HYDROMORPHOLOGY OF SINUOUS RIVER SYSTEM WITH AND WITHOUT DOWNWARD SEEPAGE

A Thesis Submitted

In partial fulfilment of the requirement for the degree of

Doctor of Philosophy

Submitted By

Jyotismita Taye

(176104022)

DEPARTMENT OF CIVIL ENGINEERING

INDIAN INSTITUTE OF TECHNOLOGY GUWAHATI

GUWAHATI – 781039, INDIA

February 2021

DECLARATION

I, Jyotismita Taye, declare that this thesis titled, "Hydromorphology of Sinuous River System with and without Downward Seepage" is part of my research for the degree of Doctor of Philosophy. All the work presented in this thesis are my own and the results generated are of the original research.

I confirm that

- The work contained in this thesis is original and was done wholly or mainly while in candidature for the research degree at this institute under the guidance of my supervisor.
- The work reported herein has not been submitted to any other Institute for any degree or diploma.
- Wherever I reported material from other sources, I have duly cited and acknowledged their respective authors and sources.
- I also affirm that no part of the thesis is plagiarized to the best of my knowledge.
- I take complete responsibility for the results and inferences reported in the thesis.

Date: Jyotismita Taye

Department of Civil Engineering
Indian Institute of Technology Guwahati
Guwahati – 781039, Assam, India

Dr. Bimlesh Kumar
Professor
bimk@iitg.ac.in
0361-258 2420

CERTIFICATE

This is to certify that the thesis entitled "Hydromorphology of Sinuous River System with and without Downward Seepage" submitted by Jyotismita Taye, in partial fulfilment of the requirements for the award of the degree of Doctor of Philosophy, to the Indian Institute of Technology Guwahati, is a record of bonafide research work under my supervision. I certify that this thesis is worthy of consideration for the award of the degree of Doctor of Philosophy of the Institute. To the best of my knowledge, no part of the work reported in this thesis has been presented for the award of any degree at any other institution.

Date:

Place: IIT Guwahati

(Dr. Bimlesh Kumar)

PUBLICATIONS

JOURNALS

1. Taye, J. and Kumar, B., 2020. Experimental study on near-bed flow turbulence of sinuous channel with downward seepage. **Proceedings of the Institute of Civil Engineers - Water management (**https://doi.org/10.1680/jwama.19.00094).
2. Taye, J., Lade, A.D., Mihailović, A., Mihailović, D.T. and Kumar, B., 2020. Information measures through velocity time series in a seepage affected alluvial sinuous channel. **Stochastic Environment Research and Risk Assessment** (https://doi.org/10.1007/s00477-020-01849-2).
3. Taye, J., Barman, J., Kumar, B. and Oliveto, G., 2020. Deciphering morphological changes in a sinuous river system by higher-order velocity moments. **Water**, 12(3), 772 **(**https://doi.org/10.3390/w12030772).
4. Taye, J., Barman, J., Patel, M. and Kumar, B., 2019. Turbulent characteristics of sinuous river bend. **ISH Journal of Hydraulic Engineering (**https://doi.org/10.1080/09715010.2019.1629843).

CONFERENCES

1. Taye, J., Caroppi, G., Gualtieri, P., and Kumar, B., 2020. Hydrodynamics of sinuous channel with seepage. **River Flow 2020**, © 2020 Taylor & Francis Group, London, ISBN 978-0-367-62773-7, Delft, Netherlands.
2. Taye, J., Barman, J., Lade, A.D., and Kumar, B., 2019. Effect of downward seepage on flow behaviour in sinuous bend. **24th Hydro 2019 International Conference (Hydraulics, Water Resources and Coastal Engineering)**, Osmania University, Hyderabad, India.
3. Taye, J., and Kumar, B., 2019. Effect of downward seepage on the flow hydrodynamics of a sinuous channel. **6th India Water Week-2019, Ministry of Jal Shakti, Government of India**, Vigyan Bhawan, New Delhi, India.

ACKNOWLEDGEMENTS

A thesis is written by an individual, but sculpted by many. My journey as a doctoral candidate in IITG would not have been possible without the care, support and guidance that I received from several people.

Most of all, I would like to extend my sincere thanks to my supervisor Dr. Bimlesh Kumar, for giving me the opportunity to work with him. His relentless support and commitment highly lifted the aspiration in me to work towards the completion of my thesis. He is a great mentor and an extraordinary human being. His knowledge towards research is commendable, and I look forward to work with him in the future. It is truly a blessing to have a supervisor and mentor like him.

I am thankful to the members of my doctoral committee; Dr. Ajay Kalamdhad (chairman), Dr. Rishikesh Bharti, and Dr. Vinayak Kulkarni for their insightful comments, encouragement, and valuable time through this research. I would like to acknowledge Department of Civil Engineering at IIT Guwahati, for providing me the required resources and a fruitful work environment.

I would like to extend my genuine gratitude to Dr. Abhijit Lade, Dr. Bandita Barman, Dr. Anurag Sharma, Jyotirmoy Barman and Sukhjeet Arora for their valuable inputs. My special thanks to Abhijit and Jyotirmoy for their incessant support during my experiment in the laboratory. I will always treasure the time spent with you two in the Water Resources Laboratory. I am grateful to Bazal Da for his spontaneous and persistent support for any laboratory complications during my experiment.

I am very grateful to my friends Kankana Ba, Namrita, Jitesh and Krishna Sir for being there for me. I will forever cherish the time spent with you all. Thank you for the unconditional support you all have given me. I would like to thank Apoorva and Paramita for the support and the beautiful time spent in campus. I consider myself truly blessed to have found you all.

I express my gratitude to Geetanjali Doley and Alakesh Deka for being there for me since undergraduate. Thank you for everything you do for me Geetu and Deka. I extend my thanks to my sisters Dr. Parishmita Taye and Sumi Taye for the love, care and understanding they bestowed upon me. I would like to thank my beloved friends Alakesh Sharma, Aizawlata, Upasana, Shyamalee, Garima, Chiranjeet, Swastika and Subhalikha.

I take this opportunity to extend my most sincere gratitude to my parents. Papa and Maa being the biggest pillar in my life, without whom this journey would not have been possible. I am thankful to my brothers, Bablu Da and Chintu Da, sister-in-law Moonlee and my niece Jiya and Aarna, for the love and support. I am thankful to Aitamaa, my cousins and relatives for their love and support.

ABSTRACT

Alluvial channels with sinuosity follow an altered flow behavior, contradictory to straight flows. The usual sight of a river system consists of bends or loops along a its course. Flow through bends is complex where erosion and deposition is a continuous process. The boundary of these river systems may be pervious or impervious. Pervious channel boundary allows the transfer of water between the surface and sub-surface of a river system. Extensive use of groundwater causes depletion or lowering of the groundwater table. This has led the channel water to seep away and join the water table underneath, commonly known as downward seepage or suction. At the interface of surface water and groundwater, seepage is a significant phenomenon occurring at the boundary of alluvial channels. Some of the practical issues due to seepage are stability of hydraulic structures, transport of contaminants, bank failure, reduction in conveyance efficiency in irrigation channels and increased sediment transport.

The association between surface water and groundwater is of great importance in the field of hydraulics and a large information can be gathered by analyzing the streamflow data. Seepage has its effects on both the flow parameters and the rate of sediment transport. To address the nature of turbulence and the morphology in sinuous channel with downward seepage an experimental framework was designed. The flow and the morphology studies were conducted in three different sinuous channels, namely, rigid rectangular channel, mobile rectangular channel and mobile trapezoidal channel.

A noticeable shift in the mean velocities, Reynolds stresses, bed shear stress, turbulence intensities and turbulent kinetic energy near the channel bed were observed in the sinuous channel. High streamwise velocity was found near the deposition region, which confirmed that maximum velocity is not always towards the outer bend. Increase in entropy measures of the transverse velocity was found with downward seepage. The octant analysis helped in recognising the behavior of the bed changes, where the transverse motion of sediment was observed across the channel. The morphological changes can also be attributed to the

radial or transverse velocity across the channel, which was also confirmed from the circulation cells observed in the bend.

With downward seepage, the low momentum flow near the boundary of the channel gets detached from the main flow; therefore, there is an appreciable increase of flow parameters near the channel bed. Downward seepage promoted significant modifications along the channel bed. The flow alternations with seepage have led to enhanced sediment transport with active erosion at the outer bend and deposition at the inner bend. Pronounced streambed morphology was observed in the rigid rectangular channel. The channel was modified extensively in the mobile rectangular channel, which bankline shifting and transport of sediment load to the downstream. The mobile trapezoidal channel was observed to be stable with minimum changes along the channel boundary. These results have highlighted the processes in a sinuous channel affected by downward seepage and provide interesting information of the natural alluvial channels, where groundwater table depletion is a significant concern.

CONTENTS

LIST OF FIGURES

LIST OF TABLES

NOTATIONS

σ	Sinuosity of the channel
λ_m	Wavelength of the channel
A_m	Bend amplitude
b	Channel width
θ	Angle at any distance along the centerline of the channel
m	Distance along the centerline of the channel
θ_o	Maximum angle the channel makes with the horizontal axis (Deflection angle)
$J_o\theta_o$	Bessel function of the first kind and zeroth order
L_a	Arc length
R	Bend radius
h	Flow depth
D_{50}	Median particle size
σ_g	Geometric standard deviation
τ_c	Critical bed shear stress
u_{*c}	Critical shear velocity
ρ	Mass density of water
τ_o	Average bed shear stress
u_*	Average shear velocity
Q	Flow discharge
Q_s	Seepage discharge
L_n	Width of the notch
C_d	Coefficient of discharge
g	Acceleration due to gravity
H	Water head over the notch
E	Voltage generated in a conductor
u_c	Velocity of the conductor

B_s	Strength of the magnetic field
D	Length of the conductor
A_p	Area of the pipe
V_S	Seepage velocity
P	Perimeter
u, v, w	Instantaneous velocities in streamwise (X), transverse (Y), and vertical (Z) directions.
u', v', w'	Instantaneous fluctuations in streamwise (X), transverse (Y), and vertical (Z) directions.
$\overline{u}, \overline{v}, \overline{w}$	Average velocities in streamwise (X), transverse (Y), and vertical (Z) directions.
N	Total sample number
z	Point of measurement from the channel bed
$-\rho\overline{u'w'}$	Reynolds shear stress in streamwise direction
$-\rho\overline{v'w'}$	Reynolds shear stress in transverse direction
$\sqrt{\overline{u'u'}}$	Turbulence intensity in streamwise direction
$\sqrt{\overline{v'v'}}$	Turbulence intensity in transverse direction
$\sqrt{\overline{w'w'}}$	Turbulence intensity in transverse direction
P_k	Contribution probability of k events
n_k	Number of occurrences of bursting events
$\psi_{a,b}$	Wavelet function
v_c	Celerity or the speed of evolution

1

Introduction

1.1 Background

The rivers of our planet earth are an intrinsic part of the ecosystem. River channels choose their path and make their way downstream in the alluvial plains. Flow in channels is rarely straight; instead, they select the most probable path to minimize the energy loss. They lose their symmetry in the very few meters at the upstream of the channel and make their way with varying discharge and degree of sinuosity. Rivers mostly exhibit sinuous patterns, composed of series of loops, turns, or bends in their course. Rivers provide water for irrigation and drinking and connect important navigation links, but at the same time, they may cause bank erosion, loss of land and property during high discharge or flood events. Rivers mostly exhibit sinuous patterns, composed of series of loops, turns, or bends in their course, constituting a sinuous river system. The degree of turns or bends of a river is defined by the sinuosity, which is the ratio of curved centerline length to the channel straight-line length. The measure of sinuosity of a river (degree of the turn or curve) channel provides a clear distinction among the natural river system. The rivers with sinuosity greater than unity are termed sinuous or meandering rivers. In this thesis, the terms sinuous and meandering are used to define the same characteristics.

In practical situations, along with the main channel flow, the channel boundary exchanges water between the main channel and the groundwater through the porous boundary of the channel. Along the river reach, the nature of sediment is heterogenous, which may lead to varied channel bed characteristics. Through the porous boundaries of the alluvial channel, the main channel may receive water and deliver water, depending on the nature of groundwater level. Depletion of groundwater is valid with the maximum practice of its use. Therefore, with the lowering of the groundwater level, the water tends to move towards the

empty space created, causing downward seepage. The impact of downward seepage is found to have its maximum effects near the sediment bed of the river system. With seepage, the channel may experience changes in sediment transport processes and formation of bed features.

1.2 Definition of River Channels

Sinuous river channels are a representation of sine-generated curves. Natural rivers have distinctive features and planforms and are characterized by single-thread or multiple-thread river systems (Figure 1.1).

Figure 1.1 (a) Straight river channel (Courtesy: Richard Humphrey, Location: River Nene, Peterborough), (b) Sinuous or meandering river channel (Courtesy: Debashish Mukherjee, Location: Walong, Arunachal Pradesh), and (c) Braided river channel (Courtesy: Nic McPhee, Location: Teklanika River, Alaska).

Meandering rivers have sinuous channels that are single-thread river system, whereas braided channels are multiple-thread river system. Understanding the river pattern is important to predict the river's response with the various natural and non-natural

characteristics. The deepest path along the channel is called the thalweg. The flow along the sinuous channel swings through the deepest (outer bank) and the lowest (inner bank) regions causing undercutting and deposition. Therefore, sinuous channels are developed by the flow swinging along the thalweg. River channels can be broadly classified as straight, meandering, and braided channels (Leopold and Wolman, 1957).

- Straight rivers are characterized by minimum sinuosity less than unity. They are usually open channels for a very short reach, as long straight rivers are rarely found in nature.
- Sinuous or meandering rivers are characterized by sinuosity greater than unity. However, sinuous rivers are described to have less curvature than meandering rivers. The meandering rivers are known to have sinuosity greater than 1.5, and the sinuous rivers are described with sinuosity between 1.1 and 1.5. These descriptions are arbitrary, with no physical differences between the two. In both sinuous and meandering, the thalweg swing from side to side along the river. The river channel is associated with the development of alternate bars and pools.
- Multiple branches of channels characterize braided rivers. The branching of such a river system is such that one is the main stream, and the others are subsidiary channels. They are wide and shallow, and the water flows into different routes along the alluvial plain. Exposed alluvial bars are often observed in such rivers.

1.3 Planform Characteristics of Sinuous Channel

The planform of a meander or sinuous channel can be defined quantitatively by the sinuosity (σ), wavelength (λ_m), bend amplitude (A_m), and channel width (b). Representation of the planform is given in Figure 1.2. The path of the channel is composed of series of reversing curves, which is known as meander trains. The individual curves within the meander train are known as meander bends. Starting from an inflection point, these curves transition from one meander bend to the other along the downvalley axis. The belt width is the width of the meander between the active bends. The apex of a bend is referred to the point where a meander bend reaches its greatest lateral distance from the reference line. The amplitude is the lateral distance between the apexes of the successive

bends. The wavelength is defined as the distance between the bend apexes on the same side of the valley.

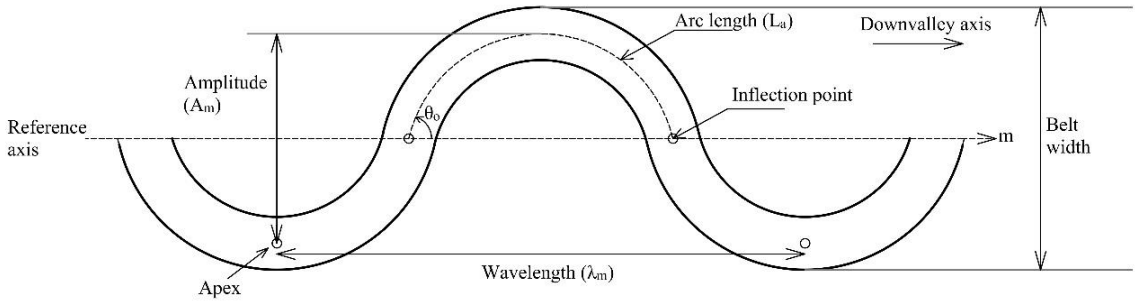

Figure 1.2 Planform of a sinuous or meandering river.

von Schelling (1951) gave the idea of a sine-generated curve to outline the most probable path between fixed points. He considered the Gaussian distribution for a given number of steps, which changes direction at the end of each step. He showed the minimum variance concept, i.e., the most probable path of a curve is obtained when the variance or overall curvature is minimum. Langbein and Leopold (1966); Leopold and Langbein (1966) proposed a sine-generated function of a regular meandering path following the minimum variance concept.

$$\theta = \theta_o cos\left(2\pi \frac{m}{L_a}\right) \tag{1.1}$$

Equation (1.1) produces a sine-generated curve that fits a meandering path of a river. The function approximates the shape of real meanders and depicts a continuous variation of the centerline curvature. In equation (1.1), θ is an angle at a distance m along the centerline of the channel, θ_o is the maximum angle the channel makes with the horizontal axis (deflection angle), and L_a is the arc length, i.e., the length between two repeating points.

1.4 Flow in Channel Bends

The centrifugal acceleration influences the flow in channel bends. This results in a three-dimensional flow that is characterized by helical motion with a superelevated free surface. Across the cross-section of the channel bend, this helical motion is viewed as transverse circulation. This flow behavior induces the transverse shear stress leading to the transverse movement of sediment across the bend. A helical flow pattern is initiated when the flow

enters the curved part of the sinuous channel. The flow near the free water surface moves towards the outer bend, and the flow near the channel bottom move towards the inner bend. When the flow passes through the curve, the flow erodes the outer bank. The eroded sediment from the channel bend is carried towards the inner bank (Figure 1.3). There is a dynamic interaction between three-dimensional flow structure, sedimentation, erosion, and channel geometry (Frothingham and Rhoads, 2003). Alluvial sinuous rivers are characterized by shallow zones at the inner bend with the development of point bars. At the outer bend, deeper zones are formed called scour or pools. The location of the pool and the maximum bend scour within the pool are the major parameters with respect to erosion at the outer bank and meander migration (e.g., Ikeda et al.,1981; Camporeale et al., 2007; Crosato, 2008).

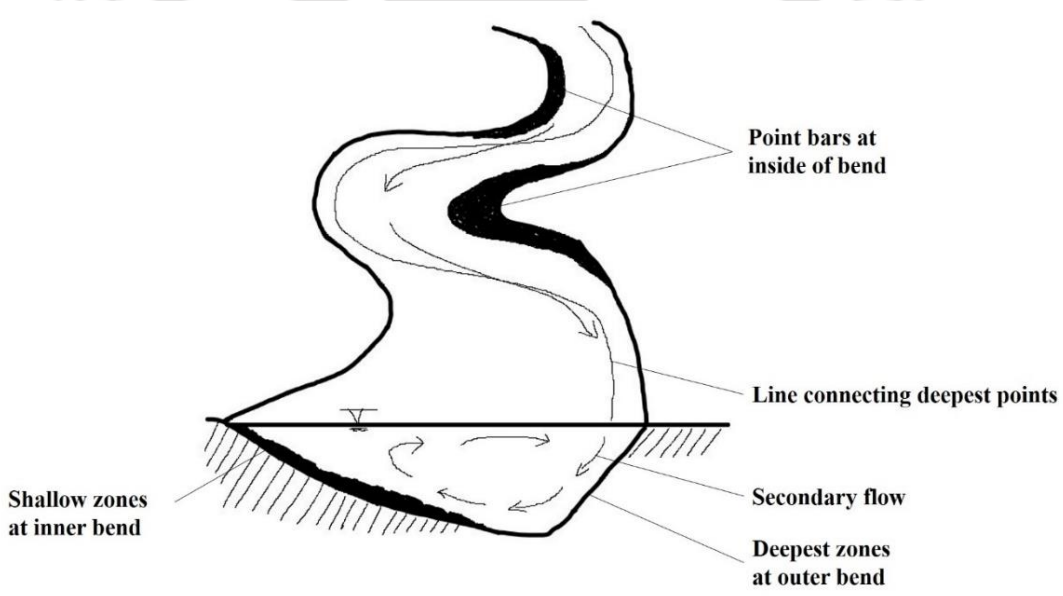

Figure 1.3 Schematic diagram of the flow conditions in sinuous channel.

Flow in sinuous alluvial bends promotes deposition and erosion at the inner and outer bank of the channel, respectively (Huggett, 2016). The flow behavior in the bend, nature of the sediment, and the channel geometry are the key factors concerning erosion at the outer bank and meander development (Crosato, 2008). Previous studies have testified the morphological changes in a sinuous channel (Binns and da Silva, 2015; da Silva and Ebrahimi, 2017). Experiments conducted with erodible beds in a meandering channel have reported bed formations as point bars, mid-channel bars, free bars, and sand bars (Whiting

and Dietrich, 1993a; Whiting and Dietrich, 1993b; Termini, 2009; Luchi et al., 2010). Xu and Bai (2013), in their experiments with erodible bed and fixed walls, observed depositional bars at the inner bank and pools at the outer bank. Under natural conditions in rivers, the flow turbulence governs the bed deformation and channel migration (Engel and Rhoads, 2012). Several laboratory experiments conducted in sine-generated channels have reported bed development with different values of deflection angle θ_o (Binns and da Silva, 2015; da Silva and Ebrahimi, 2017). da Silva et al. (2006) mentioned that, for small θ_o, the erosion and deposition features are prominent around the cross-overs, whereas, for large θ_o, they are centered around the bend apexes. Researchers have examined the timescale processes of meander bends occurring over a few decades. Engel and Rhoads (2012) studied the bed morphology, channel planform and the evolution of flow in a compound meander loop for 11 years. They concluded that the near-bank velocity and turbulence are the main causes of bank erosion and channel migration. Rahman et al. (1996) performed laboratory experiments in a mobile trapezoidal channel having bed width of 14 cm and depth of 4 cm. They have shown the morphological process of meandering channels, which indicated bank erosion and bed deformation. They concluded that the channel curvature and sediment bars play an important role in the erosion of the banks.

Literature was found regarding various aspects of meandering river like mechanics of the meandering river, bed topography of the sinuous channel, flow parameters, etc. Each of these aspects forms a separate and ongoing research topic. Thomson (1876) was the first person to explain the formation of cells in secondary currents in curved open channels. Before Thomson, Boussinesq (1868) obtained the two layers solution flowing in the opposite direction by solving the problem of viscous fluid flowing in the curved and prismatic open channel of slowly varying curvature. Rozovskii (1957) revised the solution incorporating the mechanics of river bends, which was later revisited by Engelund (1974) and Johannesson and Parker (1989). In natural meandering rivers, researchers have investigated different parameters like mean flow, Reynolds shear stress, turbulent kinetic energy, etc., and how it affects the various aspects like morphology, bed topography, the stability of banks, etc. A review of the significant studies in sinuous or meandering channels covering the flow and channel bed characteristics is in the following sections.

Rozovskii (1957) was the first person to have developed a velocity rotation scheme to separate the secondary flow from the primary flow. His study was field-based in the Desna River of Ukraine. Rozovskii's method calculates the cross-stream velocity compared to the mean flow direction at each vertical, which forces a zero-net discharge in the inward and outward directions. As a result, instead of defining the velocity profile in the entire cross-section, the strength of secondary flow was investigated at each velocity profile locally. However, there were some limitations as the study presents the secondary circulation on a local basis and fails to produce the complete details of the cross-stream velocity field.

Hooke (1975) conducted an experimental study in a 1 m wide meandering flume with sand bed and uniform flow. The bed shear stresses, bed geometry, distribution of sediment and the strength of secondary flow were determined in this study. The results of the study were established based on three discharge values 20, 35, and 50 l/sec. The strength of the secondary currents increased with the increasing discharge. Their study observed the maximum bed shear stress zone and the maximum sediment discharge per unit width close towards the inside bank across the point bar and crossed the channel centerline somewhat lower in the bend. With increased discharge and flow depth, the height and size of the point bar, and the depth of scour at the outer bend increased.

de Vriend and Geldof (1983) studied the flow velocity in river bends of shorter reach in two consecutively sharp curve bends in the river Dommel, Netherlands, and compared the results with a mathematical model for the depth-averaged main flow velocity. The river bend had steep banks and pronounced cross-sectional asymmetry. The geometry of the bed and its flow velocity measurements were implemented in a 285 m long section of the river Dommel. They found that the measured and computed flow velocity distributions are almost the same in most bend except near the bend exits where deviation occurs. This indicates that there should be an inclusion of secondary flow convection in the mathematical model. Vriend and Geldof did not consider the secondary flow convection because it led to erroneous results when they applied their mathematical model. The study observed a gradual outward shift of the maximum velocity further downstream of the bend due to the retarded adaptation of the flow to the bed configuration and not due to the secondary flow convection. Their study observed a tendency of the maximum main

velocity moving towards the inner bank. This may be due to the reduction of the channel's asymmetry and not due to the slower development of the secondary flow.

Anwar (1986) conducted field experiments along a bend of a small river in Chislehampton, Oxfordshire (U.K.). He had taken a bend of 35° central angle and conducted various experiments. The inner and outer radius of the bend was 19 m and 22 m, respectively. The instantaneous velocities in all three directions, i.e., streamline, transverse, and vertical, were analyzed. He found contrasting results regarding velocity profile, normal stresses, etc., at the bend regions. The study observed that the velocity distribution does not follow the logarithmic profile in the bend region as opposed to the straight reach upstream from the bend. The isovels (stream velocity contour line) at the bend entrance were not affected by the flow curvature but affected the bend exit. The normal stress contours are the same at the bend entrance in three directions. However, at the bend it has changed greatly where maximum stress occurs near the surface of the outer bank. The shear stresses were maximum at the outer bank near the apex, and it decreased downstream. The secondary flow played a good part in showing the anomalous behavior in different parts of the bends.

da Silva (1996) developed a sine-generated meandering to compute rough turbulent steady-state flows. The cross-section of the flow was rectangular with constant width and periodic fluid motion. Silva tried to determine the initial flow both theoretically and experimentally. The theoretical part concerns the rationalization of the equations of motion. The experiment was conducted in the laboratory using two meandering channels of 40 cm width. One was of small curvature 30° angle, and another one was of large curvature 110° angle. Silva concluded that the flow in sine-generated channels with an initial bed is not standard. The flow varies depending on the angle, width by depth ratio, and resistance factor due to friction factor. In the case of a small deflection angle between longitudinal channel axis and horizontal channel axis, the flow is ingoing, whereas it is outgoing for large values. Silva also concluded that cross circulation is not necessary to explain the occurrence of point bar at the inner bank.

Graf and Blanckaert (2002) conducted some experiments at the laboratory to see the flow around bends in rivers. They took a 120° meander bend in a flume of constant curvature of sand bed with vertical banks. They observed that the velocity distribution curve in the bend

deviates from the logarithmic profile. Furthermore, they observed two circulation cells at the bend region. One is the center region cell, which turns in the clockwise direction due to the superelevation at the outer bend. This is also known as the helical motion characteristic of bend flow (Thomson, 1876; Rozovskii, 1957). The second one is the outer bank cell, which turns in the anticlockwise direction. The outer-bank cell acts as an outer bank protection buffer zone by keeping the core of maximum velocity away from the erosive bank. After analyzing the data, they found a reduction of shear stresses in the outer bank relative to the main channel. The limitation in this experiment is that the parameters were measured at one cross section (60°). Other limitations are the flume geometry had an artificially sharp outer bank/toe interface, and the velocities and turbulence quantities were extrapolated to the bed due to limitations with measuring near the boundaries.

Blanckaert (2002a) analyzed the coherent flow structures in a bend based on instantaneous velocity profiling. He illustrated ADVP measurements of two different kinds of coherent flow structures in open-channel bends, where the existence of cross-stream circulation cells characterizes the three-dimensional flow. The first kind of coherent flow structure concerns the bulk-behavior of the pattern of cross-stream circulation cells. The second kind of coherent flow structure is associated with the turbulent bursting process. He found that the Reynolds shear stress in the meander bend differs from that of the straight river.

Patra et al. (2004) conducted experiments in the laboratory to study the behavior of meandering channels with and without floodplains. They provided a modified power law for the vertical distribution of longitudinal velocity in the meandering channel. A secondary circulation across the flow is operative because the traditional power law gives different distributions in an open channel and natural or lab channels. In their study, the distribution of tangential velocity in the longitudinal, transverse and vertical directions in the meandering channels for both in-bank and over-bank flow conditions are found to give good results.

da Silva et al. (2006) studied the erosion and deposition pattern in a sine-generated meandering stream. The changes were observed on the small, intermediate, and large deflection angle (θ_o) channels. When θ_o is small, the upstream and downstream ends of each erosion-deposition zone are very near the two consecutive apex sections. This implies

that the maximum erosion and deposition in the meander loops occurs very near the crossover-sections [as in Figure 1.4(a)].

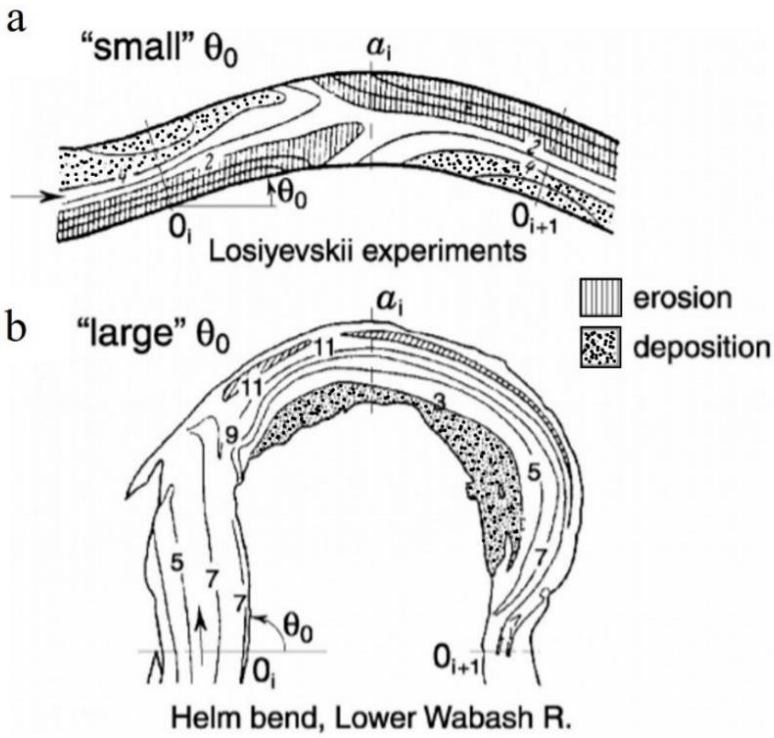

Figure 1.4 Illustration of the typical location of erosion-deposition zones in streams with small and large deflection angle (θ_o) (Courtesy: da Silva and El-Tahawy, 2008).

When θ_o is large, the upstream and downstream ends of each erosion–deposition zone are very near the two consecutive crossover sections, O_i and O_{i+1}, say. This implies that the maximum erosion and deposition in the meander loops occurs very near the apex-sections [as in Figure 1.4(b)]. When θ_o is intermediate, the erosion-deposition zones are situated somewhere in between the locations of small and large deflection angles.

Abad and Garcia (2009) conducted some laboratory experiments and used different approaches to study various parameters and their interactions. They carried the experiments in a 200° compound bend (Kinoshita) flume asymmetric in nature and with smooth rectangular channel. They considered the flow upstream and downstream skewed and compared the results. They found that the bend, which is oriented downstream valley, showed fully developed secondary flows, more developed bedforms along the bed, and

likely higher shear stresses along the bed and banks. They observed that there is a perfect correlation between turbulent kinetic energy with local curvature. The normal stresses have a major contribution to turbulent kinetic energy, except downstream of the apex, where shear stresses are prevalent.

Termini (2009) conducted experiments to study secondary circulation and how it affects bank shear stress distribution and influences bank stability. The investigation was conducted in the laboratory that follows a sine-generated curve of deflection angle 110°. The width of the channel was 0.5 m and had a rectangular cross-section. The experiment was conducted with two width to depth ratio, i.e., one is $b/h < 10$ and other $b/h > 10$, where b is the width of the channel and h is the total water depth. Termini concluded that for $b/h < 10$, a counter-rotating circulation starts to form near the outer bank's free surface, which increased until it reached the apex section and decays at the bend exit. This conclusion was in contrast with $b/h > 10$, where outer bank circulation forms only at the apex section. The formation of outer bank circulation cell, mainly with $b/h < 10$, allows the banks to be stabilized, as the values of bank shear stress were low.

Jamieson et al. (2010) performed laboratory experiments in two different cases: developing and equilibrium beds. They performed the experiments on a 135° constant curvature flume with sand bed. The thalweg migrated towards the outside wall through the bend rather than encroaching the outside wall (Matsuura and Townsend, 2004). This result indicated an outer bank circulation cell, which rotates opposite to that of the principal secondary flow cell. Due to this, it prevents the increase in flow outward from impinging on the outer bank. The study concluded that the magnitude and distribution of normal stresses and turbulent kinetic energy were concentrated over the thalweg and the magnitude increased through the first half of the bend. The streamwise cross-stream and cross-stream vertical Reynolds stresses increased as flow moved through the bend, and the streamwise vertical stresses near-bank becomes less dominant. It was found that the magnitudes of streamwise cross-stream stresses at the outer bank are high relative to other stresses.

Sukhodolov and Kaschtschejewa (2010) performed their experiments in the meander bend of the lowland river Spree in Germany. The channel considered was a 30 to 40 m width river with the bathymetry characteristic of meander patterns, which includes a riffle-

pool sequence. The river bend had an arc angle of 150°, bend wavelength of 485 m, and sinuosity of 1.57. The study focused on the cross-sectional patterns of principal statistical characteristics of flow, spatial variation of the patterns induced by the curvature of the channel, and comparing the measured data with available analytical models. The study reported that the mean velocity profile is not logarithmic and only valid near the riverbed. They found that the mean and turbulent flow structure in the meander bend is three-dimensional and highly heterogeneous. The field experiment also concluded that a small counteracting cell was observed near the outer bank, similar to those observed in the laboratory by various researchers.

Engel and Rhoads (2012) studied the co-evolution of flow, bed morphology, and channel planform in a compound meander loop. They collected data from the upper portion of Embarras river watershed in Champaign County, Illinois, taking two different measurements in 11 years. The compound meander bend angle was 200°, asymmetrical in nature. They found the turbulent kinetic energy magnitudes are greatest near the bank toe, downstream of bend apex. In the span of 11 years, they have seen the migration of the channel within the loop. They concluded that spatial variation of bank velocity and turbulence documented at the beginning control the pattern of bank erosion. The qualitative near bank erosion pattern was evaluated between turbulent kinetic energy and boundary shear using an empirical relationship. The study suggests that the failed blocks of bank material affect the flow locally and, thus, it influenced the bank erosion rates and patterns.

Kashyap et al. (2012) studied the flow within an alluvial channel bend with varying curvature ratio (bend radius/channel width, R/b) and aspect ratio (channel width/flow depth, b/h) by numerical simulation. Validation of the numerical predictions was done from three physical experiments in a high-curvature 135° bend. With the change in aspect ratio between 5 and 12.5, the secondary flow distribution was substantially impacted. With curvature ratio, $R/b = 3$, the streamwise depth-averaged velocities showed significant differences within the bend. With decrease in R/b from 8 to 1.5, the peak bed shear stress in the bend increased by 70%.

Khatua et al. (2012) predicted stage-discharge for the meandering channel. The stage-discharge relationship is relatively easy to find in straight channels, but due to variation of

river geometry and hydraulic properties, it is quite difficult in the meandering river. The experiment was conducted in the laboratory using straight and meandering channels. The experiments were carried out to study channel geometry and sinuosity on the variation of roughness coefficient in a meandering channel. It depends on sinuosity, aspect ratio, the longitudinal slope of the channel, and Reynolds number of the flow. With flow depth, flow resistance in terms of Chezy's C also changes. After finding the roughness coefficient using dimensional analysis, the stage-discharge relationship can be adequately predicted in a meandering channel.

Vermeulen et al. (2015) presented field measurements of a sharp bend in the Mahakam River, Indonesia. The flow structure was analyzed with the increased cross-sectional area in the bend. The flow pattern in the bends is characterized by two zones of horizontal recirculation and high vertical flow velocity. The field measurements are analyzed together with the numerical simulation results with a three-dimensional finite element model, which yields a comprehensive view of the flow structure. The results show the importance of the increase in cross-sectional area in the development of horizontal recirculation. Vertical acceleration of flow into the scour causes the pressure to deviate from a hydrostatic pressure distribution.

Song et al. (2016) studied the development of different planforms to understand the influence of initial river system parameters on the changing process of planforms. The initial river system parameters were the channel sinuousness, width, and water discharge. Transport of sediment increased with the increase in channel sinuousness but stopped growing due to the excessive increase of flow route and flow friction. In high flow runs, the initial channel showed remarkable bank-line migration, which was mainly controlled by sinuousness and water discharge.

Engel and Rhoads (2017) studied the compound meander bend along Sugar Creek in McLean County, Illinois, USA. They examined the turbulent structure in the near-bank of the meandering channel. The results showed a difference in vertical profiles of streamwise-vertical Reynolds stresses near the outer bank of meander bends to that of wide straight channels due to the effects of curvature-induced helical motion and local frictional effects associated with complex bank morphology in meandering channels. Some of the past work

have shown the presence of outer bank circulation cell which acts as a counteracting effect at the outer banks of the meander bends (Blanckaert and Graf, 2001; Blanckaert et al., 2013). This outer bank cell was not observed clearly in this study either by ADCP or by ADV measurements.

da Silva and Ebrahimi (2017) provided comprehensive insights regarding the nature of meandering flow and how the flow shapes the bed of the meander. They also conducted an experimental study in an existing 70° sine-generated channel to observe the planimetric evolution of meandering rivers. Analyzing the results of previous known studies, they mentioned that the pool-bar complexes are strongly dependent on sinuosity (or, equivalently deflection angle θ_0). For small θ_0, the pool-bar complexes centered around the cross-overs, and for large θ_0, they are centered around the apexes. The authors made a clear statement that the bank erosion did not occur at the location of the largest flow velocity near the bank or the largest downstream gradients of flow velocity. Instead, the bank erosion occurred between those of maximum downstream gradient of velocity and maximum flow velocity. The authors mentioned the scope of further study on the influence of b/h on the various aspects of meandering streams. However, with the increase in b/h would cause a reduction in cross-circulation flow and therefore have a remarkable effect on morphology.

Russell and Vennell (2019) made a study using high resolution ADCP measurements from a natural river bend of moderate curvature to show the secondary cell formation and the deformation of the vertical profile of the primary flow. The paper showed evidence of advection of momentum due to secondary circulation. The vertical distribution of the primary flow was found to be deformed, as the maximum value was well below the water surface. The outer-bank cell was larger and stronger than found in a laboratory flume, perhaps due to the outer bank roughness. The strength of this outer-bank cell was approximately 0.5 of the main cell.

Biswas and Barbhuiya (2020) conducted experiments in two laboratory flumes having 90° and 180° bends to study the influence of different parameters on scour at bends. The study used uniform non-cohesive sediment of varying size 0.28 to 1.18 mm as bed material under different flow conditions. Three different cross-sectional shapes, flat, trapezoidal and

parabolic, were used to study the effect of shape on scour. In this study, the scour mainly occurred along the outer bank for both 90° and 180° bend, which is due to the vortex and cross-flow. For parabolic bed, the magnitude of scour was maximum at the outer bank under flooded condition. For flat bed, the deposition was maximum at the inner region. The deposition pattern for the parabolic and trapezoidal bed was different. Therefore, the authors stated that the bed cross-section is an important parameter to study the effect of scour in bends.

Yan et al. (2020) made a numerical study of the flow characteristics in strongly curved channel bends with different side slopes. They investigated five different turbulence models' performance against experimental data on the flow field in a high curvature 135° channel bend. The Reynolds-Averaged Navier-Stokes (RANS) turbulence models used for the study are the standard $k-\varepsilon$, Re-Normalisation Group (RNG) $k-\varepsilon$, realization $k-\varepsilon$, $k-\omega$, and shear stress transport (SST) $k-\omega$. The objective of the study was to evaluate the influence of the side slopes on the flow distribution, secondary flow cells, and the flow vorticity in channel bends. Among the five turbulence models, the study found the realization $k-\varepsilon$ model to simulate the flow field in the channel bend. In this study, with side slope zero (rectangular channel), the secondary flow was characterized by a double-cell pattern. One cell is a clockwise-rotating primary circulation cell at the inner bend, and the other is the counterclockwise-rotating outer-bank cell. In the trapezoidal channel, with an increase in side slope run-to-rise ratio increases to 1, an additional clockwise-rotating cell was formed. With the increase in the run-to-rise ratio, the cell split into smaller cells. The local aspect ratio may contribute to the splitting of cells. The normalized streamwise unit discharge in the rectangular channel appears high near the inner bend, which may have been due to the potential-vortex effect. In trapezoidal channel bends, the side slopes deflected the flow towards the middle region of the channel.

Das et al. (2020) studied the turbulence characteristics and planform evolution based on field investigation. The study was carried out within a distinct dynamic lobe of an outer bend of the Hooghly river. The strong secondary current was present within the lobe, and streamwise mean velocity were minimal at the apex region and maximum towards the lobe ends. Erosion and evolution of the lobe were related to the presence of helical motion. The

Reynolds shear stress was maximum at the bend apex. Bursting events were analyzed, which showed the contribution of ejection and sweep to be dominant at the apex of the lobe.

1.5 Effect of seepage in alluvial channels

Natural channels with grainy beds and banks are porous, allowing water to infiltrate through the lateral downward direction. Channel water infiltrates through the porous boundaries of the alluvial channel and joins the groundwater table, termed as downward seepage. The association between surface water and groundwater is of great importance in hydraulics, and large information can be gathered by analyzing the streamflow data. Recent practices of drawing water for use from the tube-wells or bore wells in the territory of natural channels caused depletion of groundwater, resulting in downward seepage. Thereby, downward seepage is a vital parameter occurring in natural channels. Richardson et al. (1985) observed that water moves out as well as into the alluvial channel. The seepage water can either flow as suction (losing streams) or injection (gaining streams), based on the depth difference between the channel water and the nearby groundwater table (Figure 1.5).

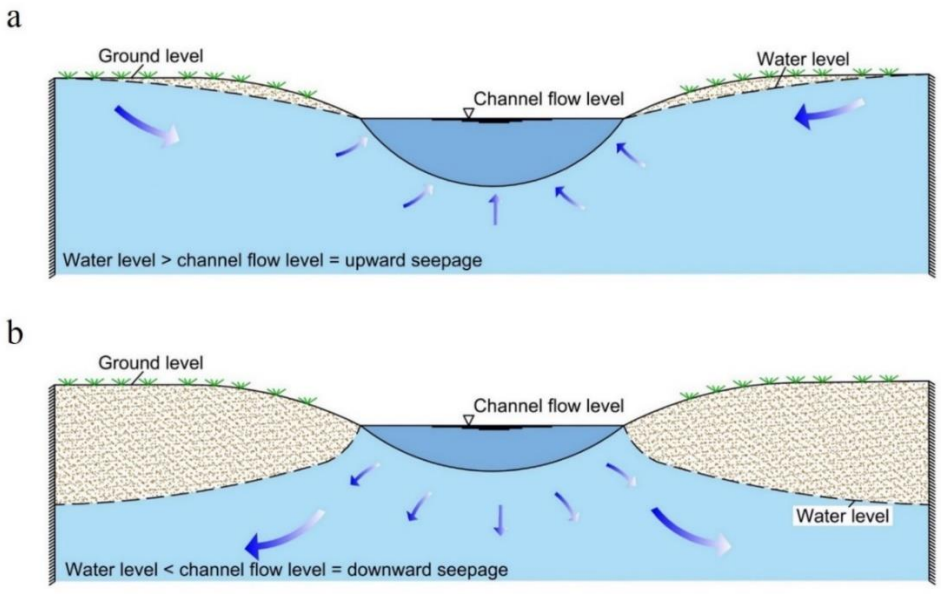

Figure 1.5 Explanatory diagram showing (a) Flow into the channel (upward seepage) and flow out from the channel (downward seepage).

The seepage velocity in most cases is small compared to the free-stream velocity above the sediment bed. Yet, this small seepage velocity exerts an extra hydrodynamic force on the sediment bed. In unlined irrigation canals with permeable soils, the downward seepage leads to a reduction in conveyance efficiency (Krishnamurthy and Rao, 1969; Sharma and Chawla, 1975; Fipps, 2005). The water supplied at the head of the canal is lost downstream of the canal. Researchers have employed different methods to estimate the seepage loss in irrigation canals and alluvial streams and channels. Krishnamurthy and Rao (1969) investigated seepage loss of 2.2 m^3/day/m at the Ganga canal using radioisotopes. Raja et al. (1983) estimated seepage loss in an unlined channel using nuclear technique and found the loss to vary from 1.3 to 4.3 m^2/106 m^2 of the wetted surface area. Dukker (1994) measured the seepage loss at the Lower Gugera Branch canal using the inflow-outflow technique and found the seepage loss to vary vastly from 3.54 cm/day to 62.04 cm/day, where errors and uncertainties might have occurred during measurements.

Field measurements of seepage loss in canals and alluvial channels were reported in previous studies to provide the real scenario of the seepage condition. Shukla and Mishra (1994) based on field investigation, quantified that about 45% of the water supplied at the head of the canal was lost due to seepage. At the New York Canal, the cumulative seepage loss was 12% to 20% (Berenbrock, 1999; Carlson and Petrich, 1999). Tanji and Kielen (2002) estimated 20% to 50% of water loss by volume of the total flow in earthen canals of semi-arid regions. Martin and Gates (2014) carried out a water balance analysis on earthen irrigation canals and estimated a loss of about 15% of the upstream flow because of seepage. The interaction of streamflow with groundwater is essential for the river system. Transport of contaminates may also occur during the exchange of water (Jones and Mulholland, 1999).

Seepage has its effects on both the flow parameters and the rate of sediment transport. Extensive laboratory studies and on-site location studies were conducted to study the impact of seepage. A review of the seepage flows is provided in the following section.

Watters and Rao (1971) carried out an experimental study to observe the effect of seepage on the stability of bed particles. They evaluated the drag and lift forces on bed particles in

the injection and suction scenarios and observed that injection inhibits the particle motion, whereas suction increases the sediment movement.

Oldenziel and Brink (1974) reported an increase in shear stress causes an appreciably increase in the bed particle movement on the plane bed channel. They suggested that the rate of sediment transport decreases for upward seepage and increases for downward seepage.

Willetts and Drossos (1975) conducted experiments on a narrow flume provided with a small seepage zone and found that downward seepage causes localized scour holes around the seepage affected zone. Besides, faster movement of sediment grains was observed over the length of the seepage zone rather than elsewhere in the flume.

Maclean and Willetts (1986) investigated bed shear stress changes with and without seepage conditions by visualizing the initiation of motion of the indicator grains. The bed shear stress increased with the application of downward seepage.

Maclean (1991a) performed two sets of experiments in an open channel and a wind tunnel to measure the velocity by providing high downward seepage rates. He observed that velocity decreases near the water surface and increases close to the channel bed under downward seepage in the open channel.

Maclean (1991b) observed that the increase in bed shear stress in the presence of downward seepage leading to local scour around the seepage zone. He found that an increase of downward seepage velocity by 10% causes around two times an increase in bed shear stress compared to uniform shear stress.

Prinos (1995) studied the effects of bed suction (downward seepage) numerically on flow turbulence structure by solving the Reynolds-average Navier Stokes equations. The bed suction rates taken for the study were 0.3%, 4%, 6%, and 9% of the free stream velocity. The velocities deviate from the law of the wall with suction. They observed a sudden change of the near-bed conditions at the suction inlet, which ascertained that the law of the wall with suction does not hold good. In the seepage zone, the bed shear stress increased when the downward seepage rate increased. The quantitative analysis signified that with

increased seepage velocity up to 9%, the bed shear stress increased eight times as compared to without seepage case.

Cheng and Chiew (1999) carried out analytical and experimental studies considering additional force because of seepage on a sediment particle in threshold condition. They showed that the critical shear velocity decreases with the application of upward seepage.

Rao and Sitaram (1999) studied the effect of seepage on the stability and mobility of bed particle by performing extensive flume experiments in the laboratory. They observed that downward seepage reduces the stability of bed particle and can initiate particle movement, whereas upward seepage increases stability and hinders the movement of sediment. Besides, they found that bed erosion increased with an increase in the downward seepage rate, while upward seepage holds the opposite result. They emphasized that the presence of seepage disturbs the stability of bed particles, and needs to be considered during the design of the stable alluvial channel.

Krogstad and Kourakine (2000) showed the effect of localized upward seepage on turbulent flow structure close to the channel bed in their experimental study. They found that bed shear stresses significantly reduced when water entered through the channel boundary in the form of upward seepage.

Chen and Chiew (2004) investigated the influence of downward seepage on the flow hydrodynamics in open channel theoretically and experimentally. They observed that near-bed velocities increased with the application of downward seepage. It was observed that the vertical distribution of streamwise velocities does not follow the universal law of the wall in the presence of seepage. The origin displacement, slip velocity, and shear velocity increases with an increase in relative downward seepage. Figure 1.6 presents the velocity distribution over a permeable bed in a straight open channel. In the Figure, y_o is the vertical displacement of the origin of the mean velocity profile, and u_s is the slip velocity at the bed surface. By determining the values of u_s, by fitting the measured data, it was reported to be about 30 – 40 % of the maximum velocity.

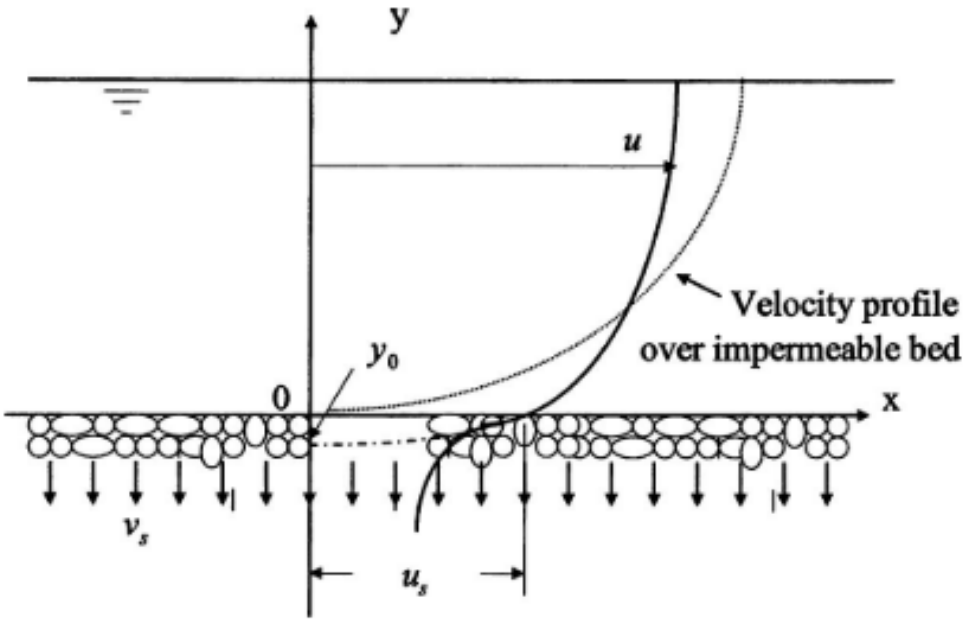

Figure 1.6 Velocity profile over porous bed in a straight open channel with downward seepage (Courtesy: Chen and Chiew, 2004).

Langhoff et al. (2006) quantified the groundwater-surface water interaction at nine site locations along an alluvial stream in central Jutland, Denmark. They reported that from 40% of the in-situ measurements, 50% of the seepage flows are through the streambed.

Rao (2007) studied the seepage losses at 24 locations in the Mahi Right Bank Canal Irrigation Project in Western India. He used the physical and the geological data available for the study. The study found that the vertical flow rate (seepage flow from the canal) varies from 0.2 – 2.1 m^3/day.

Lu et al. (2008) carried out an extensive review on the effects of seepage on the movement of sediment particles. They showed that the effective weight of a sediment particle increases with the application of downward seepage. The graphical representation of the effective weight of particles and bed shear stress variations according to the downward and upward seepages is shown in Figure 1.7.

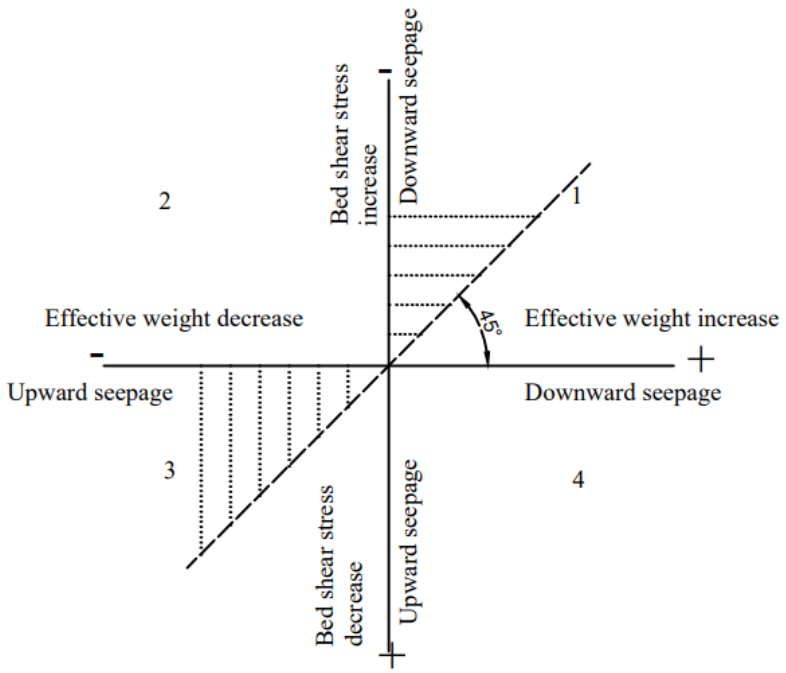

Figure 1.7 Description of bed particle stability under the influence of seepage using quadrant analysis of various forces acting on a particle (Courtesy: Lu et al., 2008).

In Figure 1.7, the positive and negative signs signify the increase and decrease in the movement of bed particles, respectively. As discussed earlier that downward and upward seepage cause increase and decrease in bed shear stress, respectively. Apart from this, it can be observed from Quadrant 1 that downward seepage increases the effective weight of particles, resulting in increasing the stability. In contrast, downward seepage can increase bed shear stress, causing a reduction in the stability of bed particles. From these scenarios, it is signified that the particle movement depends on the relative magnitude of these opposing effects. Thus, the stability of a sediment particle can be defined in terms of the equilibrium of forces. For example, if the effective weight of a sediment particle is less (more) than the force acting on it caused by flow then greater (no) movement occurs.

Rao and Sreenivasulu (2009) pointed out the significance of seepage in canal design. They showed that downward seepage in any direction, either upward or downward, influences the resistance to flow and mobility of sediment particle on a stable channel bed. They observed that suction reduces the stability of the sediment particles and can initiate

the bed particle movement, whereas, injection does the opposite. Thereby, it was concluded that the effect of seepage should be examined before designing the earthen canals.

Rosenberry and Pitlick (2009) measured the seepage rate along a 300 m long reach of the South Platte River, Colorado, USA. The average seepage rate made at 24 locations along the reach was about +24 cm/day (upward seepage). They also determined the seepage rates at specific reach locations, which ranged from -340 cm/day (downward seepage) to +237 cm/day (upward seepage). The seepage rates at one location site were measured temporally, where the seepage ranged from +5 cm/day to -41 cm/day over 2 hours.

Kavcar and Wright (2009) modified the Shields parameters by considering the influence of vertical pore water flux (downward seepage) on the movement of sediment particles. Required bed shear stress for incipient motion of bed sediment has increased as the amount of downward seepage was increased. They also found that the hydraulic bed slope plays a significant role to characterize the initiation of sediment motion.

Kinzli et al. (2010) measured the canal seepage loss by the inflow-outflow method using an ADCP in the Middle Rio Grande Valley. They found an average seepage rate of 0.64% per kilometer for the main canals, 1.93% per kilometer for the lateral canals, and 1.84% per kilometer for the acequia canals.

Hatch et al. (2010) investigated the streambed seepage loss of the Pajaro River, California. The seepage loss was determined for an 11.42 km long experimental reach, and point-specific seepage rates were determined along the reach using time series thermal methods. Along the reach, the seepage loss was in the range of 0.1 – 0.3 m^3/s. The seepage loss rate at a specific point was found to be 1.4 m/day (downward seepage).

Sreenivasulu et al. (2011) presented the variation of stream power in the presence of downward seepage affected channels. They observed higher stream power at the upstream end of the channel, and it decreases towards downstream direction because of changes in seepage quantity. It was observed that the higher stream power caused erosion at the upstream end. Consequently, eroded material deposited at the downstream end due to reduction in stream power.

Rao et al. (2011) considered the effect of downward seepage on the geometry of sand bed channels. They found that the presence of seepage alters the stability of the regime channel and flow characteristics. They defined that the regime channels are free to adjust section, pattern, geometry, and shape in response to hydraulic changes. The bivariate and trivariate regression relationships was developed for an alluvial channel under the influence of downward seepage.

Liu and Chiew (2012, 2014) performed both theoretical and experimental investigations to understand the seepage effects on the initiation of cohesionless sediment particles. In their theoretical analysis, the external force exerted by downward seepage was examined. They conducted five experiments on the uniform sand bed to quantify the effect of downward seepage on sediment entrainment. These analytical and experimental works provide an overall understanding regarding seepage effects on sediment movement. In Figure 1.8, with an injection or upward seepage, the velocity decreased near the bed and increases near the water surface compared to that without seepage; the reverse occurs with suction or downward seepage.

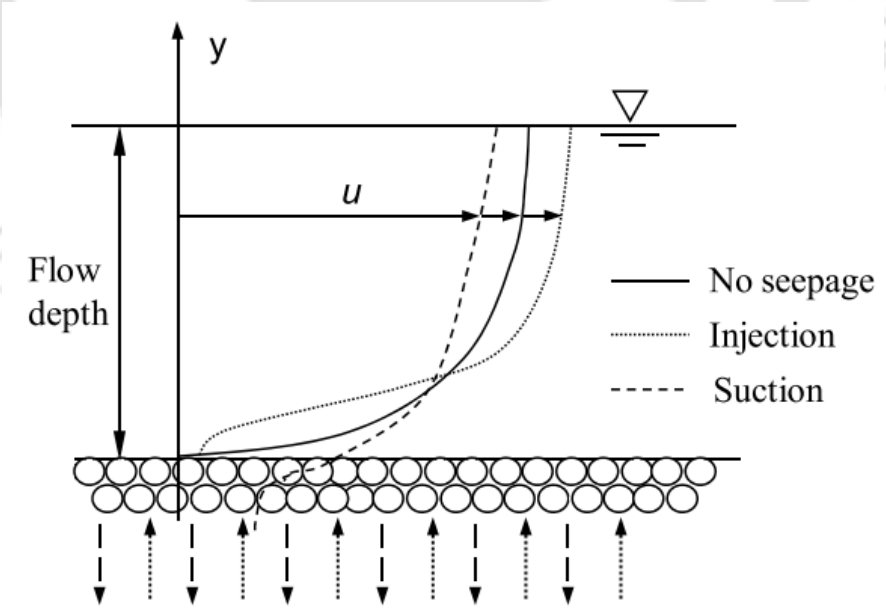

Figure 1.8 Velocity profiles over a permeable bed in straight open channel subjected to upward seepage (injection) and downward seepage (suction) (Courtesy: Liu and Chiew, 2012).

Cao and Chiew (2014) conducted laboratory experiments and theoretical analysis to investigate the influence of downward seepage on sediment transport in closed-conduit flows. The small seepage rate did not influence the overall sediment transport, and the movement of bed particles remained unchanged. Theoretical analysis showed that the bed particle experiences additional force because of downward seepage, which caused external vertical drag induced by suction on the bed particle. In the flow analysis, they found that suction causes an increase in horizontal and vertical near-bed velocities ascribed to driving force on the bed particle, indicating sediment transport in the presence of downward seepage.

Deshpande and Kumar (2016) observed that downward seepage alters the channel morphology and increases the bed shear stress. They developed an empirical relationship for the thickness of the sheet flow layer by considering downward seepage as an independent parameter. Lu and Chiew (2007), Dey and Nath (2010), and Dey et al. (2012) investigated the effect of seepage on turbulent characteristics of flow in open channels. They observed that near-bed velocities increased after the application of downward seepage.

Patel and Kumar (2017) conducted an experimental study on a parabolic cross-sectional straight channel under no seepage and seepage conditions. The study addresses the turbulent flow characteristics behind the development of bedforms with seepage application on a threshold channel. Without seepage at the threshold channel, no appreciable deformation occurred. However, with downward seepage, bed deformation was noticed with the development of bedforms in the channel. With an experimental run for 24 to 31 h with seepage, the channel attained stability with deformation at high Shields stress. The flow parameters were observed to alter near the channel bed with seepage. The velocities increased 1 – 4%, and the Reynolds shear stress increased 25 – 30% near the channel bed. The streamwise and the vertical TKE fluxes have shown a significant increase. Daughter Ripples across the channel were observed after the seepage application, which further transformed into linguoid ripples with the passage of time.

Jewel et al. (2019) made an experimental study to investigate the effect of upward seepage on the critical shear stress of cohesionless soil bed. The experiment aimed to determine the

incipient motion of particles subjected to upward seepage with different hydraulic gradients. The dimensionless critical shear stress decreased slightly with the increase in the hydraulic gradient of the seepage flow, in upstream of the seepage zone. The dimensionless critical shear stress at the seepage zone decreased sharply with the increase in the hydraulic gradient of the seepage flow.

Sharma et al. (2020) studied the effect of hydrodynamic on the mobility of phosphorous in an upward seepage affected alluvial channel. They observed that the concentration of phosphorous (P) has reduced by 25% - 40% in the presence of upward seepage for no seepage. Additionally, the flow turbulence intensities and Reynolds shear stress have decreased in the presence of upward seepage.

1.6 Research Gap

Seepage effects are assumed to have minimal effects on river channels, and therefore their effects are neglected in the field of fluvial hydraulics. River engineers mostly ignore the impact of seepage because of its small magnitude. In recent years, with the declining groundwater level, the study of downward seepage is gaining interest in the research community. With downward seepage, a substantial amount of water is lost through the channel bed. This water transfer through the porous boundary of the channel and joins the groundwater. Researchers in the laboratory and on-site location extensively studied the effect of seepage in open-channel flows. After an extensive review of the literature, it may be concluded that seepage loss depletes the water resources and alters the hydro-morphology of the channel boundary.

Downward seepage induces transfer of mass and momentum that significantly influences the flow structures and sediment transport processes. Some of the practical issues due to seepage are the stability of hydraulic structures, bank failure, and abrupt changes in the channel bed. In coastal environments, complex situations arise, such as in the swash zone, where seepage varies temporally and spatially (Turner, 1995; Karambas, 2003). Considering this situation, understanding surface water interaction with seepage flow through porous media was essential to quantify the erosion processes.

From the review of the present literature, the effect of seepage reported so far is investigated in straight channel and has not considered the bends or loops in the channel's course. Even though the understanding of the physical processes of seepage in straight open channel flow is largely present, comprehensive study around the porous boundary of sinuous channel is felt necessary. The banks of sinuous channels are weak locations where the effects of fluctuating velocity components are significant. They are vulnerable to deposition and erosion activity. The phenomenon of downward seepage is yet to be explored sufficiently in sinuous or meander channels. Practical differences may arise to obtain accurate results in actual field experiments; therefore, well-designed laboratory investigation is preferred as a truthful method to provide detailed information of the hydrodynamics and morphological parameters. Moreover, to find a solution to a specific problem to understand the fundamentals of river processes, experimental channels are quite useful to explore the mechanisms associated. In the present work, the aim is to explore and understand the near-bed turbulent flow and bed morphology in a sinuous bend without seepage and with downward seepage (suction).

1.7 Objectives

The study addresses the nature of the flow field and morphology of the sinuous channel with and without downward seepage. Following are the objectives:

1. Effect of downward seepage on the turbulent flow behavior in sinuous channels.
    - Effect of downward seepage on the flow turbulence in a rectangular sinuous channel with non-erodible banks.
    - Experimental study on near-bed flow turbulence in a rectangular sinuous channel with non-erodible banks with downward seepage
    - Effect of downward seepage on the flow turbulence in a rectangular sinuous channel with erodible banks and bed.
    - Effect of downward seepage on the flow turbulence in a trapezoidal sinuous channel with erodible banks and bed.
2. Effect of downward seepage on the morphological changes in sinuous channels.
    - Effect of downward seepage on the morphology in a rectangular sinuous channel with non-erodible banks.

- Effect of downward seepage on the flow turbulence in a rectangular sinuous channel with erodible banks.
- Effect of downward seepage on the flow turbulence in a trapezoidal sinuous channel with erodible banks.

1.8 Organization of Thesis

A brief introduction of each chapter is described below:

Chapter 1 "Introduction" presents the background of sinuous channels, describing the flow behavior and the bed development put forward by various pioneering researchers. Detail review of downward seepage in the experimental and natural condition of a river system is discussed. The problem statement and the research gap are discussed, and finally, the objectives of the study are outlined.

Chapter 2 "Methodology" describes the experimental methodology with details of experimental design, experimental program, and data collection methods. The details of the instruments used in the experimental study are also provided.

Chapter 3 "Turbulent Flow Behavior in a Sinuous Channel with and without Downward Seepage" presents the effect of downward seepage on the hydrodynamics of a sinuous channel. The turbulence structure in three sinuous channels, rectangular with rigid boundary, rectangular with mobile boundary, and trapezoidal with mobile boundary, is explored under the effect of downward seepage.

Chapter 4 "Morphological Characteristics in a Sinuous Channel with and without Downward Seepage" presents the morphological characteristics of a sinuous channel. The bed development and bank evolution are studied with different cross-sectional shapes. Contour plots and cross-sectional profiles are shown. The celerity is also analyzed in rigid boundary rectangular sinuous channel to provide evidence on sediment transport speed with seepage.

Chapter 5 "Conclusion and Recommendations" aims to address the important findings of the present research work. Recommendation and future scope of the work are also discussed in this chapter.

2

Methodology

2.1 Overview

Performing experimental studies in laboratory flumes can provide us an overview of the sediment transport problem associated with the flow characteristics. Flume results or laboratory studies are conducted to find specific phenomena and measure their effects, whereas many complicated factors play a role in field studies. The following section describes the experimental procedures, data collection, and data processing techniques.

2.2 Experimental Setup

2.2.1 The Flume

Experiments were conducted in a deep transparent glass-side recirculating flume at the Water Resources Engineering Laboratory, Civil Engineering Department, IIT Guwahati, India. The length of the flume is 17.2 m, width is 1 m, and depth is 0.72 m. The flume is a recirculating type connected to an underground sump having a storage capacity of about 70 m^3. Three centrifugal pumps having 7.35 kW power regulate the recirculation. The water was supplied to the overhead tank using the pumps. The overhead tank supplied water to the inlet tank (length 2.8 m, width 1.5 m, and depth 1.5 m) at the upstream of the flume by a supply pipe. A control valve was installed in the pipe near the overhead tank to govern the flow discharge. The sudden fall of water in the inlet tank was corrected by installing wooden baffles to achieve smooth entry into the channel. The total channel length is 17.2 m, and the first 2 m length from the upstream was made impermeable, where gravel layer was laid. The wooden baffles at the inlet tank and the gravel bed together diminished the unsteady fluctuations at the flume entrance and allowed smooth entry into the channel.

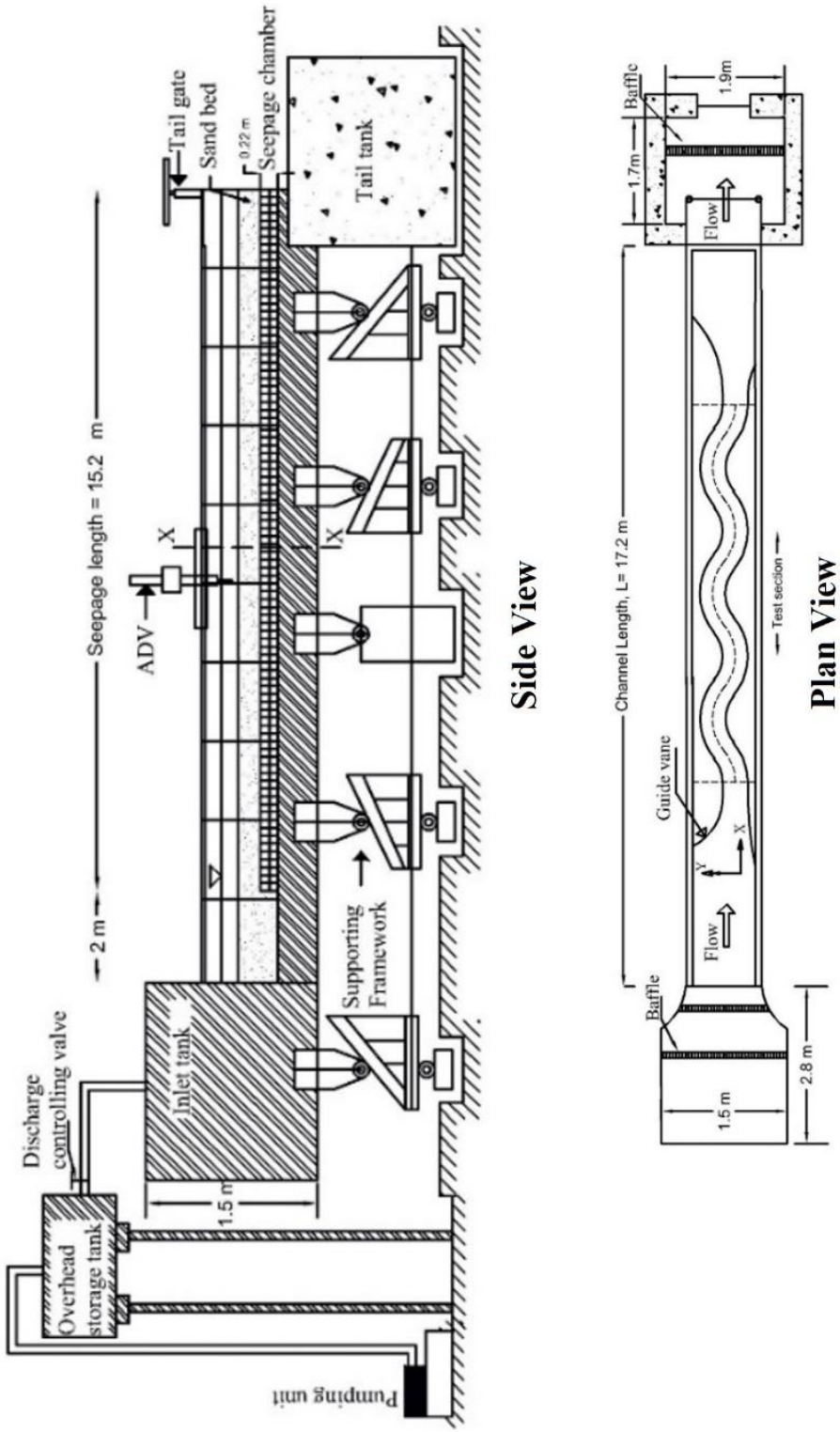

Figure 2.1 Schematic diagram of the experimental flume with facilities.

The 15.2 m length of the flume was divided into two parts, the upper one is the open channel, and the bottom part is the seepage chamber. A fine mesh (0.1 mm) supported on steel tubes of 0.22 m height separates the seepage chamber from the main channel. The sand bed was laid above the mesh to make it porous, and the mesh prevents its entry into the seepage chamber. The seepage chamber drain water from the main channel through the sand bed uniformly in the form of downward seepage. The required flow depth is achieved with the help of the control valve and the tailgate. A tailgate installed at the downstream end of the flume can be adjusted manually. The water from the flume flows out into a collecting tank and passes over the rectangular notch at the end of the flume. From the notch, the water falls into the canal or trench that is connected to the underground sump and recirculation continued.

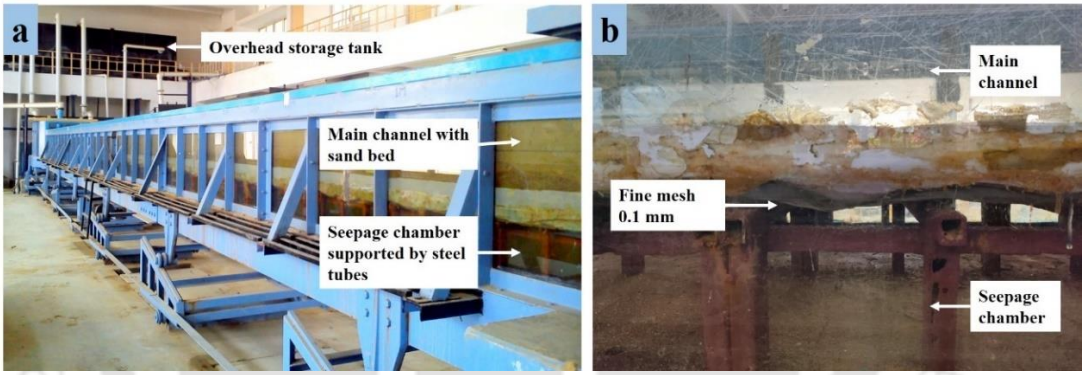

Figure 2.2 Photograph of the experimental flume (side view).

2.2.2 Bed Material

River sand was used for the experiments having 1.1 mm median particle diameter (D_{50}). The particle size distribution of the sand was uniform (Figure 2.3). The uniformity of the sand can be determined when the geometric standard deviation is less than 1.4 (Marsh et al. 2004). The geometric standard deviation was calculated as

$$\sigma_g = \frac{D_{84} - D_{16}}{D_{50}} \tag{2.1}$$

where, $D_{84}(D_{16})$ are defined as the size of grain for which 84% (16%) of the sample are finer by weight. The dry angle of repose of the sand was 31.1°. From Shield's criterion, the

critical bed shear stress (τ_c) and critical shear velocity $\left(u_{*c} = \sqrt{\tau_c/\rho}\right)$ was calculated as 0.686 N/m^2 and 0.0262 m/s, where ρ is the density of water.

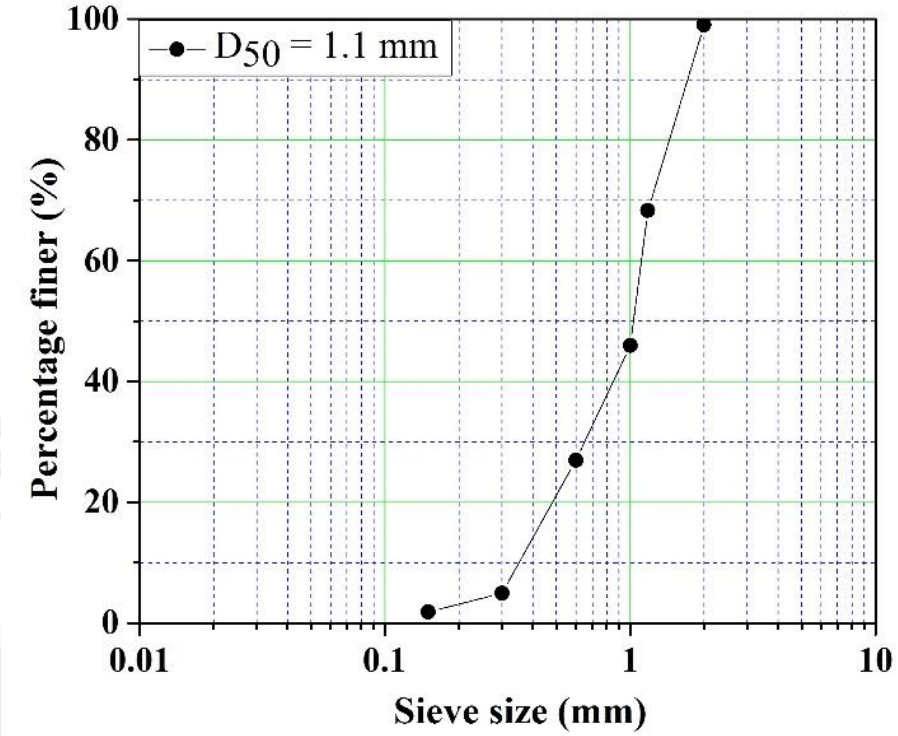

Figure 2.3 Grain size distribution of sediment.

2.2.3 Open Channel Discharge Measurement

The main channel discharge (Q) was measured over a rectangular notch located at the end of the downstream collecting tank (Figure 2.4). The water pass through wooden baffles to give a smooth flow over the notch. The width of the notch (L_n) was 0.5 m. The coefficient of discharge (C_d) was found to be 0.82 for the rectangular notch. The flow discharge for the experiments was calculated as

$$Q = \frac{2}{3} C_d \sqrt{2g} L_n H^{\frac{3}{2}} \tag{2.2}$$

where g is the acceleration due to gravity, and H is the water head over the notch.

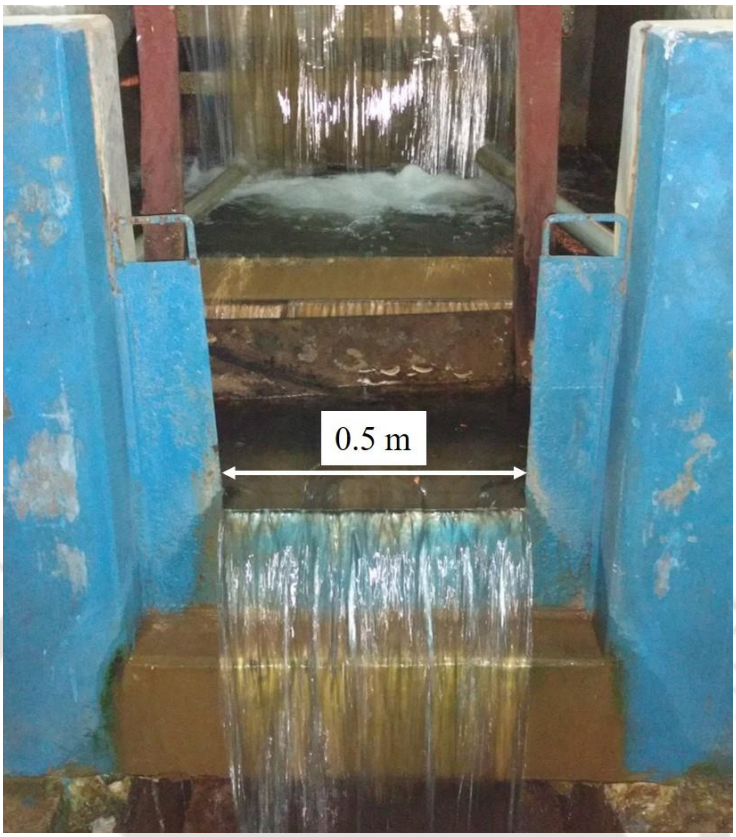

Figure 2.4 Rectangular notch for discharge measurement.

2.2.4 Seepage Discharge Measurement

The seepage discharge (Q_s) from the seepage chamber was measured by two electromagnetic flowmeters. The flowmeters are connected to the seepage chamber through a supply pipe. The operation of the flowmeter is based upon Faraday's Law. According to Faraday's Law, the voltage induced across any conductor when it moves at right angles through a magnetic field is proportional to the velocity of that conductor. To apply Faraday's Law, the fluid being measured must be electrically conductive.

$$E = f(u_c, B_s, D) \tag{2.3}$$

where, E is the voltage generated in a conductor, u_c is the velocity of the conductor, B_s is the strength of the magnetic field, and D is the length of the conductor (in this case is the distance between the electrodes). Faraday's Law indicates that the signal voltage (E) is dependent on the average liquid velocity (u_c), the magnetic field strength (B_s) and the length of the conductor (D). An electromagnetic field is generated in the whole cross-

section of the flow pipe to measure the flow discharge. If the magnetic field is considered as the measuring element of the magnetic flow meter, in that case, it can be seen that the measuring element is exposed to the hydraulic conditions throughout the entire cross-section of the flowmeter. The seepage discharge Q_s can be calculated using the following relationship:

$$Q_s = A_p u_c \tag{2.4}$$

where, Q_s is the seepage discharge (m^3/s), A_p is the area of the pipe (m^2), and u_c is the fluid velocity passing through the flow meter (m/s).

The seepage velocity (V_s) applied over the sand bed of seepage length L can be evaluated as:

$$V_s = \frac{Q_s}{PL} \tag{2.5}$$

where, P is the perimeter of the channel over which seepage is active.

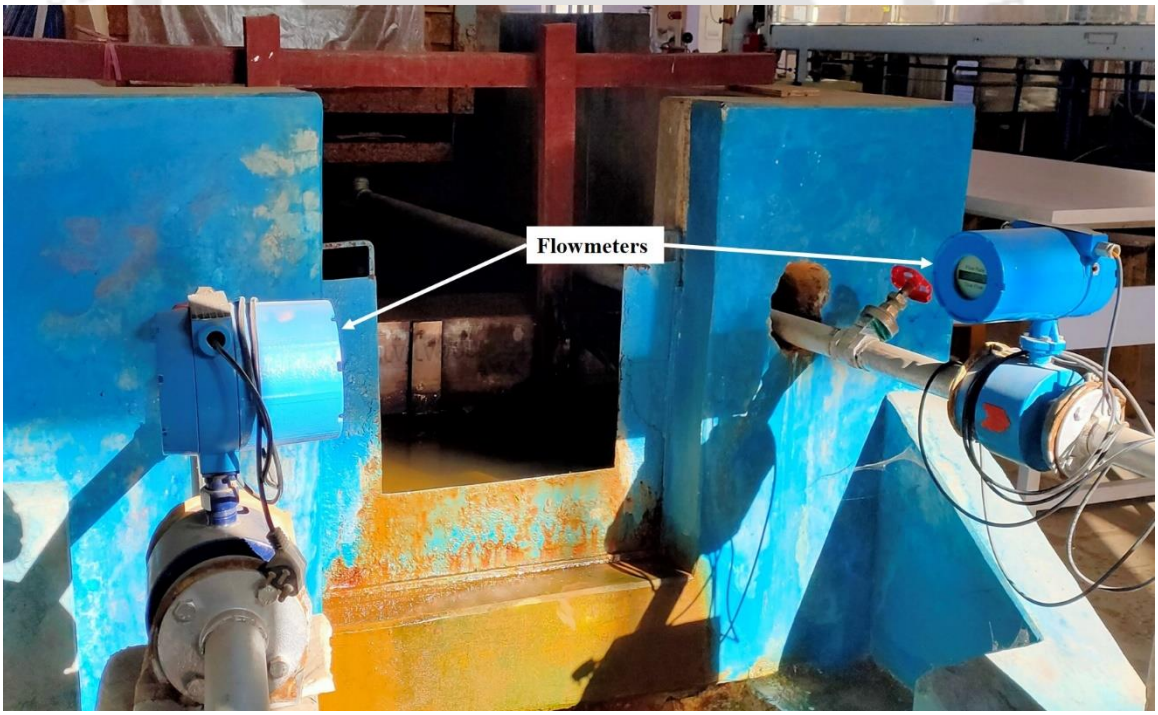

Figure 2.5 Flowmeters to measure seepage discharge.

2.2.5 Flow Depth and Bed Level Measurement

A digital point gauge was used to measure the flow depth with reference to the bed level (Figure 2.6). The point gauge has a liquid crystal display (LCD) with least count 0.01 mm. The instrument can be preset to zero initially at the channel bed before starting the experiments. It can traverse along the longitudinal (along flume length) and transverse (along flume width) directions with the help of a movable trolley. The digital point gauge was also used to record the bed deformation at the end of the experiment by draining the water.

Figure 2.6 Digital point gauge.

2.2.6 Velocity Measurement

Instantaneous three-dimensional flow velocities were measured using Nortek® (Nortek AS, Norway) Vectrino+ Acoustic Doppler Velocimeter (ADV). The velocimeter uses the Doppler shift principle for the measurement of velocity. The Doppler effect is the apparent change in the frequency of a wave caused by relative motion between the source of the wave and the observer. The Vectrino+ has one transmitter and four beam receivers (Figure 2.7). The transmitter is at the center, and it emits short pairs of sound waves, listens to their

echoes, and finally measures the change in frequency of the returned sound. The particles suspended in water (suspended sediment) have the same average speed as the water reflect the transmitted waves, and the four receivers record the returned waves. The velocimeter used in the laboratory is a fixed stem down-looking probe. The Vectrino measures the flow velocity in different beam directions (X-direction, Y-direction, and Z-direction), which are then combined geometrically to obtain the three orthogonal components of velocity. The x-direction is indicated with a red rubber band and should always be in the flow direction. Proper alignment of the beam should be ensured during data collection. The instrument collects the signals in a remote cylindrical sampling volume (6 mm Ø) of user-selectable height located 50 mm away from the central transmitter. The velocimeter transmits an acoustic frequency of 10MHz, and it allows a sampling rate up to a maximum frequency of 200 Hz. The probe has a temperature sensor with a range of -4° to 32°C, with an accuracy of ±0.1°C.

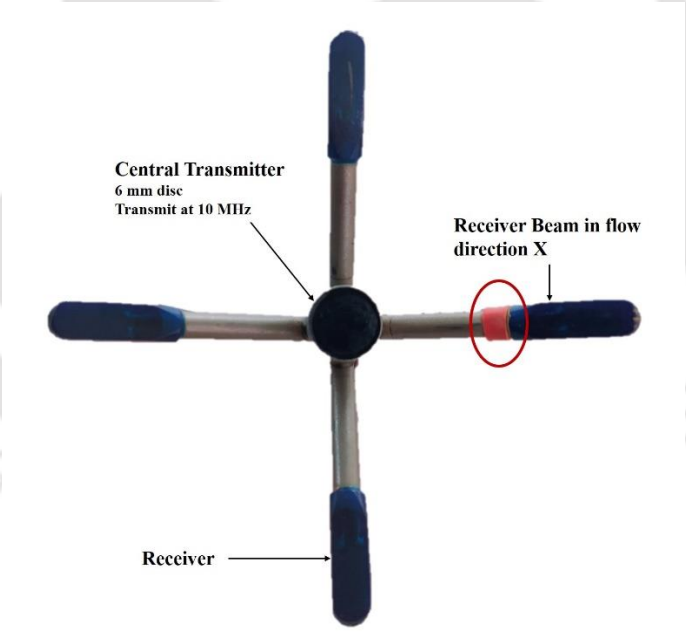

Figure 2.7 Nortek® Vectrino+ velocimeter transmitter and receivers.

The velocity measurement taken at a particular point provides the instantaneous velocities u, v, and w in the streamwise (X), transverse (Y), and vertical (Z) directions, respectively. The instantaneous velocities $(u, v, \text{and } w)$ can be resolved into time-averaged velocities $(\overline{u}, \overline{v}, \text{and } \overline{w})$ and fluctuating components of velocities $(u', v' \text{and } w')$ as $u = \overline{u} + u'$, $v =$

$\overline{v} + v'$, and $w = \overline{w} + w'$, respectively. The velocity signals are collected in a computer system using Vectrino plus software developed by Nortek®. The software records the signal-to-noise ratio (SNR) in decibels (dB) and the correlation in percentage (%).

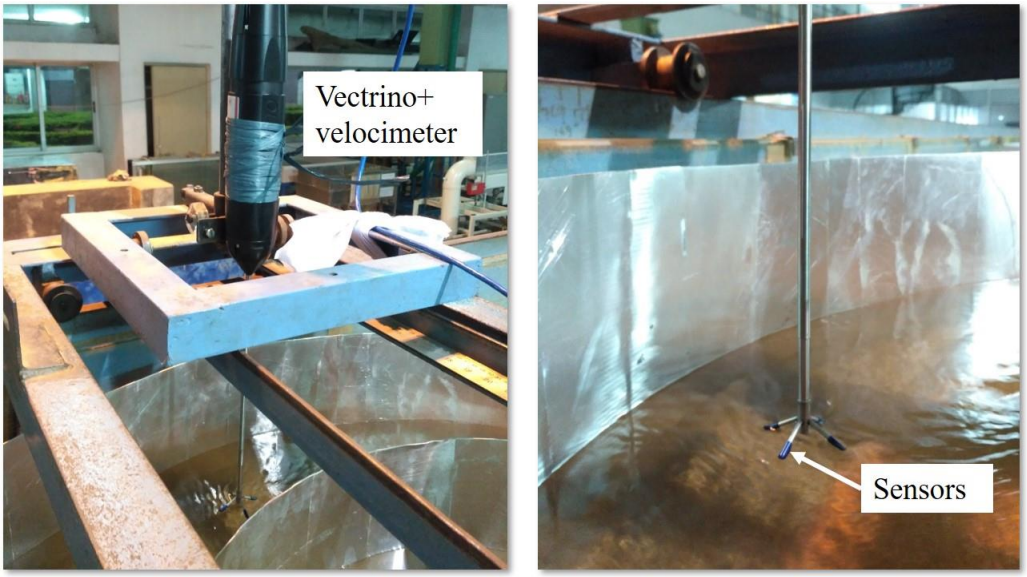

Figure 2.8 Nortek® Vectrino+ velocimeter for velocity measurement.

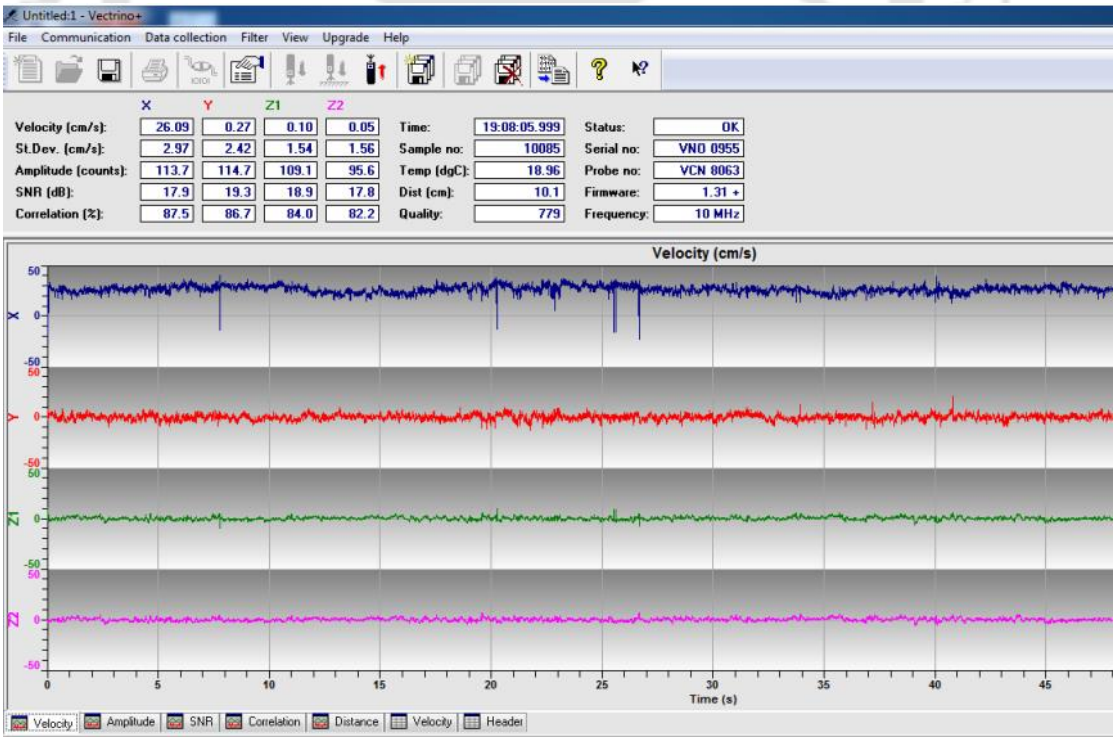

Figure 2.9 Nortek® Vectrino+ software recoding velocity data.

To determine the uncertainty associated with the velocimeter recordings, 16 pulses of velocity data was measured for 120 s near the channel bed ($z \sim 0.02\ m$), where z is the distance of measurement point from the channel bed (positive in the vertical upward direction). Table 2.1 displays the standard deviation and the uncertainty in percentage where $\overline{u}, \overline{v}$ and $\overline{w}$ are the mean velocities and $\sqrt{\overline{u'u'}}, \sqrt{\overline{v'v'}}$ and $\sqrt{\overline{w'w'}}$ are the root mean square of fluctuating components of velocity.

Table 2.1 Uncertainty of velocimeter data.

	$\overline{u}$ (m/s)	$\overline{v}$ (m/s)	$\overline{w}$ (m/s)	$\sqrt{\overline{u'u'}}$ (m/s)	$\sqrt{\overline{v'v'}}$ (m/s)	$\sqrt{\overline{w'w'}}$ (m/s)
Standard deviation	0.00074	0.00013	2.9×10^{-6}	8.7×10^{-6}	1.6×10^{-5}	1.5×10^{-5}
Uncertainty (%)	0.269	0.276	0.046	0.011	0.013	0.049

2.2.7 Ultrasonic Ranging System (URS)

A Seatek® made Ultrasonic Ranging System was used to measure the bed elevation time series in the laboratory flume. It has an accuracy of ±0.2 mm. The URS composed of six transducers, each of 20 mm diameter. They were mounted on a fixed plate, and placed on a trolley (Figure 2.10). The transducers can be placed at any location inside the flume to record the bed elevations. The transducers transmit 5MHz ultrasonic pulses and are placed such that it just touches the water surface. The pulses travel through water and reflect from the bed surface. The transducers act as both the transmitter and the receiver. The reflected signal travels back to the same transducer. The time lag between the transmitted pulse and the received signal gives the distance to the bed surface.

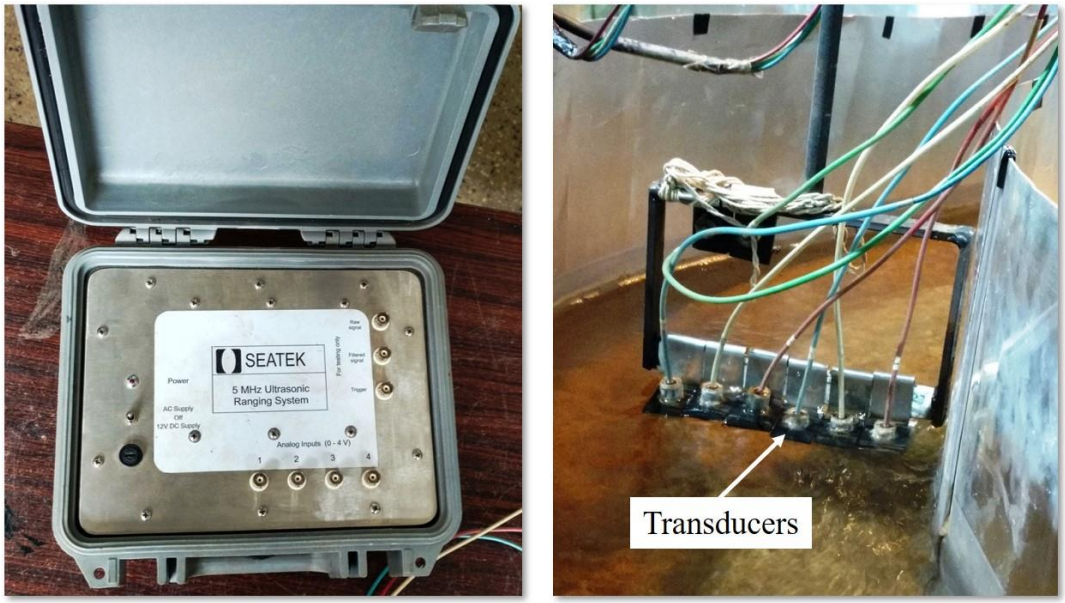

Figure 2.10 Seatek® Ultrasonic Ranging System.

2.2.8 Bed Preparation

The experimental procedure starts with the preparation of a plain channel bed before the start of every experiment. At 15.2 m length of the channel, the sand was uniformly laid above the fine mesh. The plain bed was prepared with a cutter attached to a trolley (Figure 2.11). The sand bed thickness was 25 cm above the channel bottom. The sand bed was levelled gradually starting from the downstream end of the channel. The excess sand was carefully removed from the channel. Hereafter, the sinuous channel was constructed with the help of stencils and a wooden shaper. At the end of the experiments, the water was drained out of the channel. The exposed channel bed was allowed to dry naturally, and later, the top layer of the sand bed was disturbed using trowels before the preparation of the plain bed for the next experiment.

Figure 2.11 Levelled sand bed preparation with metal cutter.

2.2.9 Preparation of Sinuous Channel

The sinuous channels were prepared with the help of a wooden shaper and stencils. The sinuous bend is symmetrical on either side of the bend axis and comprised of three wavelengths.

$$\sigma = \frac{1}{J_o(\theta_o)}\left(= \frac{L_a}{\lambda_m}\right) \tag{2.6}$$

$$\lambda_m \approx 2\pi b \tag{2.7}$$

The deflection angle specifies the shape of a sine curve channel (θ_o) at the point of inflection, therefore the sinuosity of the channel (σ) can be determined by the Bessel function of the first kind and zeroth order $(J_o(\theta_o))$ of θ_o as suggested by Yalin (1992). Equation (2.6) estimates the sinuosity, where λ_m is the wavelength of the sinuous channel. In accordance with the conditions present in natural streams, the width of the channel (b) was related to the wavelength of the sine channel (λ_m) as given in Equation 2.7 [Yalin, 1977; Yalin and da Silva, 2001]. The wavelength of the sinuous channel was determined as given in Equation (2.7).

Figure 2.12 Preparation of the sinuous channel in the flume with wooden shaper and stencil.

The width of the flume was a limitation in the preparation of high curvature sinuous channel. Three different sinuous channels, rigid rectangular, mobile rectangular and mobile trapezoidal were prepared in the flume to conduct the experiments. The channel geometry was designed so that it is maximum for the given width of the flume (1 m). Figure 2.12 shows the preparation of the mobile boundary trapezoidal channel. The channel was carved carefully along the length of the channel with the help of stencils. The cutter was moved slowly in between the stencils, and the excess sand was removed to move ahead.

2.2.10 Criteria for Seepage Velocity

The seepage effects on the hydrodynamics and morphology are significant. The interaction of surface water – ground water in the real field reports the varying range of seepage found

in alluvial channels (Langhoff et al., 2006; Rosenberry and Pitlick, 2009; Kinzli et al., 2010; Hatch et al., 2010). Section 1.5 suggest seepage percentage in alluvial channels vary in the range of 0.3% to 50% of the main channel discharge depending upon field conditions. Hatch et al. (2010) found seepage loss in the field to range from 0.1 to 0.3 m^3/s when the channel discharge was ≤ 2 m^3/s, i.e., 5% to 15% of the channel discharge. Quantification of seepage in the field has led to the advancement of seepage application in the laboratory. Seepage is a natural phenomenon and therefore the interest of its application in the laboratory has increased remarkably, primarily to understand the fluvial processes. The seepage in the field is heterogeneous and studies were performed on a large scale. Scaled model cannot be used in the experiment because of field specific conditions. Experimental studies were performed to show the influence of seepage effects, considering wide range of seepage velocities. Dey et al. (2011) suggested that the magnitude of seepage velocity can be taken as 1% or less of the average streamflow velocity. The seepage velocities ranged from 0.0 – 0.88 mm/s (Richardson et al. 1985), 0.55 – 1.5 mm/s (Faruque and Balachandar, 2011), 0.4 – 7.3 mm/s (Cao and Chiew, 2014), and 0 – 3.14 mm/s (Liu and Chiew, 2012). Patel and Kumar (2017) conducted experiments to investigate the effect of downward seepage on the turbulence in a straight parabolic channel with a seepage velocity of 0.2 mm/s. Following the range of seepage velocities found in the literature, the downward seepage velocity in the present work was in the range of 0.05 – 0.3 mm/s (Table 2.2).

2.3 Experimental Program

The experimental program starts from the construction of the sinuous channel. On the prepared plain sand bed, the designed sinuous channel was carefully made. For the smooth entry and exit of the flow, guide vanes were provided at the upstream and downstream end of the sinuous channel. The experiments were conducted in three sinuous channels: a) Rectangular cross-section with rigid banks and movable bed, b) Rectangular cross-section with mobile banks and bed, and c) Trapezoidal cross-section with mobile banks and bed. The rectangular sinuous channel with rigid banks was designed with length 5.64 m, breadth 0.3 m, and height 0.2 m. The sinuosity of the channel was 1.25. The straight approach channel length at the upstream and downstream was 6.6 m and 5 m, respectively. The

mobile rectangular sinuous channel was designed with length 5.64 m, width 0.3 m, depth 0.12 m, and sinuosity 1.25 (Figure 2.13). The mobile trapezoidal sinuous channel was designed with length 5.64 m, top width 0.5 m, bottom width 0.1 m, height 0.14 m, side slope angle 35°, and sinuosity 1.1 (Figure 2.14).

The flow in a rectangular sinuous channel with rigid banks (Case I) was investigated to focus our understanding on the turbulence structure and the morphology. The flow depth was kept sufficiently high along with adequate inflow discharge for Case I in order to explore the morphological changes throughout the sinuous bend and the turbulence in the sinuous channel.

The near-bed flow and its interaction with the sediment bed was investigated in a rectangular sinuous channel with rigid banks (Case II). Here, the inflow discharge was kept low, as with high flow rate the channel bed would make large modifications which would hinder the near-bed velocity recordings. Also, the rigid banks helped the channel to maintain its sinuosity to assist the near-bed velocity readings throughout the channel.

To study the effect of downward seepage on the hydro-morphological alterations in a mobile boundary channel, experiments were conducted in two different cross-sections, rectangular mobile boundary sinuous channel (Case III) and trapezoidal mobile boundary sinuous channel (Case IV). The trapezoidal channel and the rectangular channel were chosen to examine the bankline changes. The planform of the rigid and the mobile rectangular channel is similar except for the channel depth.

The experimental information of all the cases is presented in Table 2.2. Experiments were conducted at different flow discharges both for without seepage and with seepage condition.

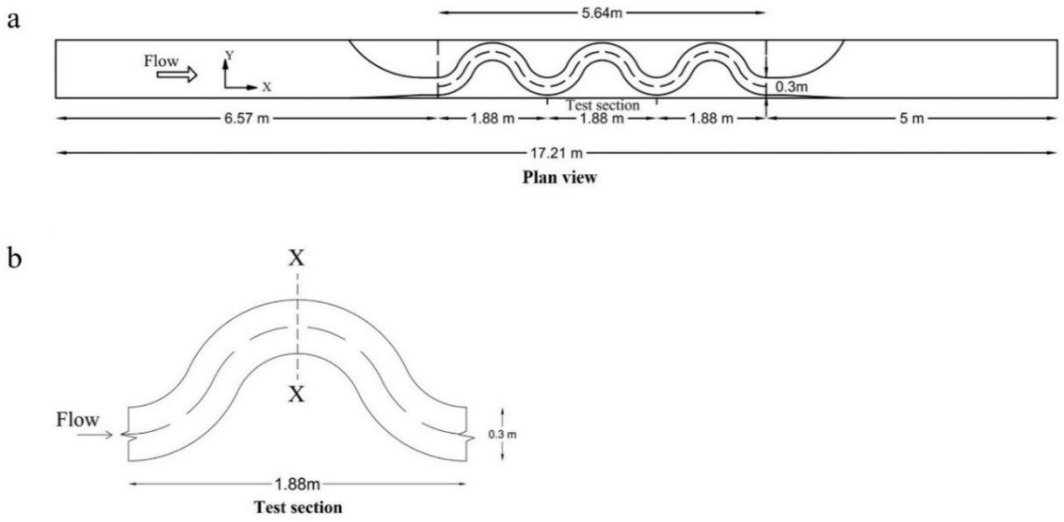

Figure 2.13 Diagram showing the (a) Plan view of the rectangular sinuous channel, and (b) Plan view of the test section.

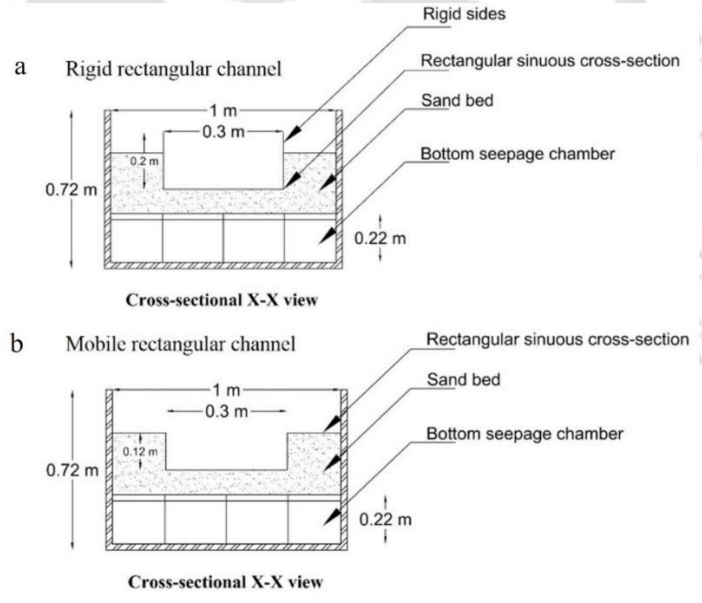

Figure 2.14 Diagram showing the (a) Cross-sectional view of the rigid rectangular channel, and (b) Cross-sectional view of the mobile rectangular channel.

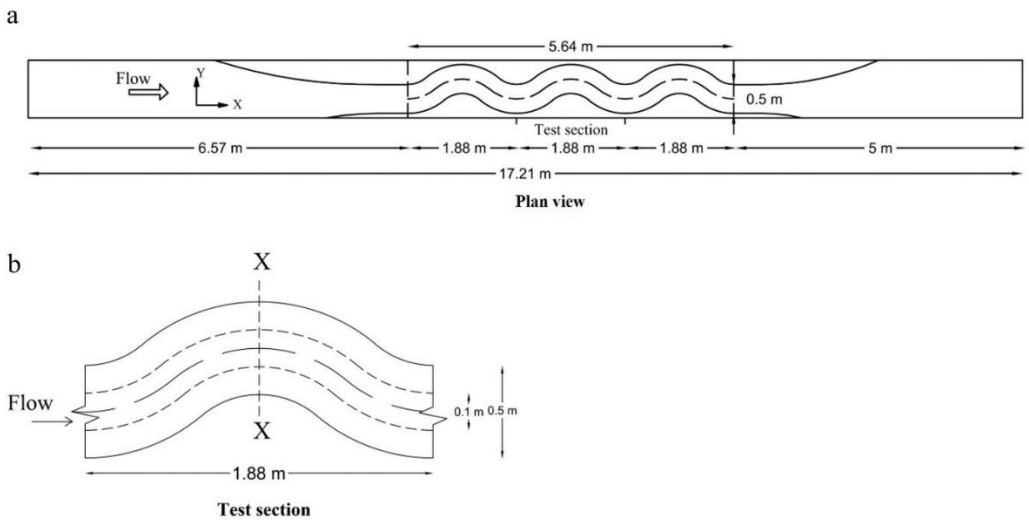

Figure 2.15 Diagram showing the (a) Plan view of the mobile trapezoidal sinuous channel, and (b) Plan view of the test section.

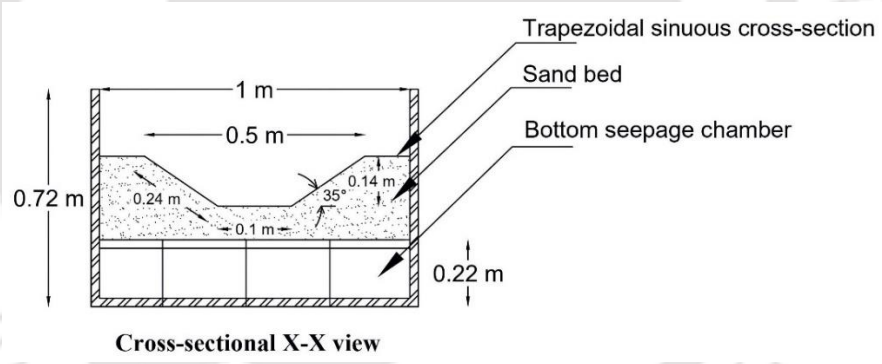

Figure 2.16 Diagram showing the cross-sectional view of the mobile trapezoidal channel.

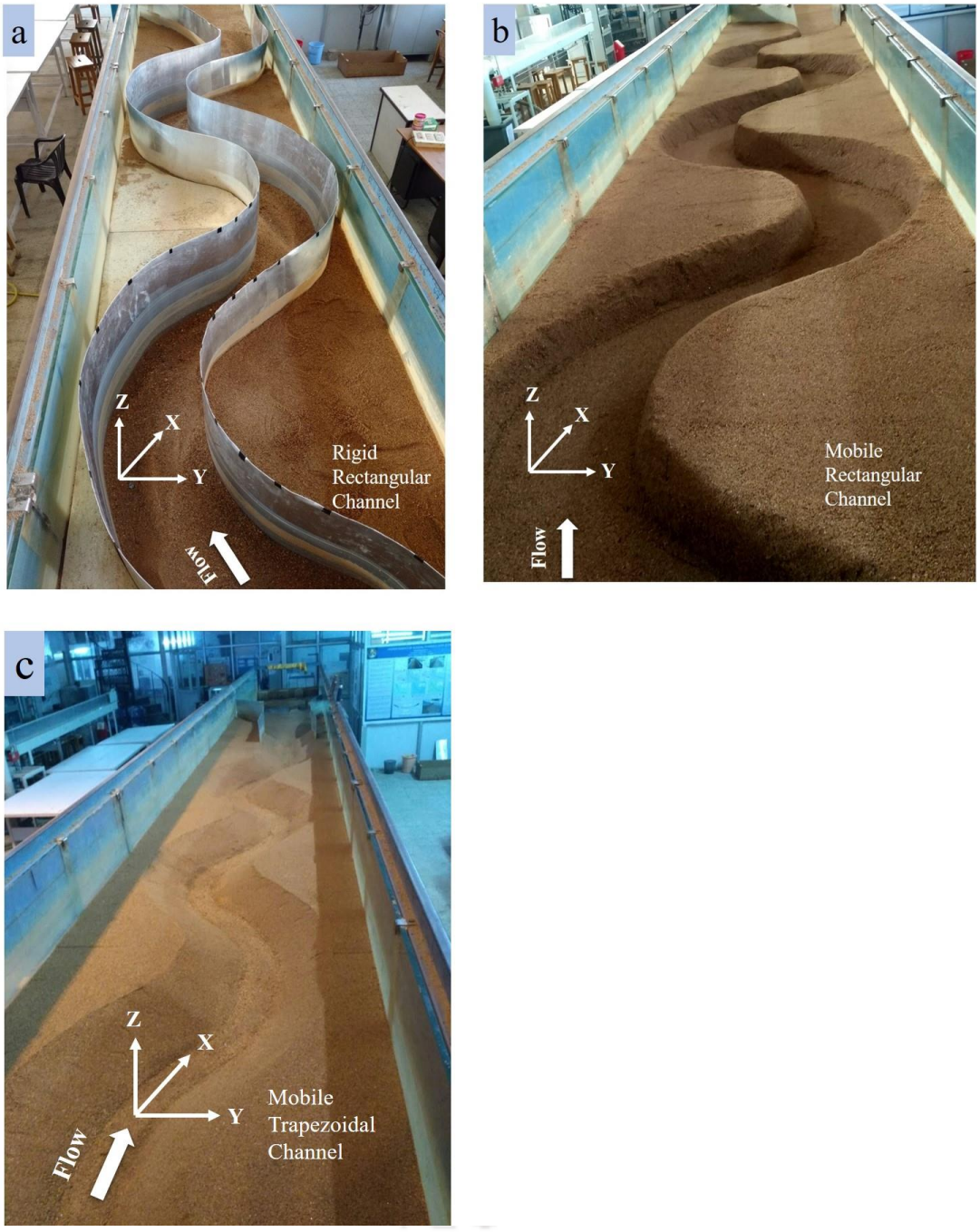

Figure 2.17 Pictures of different cases of sinuous channel (a) Rigid rectangular sinuous channel, (b) Mobile rectangular sinuous channel, and (c) Mobile trapezoidal sinuous channel.

Table 2.2 Experimental information of all the cases.

Channel	Inflow Discharge, $Q(\mathbf{m^3/s})$	Seepage condition	Average flow depth (m)	Froude number, Fr	Reynolds number, Re	Seepage velocity, $V_S(\mathbf{mm/s})$
Rigid Rectangular (Case I)	0.0156	No seepage	0.117	0.41	32116	-
		With seepage	0.117	0.41	32116	0.3
	0.0135	No seepage	0.108	0.40	29251	-
		With seepage	0.108	0.40	29251	0.3
Rigid Rectangular (Case II)	0.00968	No seepage	0.107	0.29	21134	-
		With seepage	0.107	0.29	21134	0.05 and 0.1
	0.00793	No seepage	0.107	0.24	17495	-
		With seepage	0.107	0.24	17495	0.05 and 0.1
	0.00629	No seepage	0.107	0.20	13716	-
		With seepage	0.107	0.20	13716	0.05 and 0.1
Mobile Rectangular (Case III)	0.00793	No seepage	0.104	0.25	17489	-
		With seepage	0.101	0.26	17747	0.16
	0.00629	No seepage	0.102	0.20	13978	-
		With seepage	0.100	0.21	14130	0.12
Mobile Trapezoidal (Case IV)	0.00793	No seepage	0.114	0.32	17831	-
		With seepage	0.107	0.37	18921	0.17
	0.00629	No seepage	0.109	0.28	14635	-
		With seepage	0.099	0.33	15866	0.14

3

Turbulent Flow Behavior in a Sinuous Channel with and without Downward Seepage

3.1 Introduction

The structure of turbulence in a sinuous channel with different cross-sections and boundary conditions are discussed in this chapter based on the experimental results obtained. In this study, four experimental cases were analyzed: Case I, the flow characteristics in a rigid rectangular sinuous channel, Case II, the near-bed flow characteristics in a rigid rectangular sinuous channel, Case III, the flow characteristics in a mobile rectangular sinuous channel, and Case IV, the flow characteristics in a mobile trapezoidal sinuous channel.

The nature of turbulent flow characteristics of a sinuous river varies from that of straight channels. The study of turbulence in a sinuous channel is a complex topic as compared to a straight channel. The flow is three-dimensional, and the flow characteristics across the sinuous bend would provide a complete knowledge of the hydraulic processes associated at the banks of the sinuous channel. Due to the curvature in the channel, the inner and outer bank has different flow characteristics. Investigation of the flow in the bend is important in association with the stability of banks, water intakes, navigation, and sediment transport processes. Turbulence studies in a sinuous channel have been discussed quite elaborately over the past 2-3 decades. Researchers like Rozovskii (1957), Anwar (1986), de Vriend and Geldof (1983), Blanckaert and Graf (2001), Booij (2003), Sukhodolov and Kaschtschejewa (2010), and Engel and Rhoads (2017) have studied the turbulent characteristics both in the field and in the laboratory and forwarded theories and articles regarding the uniqueness of flow behavior. A conceptual sketch of the flow processes in sinuous or meander bends is shown in Figure 3.1.

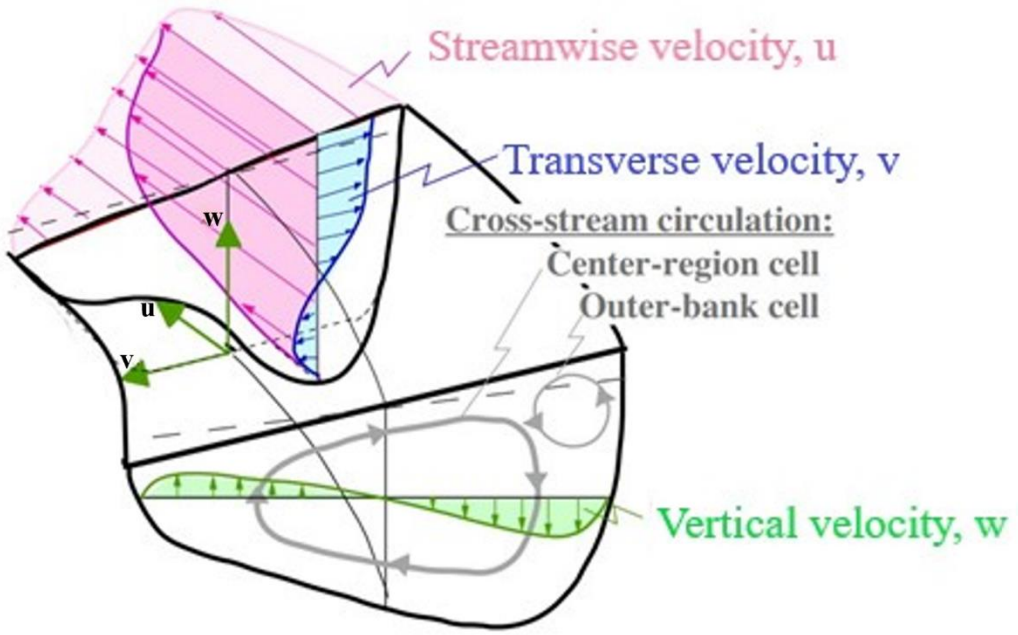

Figure 3.1 Flow in open channel bend (Courtesy: Blanckaert, 2002b).

The flow in bends comprises two components, primary flow (in the direction of flow) and secondary flow (transverse to the flow direction). Flow in curved open channel is characterized by the existence of cross-stream circulation cells (secondary flow). This secondary flow induces a transverse component of the bed shear stress, which conditions the development of a transverse bed slope with increasing flow depth in outward direction (Olesen, 1985; Camporeale et al., 2007). The classical helical motion called the center-region cell covers a large part of the cross-section (Figure 3.1). The center region cell is usually explained in terms of the local imbalance between the driving centrifugal force and the transverse pressure gradient (e.g., Rozovskii, 1957). In addition to the center-region cell, an outer bank counter-rotating cell (Figure 3.1) is found to occur in the region near the outer bank, which play an important role with respect to the stability of the outer bank and the adjacent bed (Bathurst et al., 1979; Blanckaert and Graf, 2004). Blanckaert and Graf (2001) investigated the secondary cells experimentally in a sharp narrow open channel bends with an aspect ratio 3.6. They mentioned that in the outer bank region, both the centrifugal force and the cross-stream turbulent stresses contribute to the generation of the outer-bank cell. Outer bank cells are observed in laboratory flows (Einstein and Harder,

1954; Rozovskii, 1957) as well as in natural flows (Dietrich and Smith, 1983; de Vriend and Geldof, 1983). Besides, the number of secondary flow cells and their shape depend mainly on the aspect ratio [width (b)/depth (h)] (Patnaik et al., 2014). Schumm (1963) proposed that sinuous channels signify a low aspect ratio. With a small aspect ratio $(b/h = 2.8)$, Esfahani and Keshavarzi (2011) studied the flow in the meander channel, where they observed the radial or transverse motion of sediment particles across the bend. The distribution of Reynolds shear stress (RSS) reveals the circular or helical flow in the bends. The Reynolds shear stress distribution in sinuous or meandering river diverts from the usual Reynolds shear stress as found in straight channels. The high stresses at the outer bend and low stresses at the inner bend can be linked with this radial motion of the sediment. The stresses at the banks of the channel highlights the high momentum flux at the outer zone of the bend where erosion is predominant.

The vertical distribution of the velocity measured in bends was reported as non-logarithmic in its distribution (Graf and Blanckaert, 2002; Sukhodolov and Kaschtschejewa, 2010). In most cases, the velocity at the outer bend is more than the inner bend, but this does not hold for all cases. In a sinuous river, the maximum velocity does not occur at a fixed location along the channel cross-section due to the centrifugal acceleration (Henderson, 1966; Furbish, 1988; Esfahani and Keshavarzi 2010). de Vriend and Geldof (1983) studied the flow velocity in a sharp curved short bend and found a tendency for movement of maximum velocity towards the inner bend when the flow stage is higher. In the inner flow region, the velocity is maximum, as reported by several authors (Dietrich et al., 1979; Esfahani and Keshavarzi, 2011; McKeogh and Kiely, 1989; de Vriend and Geldof, 1983). Keshavarzi et al. (2016) found scouring along the inner bank of the meander where maximum streamwise velocity also prevails. Turbulent flows are chaotic and are defined as complex multi-scale flows that needs to be classified into more elementary components, referred to turbulent structures or coherent structures. To acknowledge the coherent structures in turbulent flows, one need to deal with the shapes and the vorticity of the structures. In turbulent shear flow, the flow near the boundary is basically characterized by the sequence of events, commonly called burst-sweep cycle. Sweeps are inrushes of high-speed fluid moving towards the boundary and the bursts are violent ejections of low-speed fluid moving away from the boundary. Kline et al. (1967) first introduced the two-

dimensional bursting process (quadrant analysis) to examine the momentum transfer in the boundary layer. The sweep and ejection events contribute more towards the erosion and deposition process reported by Nezu (1993) and Thorne et al. (1989). Analyzing the turbulent bursting phenomenon in two-dimensional flow, the contribution of velocity fluctuations mainly in the direction of streamwise and vertical can be related to the production of Reynolds shear stress. Researchers (Keshavarzy and Ball, 1997; Nakagawa and Nezu, 1978; Nezu, 1993) have incorporated the bursting events to define the sediment transport in their studies. In model studies, incorporating the study of the bursting process was found beneficial to examine the sediment transport in turbulent flow (Yen, 2002). Keshavarzi and Shirvani (2002) found the Markov process effective in defining the bursting events. Keshavarzi and Gheisi (2006) introduced a new method of bursting process, where all the three-dimensional fluctuating velocities are considered. They studied the bursting phenomenon in a vortex chamber and found that the sweep events are responsible for sediment transport. Liu and Bai (2013) adopted the three-dimensional octant analysis to inspect the bursting events in a multi-bend channel. They found the ejection and sweep event dominating in the bend and the exit section.

The existing literature on seepage analysis is mainly focused on straight river channels (Chen and Chiew, 2004; Maclean, 1991a; Oldenziel and Brink, 1974; Sreenivasulu et al., 2011). The study of seepage is extensively studied in various aspects of fluvial hydraulics. Some of the previous studies include the stability of hydraulic structures due to seepage (Chavan et al., 2019; Qi et al., 2013), the effect of seepage flow around pipelines (Li et al., 2019; Liang et al., 2005), pollutant mobility with seepage (Jones and Mulholland, 1999; Sharma et al., 2020), reduction in conveyance efficiency in irrigation channels (Shukla and Mishra, 1994) and increase in sediment transport (Deshpande and Kumar, 2016). Sreenivasulu et al. (2011) stated that the flow turbulence is affected by the seepage flow. For downward seepage, researchers have observed increased bed shear stress (Deshpande and Kumar, 2016) and increased near-bed velocity (Chen and Chiew, 2004; Maclean, 1991a). The seepage affecting the near-bed turbulent flow is significant in the study of the particle motion. Rao and Sreenivasulu (2009) proposed that downward seepage increases sediment transport and reduces bed stability. Presence of downward seepage can alter the turbulent flow characteristics in a sinuous channel and consequently affect the erosion and

deposition pattern. Potential activity of downward seepage is still unexplored in hydraulics, and there is a need to address as the flow in alluvial channel experience the seepage phenomenon through their porous boundaries. This study emphasizes the seepage phenomena in sinuous channels. Sinuous channels are prone to flow acceleration and deceleration, therefore the need to understand the channel hydrodynamics and alluvial boundary interaction between the channel and the sub-surface flow holds importance. The effect of downward seepage on the flow turbulence in a sinuous channel has not been explored in previous studies. The results are discussed in the following section.

3.2 Effect of Downward Seepage on the Flow Turbulence in a Rigid Rectangular Sinuous Channel

3.2.1 Experimental Conditions and Data Recording

In this study, experimental investigation in a sinuous channel was analyzed under two conditions: (1) without seepage and (2) with downward seepage. The channel was rectangular in cross-section with rigid non-erodible banks, and the channel bed consisted of movable uniform sand. The experimental run was conducted at a high Reynolds number ($> 10\,000$) and low Froude number (< 1). The high Reynolds number denotes the turbulent nature of the flow. The flow in the channel was in the subcritical condition ($Fr < 1$).

Table 3.1 Hydraulic parameters of the experiment in the rigid rectangular sinuous channel.

Channel Condition	**Inflow Discharge, $Q(\mathrm{m^3/s})$**	**Average flow depth (m)**	**Froude number, Fr**	**Reynolds number, Re**	**Seepage velocity, $V_S(\mathrm{mm/s})$**
No seepage	0.0156	0.117	0.41	32116	–
With seepage	0.0156	0.117	0.41	32116	0.3

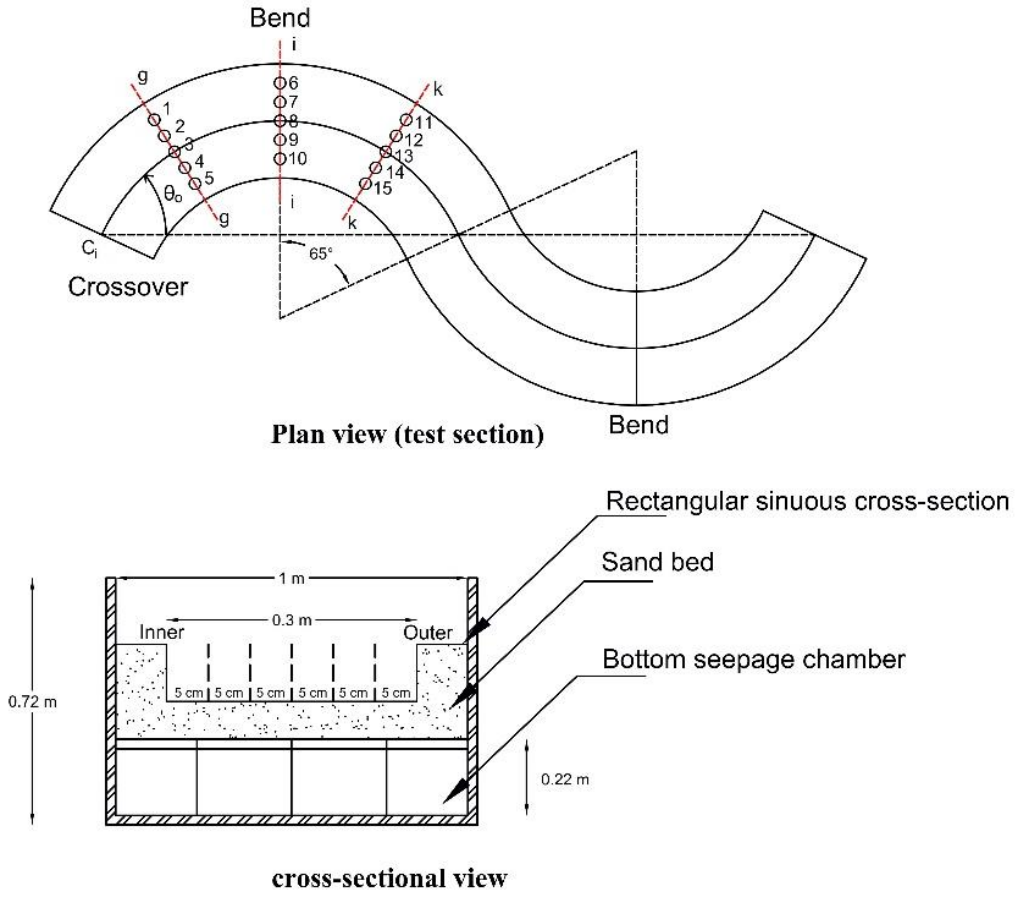

Figure 3.2 Velocity data recording locations within the rigid rectangular sinuous channel.

The hydraulic conditions of the experiments are presented in Table 3.1. At first, no seepage experiments were performed. The experiments with downward seepage were then conducted with the same flow condition as the no seepage condition. With seepage application, the main channel discharge (Q) decreased by an amount equal to the seepage discharge (Q_s), while the flow depth also decreased. However, after the seepage application, the flow depth was restored equal to the no seepage condition using the tailgate at the end of the flume so that the hydrodynamics of no seepage and seepage conditions can be comparatively studied.

The three-dimensional instantaneous flow velocity was recorded at three cross-sections of the bend (Figure 3.2). Each section has five vertical locations to capture the flow characteristics thoroughly. Section $g - g$ (location 1 to 5) is at bend upstream, section $i - i$ (location 6 to 10) is at bend apex, and section $k - k$ (location 11 to 15) is at bend

downstream. The flow in the channel was recorded after the channel achieved the desired flow depth and discharge and when quasi-equilibrium was achieved in the channel.

3.2.2 Data Filtering

In a turbulent energy cascade, transfer of energy occurs within three different range of eddy scales, i.e., firstly from the integral scale (energy containing range of largest eddies), then to the inertial subrange (intermediate scale range) and finally to the Kolmogorov scale (viscous dissipation range of smallest eddies). According to Kolmogorov's hypothesis, the inertial subrange and the dissipation range are isotropic and forms a universal equilibrium range. The energy transfer in the inertial subrange is a function of dissipation rate and the corresponding length scale, while it is independent of viscosity. One of the implications of this hypothesis is that an energy spectrum in the inertial subrange becomes $-5/3$. Therefore, this property was used for filtering the raw velocity data recorded by ADV. Initially, the power spectra for raw velocity data were plotted, which clearly shows that the slope of the spectra deviates from Kolmogorov $-5/3$ law. This indicated the presence of spikes in the velocity data; therefore, careful filtering was essential before analysis.

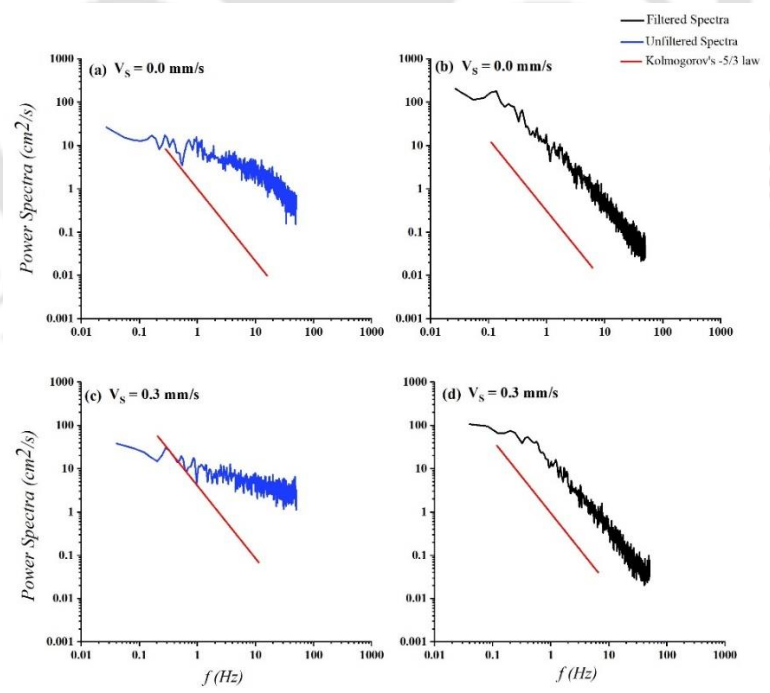

Figure 3.3 Unfiltered and filtered velocity power spectra with Kolmogorov $-5/3$ law for (a, b) no seepage ($V_S = 0.0$ mm/s) and (c, d) with seepage ($V_S = 0.3$ mm/s).

The raw velocity data recorded by ADV may be contaminated with spikes due to signal interference. The spikes were filtered with the help of the acceleration threshold method (Goring and Nikora, 2002). This method was performed by trial and error where the value of acceleration threshold ranges from 1 to 1.5 (Deshpande and Kumar, 2016). Spike removal using the trial and error method was truncated when the slope of the power spectra of the filtered data was $-5/3$ in the inertial subrange, as shown in Figure 3.3. It indicates that the turbulent energy dissipation in the inertial subrange follows the Kolmogorov hypothesis of local isotropy. Thus, further analysis of the velocity data could be conducted from this filtered velocity data.

3.2.3 Mean Streamwise Flow Velocity

The time-averaged streamwise velocity profile is shown in Figure 3.4 at the center of the channel bend. The time-averaged velocities $\overline{u}, \overline{v},$ and $\overline{w}$ in streamwise, transverse, and vertical directions, respectively, were calculated as:

$$\overline{u} = \frac{1}{N}\sum_{i=1}^{N} u_i \tag{3.1}$$

$$\overline{u} = \frac{1}{N}\sum_{i=1}^{N} v_i \tag{3.2}$$

$$\overline{w} = \frac{1}{N}\sum_{i=1}^{N} w_i \tag{3.3}$$

where, N is the total sample number. The time-averaged velocity $(\overline{u})$ was plotted along with the normalized flow depth (z/h).

The figure shows non-logarithmic profiles measured at the center of the bend width. Close observation report that with seepage, the velocities increased near the channel bed. The shift in velocity increased due to seepage results in more sediment transport near the bed. With downward seepage, the flow near the channel bed undergoes disturbance with which the velocity shifts from the original. The streamwise mean velocity at the centerline was found to increase by 20% to 40% at average near the channel bed.

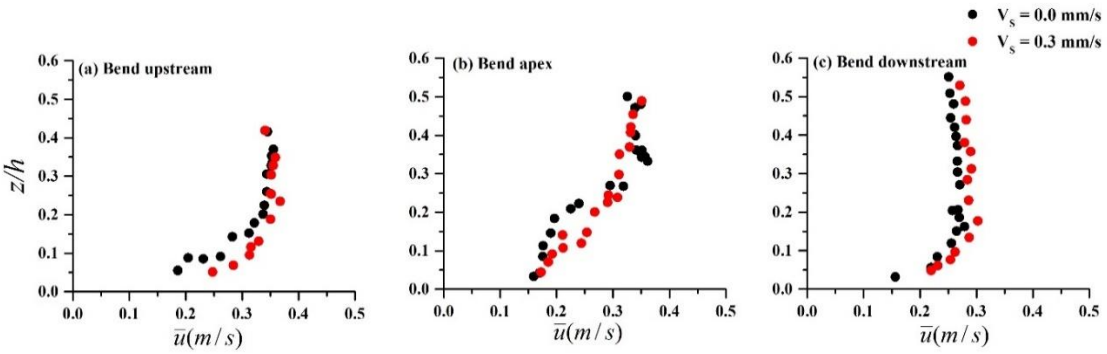

Figure 3.4 Time-averaged velocity distribution for no seepage ($V_S = 0.0$ mm/s) and with seepage ($V_s = 0.3$ mm/s) at (a) Bend upstream (location 3), (b) Bend apex (location 8), and (c) Bend downstream (location 13).

3.2.4 Reynolds Shear Stress (RSS)

The Reynolds shear stress in the streamwise direction is calculated as:

$$\tau_{zx} = -\rho\overline{u'w'} \tag{3.4}$$

$$\overline{u'w'} = \frac{1}{N}\sum_{i=1}^{N}(u-\overline{u})(w-\overline{w}) \tag{3.5}$$

τ_{zx} is the Reynolds shear stress in streamwise direction and perpendicular to the plane in vertical direction. In Equations 3.4 and 3.5, ρ is the density of water, and N is the total number of samples. Blanckaert (2002a) showed the representation of Reynolds shear stress in bends. They found that the RSS distribution has revealed circular flow in bends as depicted with positive and negative values. The revelation of discontinuous distribution of RSS may attribute the presence of helical flow in bends. The quantity of RSS can be attributed to the bursting process near the channel bed, as reported by Nezu (1993). The distribution of RSS at the centerline of the bend are plotted against the normalized flow depth as shown in Figure 3.5.

It was observed that the flow reversal exists with negative values in the upper half of the water depth for both no seepage and seepage run. At the upstream and downstream sections of the bend, the change in sign was not so prominent from the distribution of RSS. At all the three sections (g, i and k) of the bend, it was observed that RSS increased near the

channel bed with seepage. However, at the upstream bend, the magnitude of increase is less as compared to the apex and the downstream bend. The distribution of the RSS profile is sporadic at all the three locations. With the flow passing through the bend, the change in seepage magnitude at the upstream and downstream of the bend may be due to local bed features. At the center of the downstream bend, the change in bed level might likely induced high velocity fluctuations.

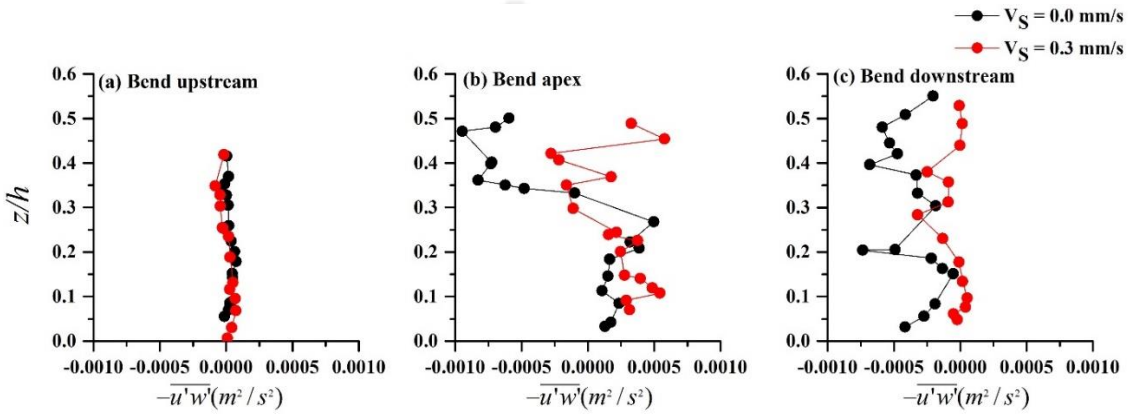

Figure 3.5 Streamwise Reynolds shear stress distribution for no seepage ($V_S = 0.0$ mm/s) and with seepage ($V_S = 0.3$ mm/s) at (a) Bend upstream (location 3), (b) Bend apex (location 8), and (c) Bend downstream (location 13).

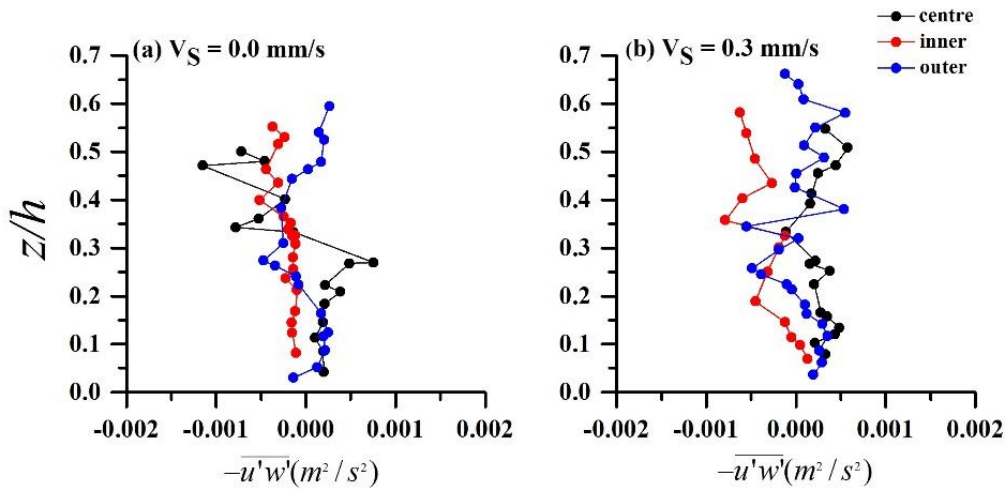

Figure 3.6 Streamwise Reynolds shear stress distribution at the center (location 8), inner (location 10) and outer (location 6) region of the bend section i for seepage velocity (a) $V_S = 0.0$ mm/s, and (b) $V_S = 0.3$ mm/s.

The analysis of RSS provides the momentum flux at three locations of the bend apex (section i): center (location 8), inner (location 10), and outer (location 6). At the outer region of the bend, because of the greater momentum transport results to higher turbulent Reynolds shear stress compared to the inner region (Figure 3.6). The flow in bends erode the sediment in the outer bend (conforming to high stresses) and deposit in the inner bend (conforming to less stresses). For no seepage condition, the RSS distribution in the outer and central part of the flow follows a helical profile with positive values near the channel bed ($z/h < 0.2$) [Figure 3.6(a)]. The intermittent flow distribution relates to the formation of circular flow across the bend. The distribution of RSS can be helpful in understanding the flow circulation in the bend. From the center of the bend towards the outer region, the flow circulation occurs where scouring action is prominent. Therefore, the streamwise RSS distribution is dominant at the outer and central part of the flow. As shown in Figure 3.6(b), the distribution of RSS with downward seepage reveals an increase in RSS near the channel bed. The additional forces induced by the increasing seepage velocity near the channel bed involve enhancement in sediment transport. There is a 20% increase near the channel bed in the outer region for streamwise RSS for seepage flow.

3.2.5 Reynolds Normal Stress (RNS)

The turbulence intensity defines the strength of turbulence in the flow. Figure 3.7 show the vertical distribution of the turbulence intensity in streamwise $\left(\sqrt{\overline{u'u'}}\right)$, transverse $\left(\sqrt{\overline{v'v'}}\right)$ and vertical $\left(\sqrt{\overline{w'w'}}\right)$ directions, respectively. Blanckaert and de Vriend (2005) analyzed the streamwise and vertical turbulence intensity in the outer half of the bend. They found velocity fluctuations to be higher in the mid-depth and top-depth of the water column. In this study, the higher intensity was found at the mid-depth of the flow depth. The higher the fluctuations (intensity), the more is the strength of turbulence. Blanckaert and Graf (2001) found that the streamwise fluctuations contribute more to the total turbulent momentum flux.

Turbulence intensity distribution for seepage flow in comparison with no seepage flow is shown in Figure 3.7. The geometry of the channel bed influenced the magnitude of the turbulence intensity at the bend. From the bend apex towards the bend downstream, the

changes in bed level are maximum which might have induced higher fluctuating velocity in the downstream bend. The intensity in all three directions has increased near the channel bed ($z/h < 0.2$) after the application of downward seepage. The magnitude of turbulence intensity in the streamwise and transverse direction was observed to be dominant in the flow over the vertical turbulence intensity.

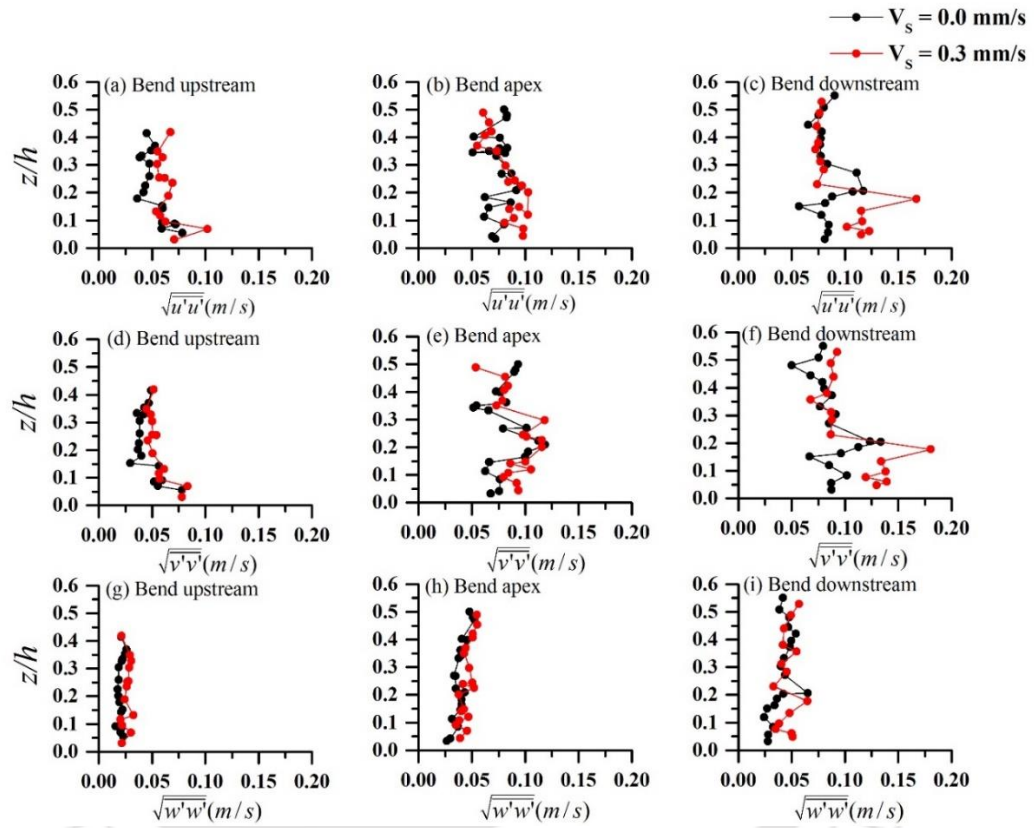

Figure 3.7 Streamwise turbulence intensity distribution for no seepage ($V_S = 0.0$ mm/s) and with seepage ($V_S = 0.3$ mm/s) at (a) Bend upstream (location 3), (b) Bend apex (location 8), and (c) Bend downstream (location 13). Transverse turbulence intensity distribution for no seepage ($V_S = 0.0$ mm/s) and with seepage ($V_S = 0.3$ mm/s) at (d) Bend upstream (location 3), (e) Bend apex (location 8), and (f) Bend downstream (location 13). Vertical turbulence intensity distribution for no seepage ($V_S = 0.0$ mm/s) and with seepage ($V_S = 0.3$ mm/s) at (g) Bend upstream (location 3), (h) Bend apex (location 8), and (i) bend downstream (location 13).

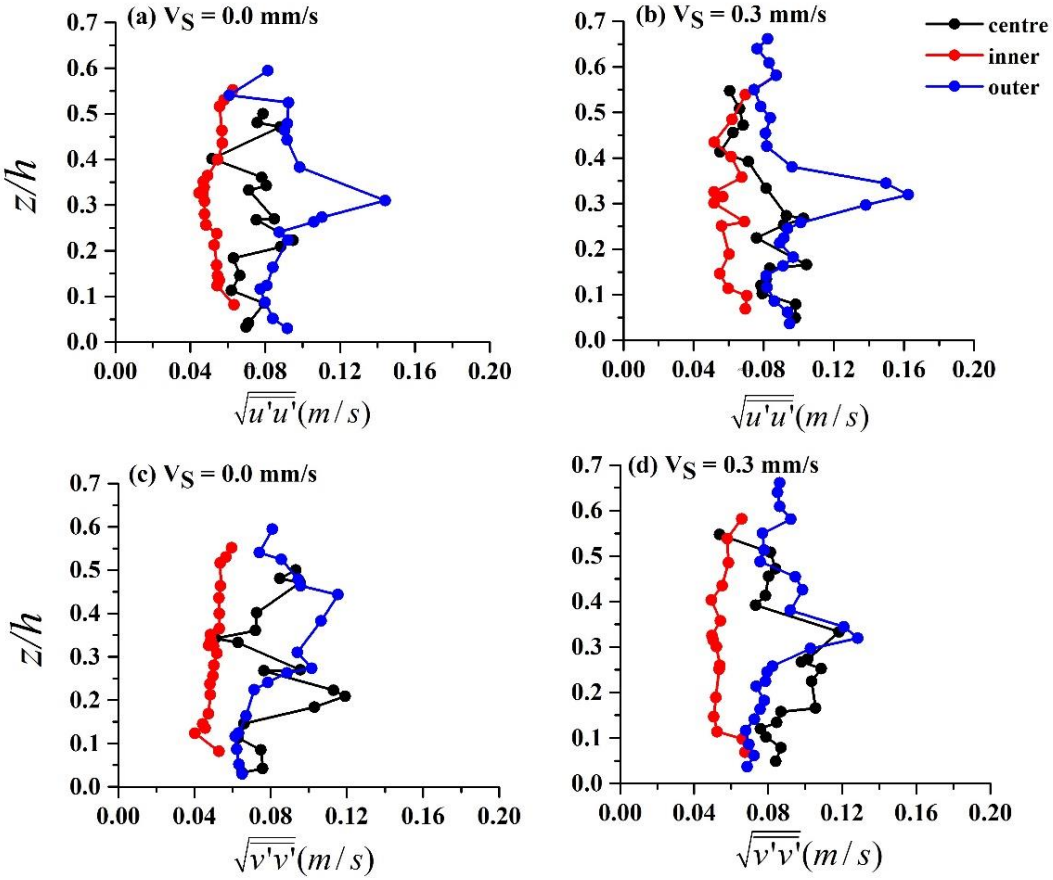

Figure 3.8 Streamwise turbulence intensity distribution at center (location 8), inner (location 10), and outer (location 6) regions of the bend for seepage velocity (a) $V_S = 0.0$ mm/s, and (b) $V_S = 0.3$ mm/s. Transverse turbulence intensity distribution at center (location 8), inner (location 10), and outer (location 6) regions of the bend for seepage velocity (c) $V_S = 0.0$ mm/s, and (d) $V_S = 0.3$ mm/s.

At the outer bend (Figure 3.8(a)), the streamwise turbulence intensity fluctuations are higher when compared to center and inner regions of the bend. Higher fluctuation relates to more turbulence generation in the outer region of the bend. However, the transverse turbulence intensity (Figure 3.8(c)) is higher at the center of the bend. At the inner bend, velocity fluctuations are least for both streamwise and transverse turbulence intensity.

With downward seepage, the turbulence intensity has increased near the channel bed across the bend. At the inner, center, and outer regions of the bend, the average streamwise turbulence intensity has increased about 18.5%, 4.4% and 3.8%, respectively (Figure

3.8(b)). The average transverse turbulence intensity has increased by about 10.6%, 8.1%, and 4% at the inner, center, and outer part of the bend, respectively (Figure 3.8(d)). The increase in fluctuating velocity with downward seepage may enhance sediment transport leading to modifications in the alluvial channel bed.

3.2.6 Turbulent Kinetic Energy

Turbulent kinetic energy (TKE) is a measure of the intensity of turbulence. TKE is defined as TKE = $1/2\ \left(\overline{u'u'} + \overline{v'v'} + \overline{w'w'}\right)$. The distribution of TKE is shown in Figure 3.9 at the center (location 8), inner (location 10), and outer regions (location 6) of the bend along the normalized depth (z/h). Observation reveals that TKE at the outer zone is higher, which corresponds to higher velocity fluctuations. TKE is less at the zone of sedimentation (inner zone) owing to lesser velocity fluctuations. With downward seepage, an average rise of 5% is observed in TKE in the near-bed region of the outer bend.

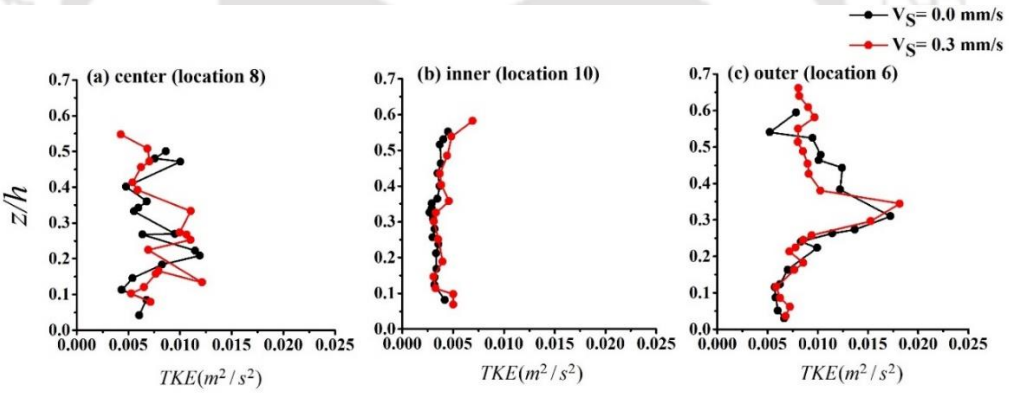

Figure 3.9 Turbulent kinetic energy (TKE) distribution for no seepage $(V_S = 0.0\ \mathrm{mm/s})$ and with seepage $(V_S = 0.3\ \mathrm{mm/s})$ at (a) center (location 8), (b) inner (location 10), and (c) outer (location 6) regions of the bend apex.

3.2.7 Entropy Measures

The time series data can be used as an informative measure by employing entropy. There are many entropy methods, such as Permutation entropy (PE) (Bandt and Pompe, 2002), Approximate entropy (ApEn) (Pincus, 1991), Sample entropy (SampEn) (Richman and Moorman, 2000), and Range entropy (RangeEn) (Omidvarnia et al., 2018). From a given time series, PE captures the permutation patterns-ordinal among individual values of the

time series and provides a probability distribution of an available pattern to quantify the degree of complexity of a system. Ordinal patterns describe the total order between two or more neighbours, encoded by permutations. The permutation entropy algorithm applies to regular, chaotic, noisy, and experimental or reality-based time series. Until now, PE was used extensively in various fields such as finding fault in diagnosis (Li et al., 2018; Zhou et al., 2018), biomedical signal processing (Azami and Escudero, 2016; Li et al., 2008; Li et al., 2007; Zhu et al., 2017), stock market analysis (Xu and Wang, 2017; Zunino et al., 2009), and economic downturns (Henry and Judge, 2019).

Permutation entropy (PE) is an appropriate complexity measure for disordered time series. Bandt and Pompe (2002) proposed an algorithm for permutation entropy and defined an arbitrary time series $\{x_t, t = 1, \dots, N\}$ into the m-dimensional space:

$$X_t = \{x[t], x[t + \tau_e], \dots, x[t + (m-1)\tau_e]\} \quad (3.6)$$

In the PE algorithm (Equation (3.6)), m and τ_e are the two basic physical quantities. To symbolise a time series, each time point is assigned its ordinal pattern of order m. The quantities m is the embedding dimension and τ_e is the embedding time delay. The embedding dimension determines the information contained in each vector with which an ordinal pattern is associated. The embedding time delay is the delay between successive points in the time series. Rearranging X_t in ascending order:

$$X_t = \{x[t + (r_1 - 1)\tau_e] \leq x[t + (r_2 - 1)\tau_e] \leq \cdots \leq x[t + (r_m - 1)\tau_e]\} \quad (3.7)$$

where, r_m denotes a size to distinguish two identical numbers. For any X_t, an ordered pattern is defined as $s = (r_1, r_2, \dots, r_m)$, where, s is one of $m!$ permutations consisting of m symbols $(1, 2, \dots, m)$ and r_m is the order in which $x[t + (r_m - 1)\tau_e]$ is replaced in the original $x[t + (m-1)\tau_e]$. For practical purposes, Bandt and Pompe (2002) recommended m equals 3 to 7, depending on the length of the time series. They pointed out that the length of the time series or sequence N should be large enough to satisfy $N \geq m!$ in order to obtain more reliable probability distribution. In the current study, for the calculation of PE, we have considered $m = 3$. The order m should be much smaller than the time series to look at small windows in a time series and their distributions of up and down movements.

For all probability distribution $P = \{p(s), s = r_1, r_2, \dots, r_m\}$, we define the normalized permutation entropy as:

$$H[P] = -\sum p(s)\, log\, p(s)/\, log(m!) \tag{3.8}$$

where $H[P]$ ranges from 0 to 1. The value of $H[P]$ depends on the sequence of the time series. When $H[P] = 0$, the time series is regular and when $H[P] = 1$, the time series is random and unpredictable. Therefore, the complexity of the signal is higher if the value of $H[P]$ is higher.

Pincus (1991) proposed approximate entropy (ApEn), a statistical parameter that applies to time series to measure the complexity of a system. ApEn measures the predictability of the existing amplitude waves of a signal on its previous amplitude waves (Srinivasan et al., 2007). ApEn is the negative logarithm where two similar sequences of m points remain similar to the next point. The algorithm of approximate entropy (ApEn) considers each sequence as matching itself to prevent the occurrence of $ln\,(0)$ in the computation. This condition in the algorithm confirms ApEn to be biased (Pincus, 1995; Richman and Moorman, 2000; Song et al., 2012). Therefore, Richman and Moorman (2000) introduced sample entropy (SampEn) as they believed that approximate entropy leads to inconsistent results. SampEn (m, r, N) is the negative logarithm where two similar sequences of m points remain similar to the next point and where self-matches are not considered in calculating the probability.

There is a combination of three parameters: $m, r,$ and N, based on which we can calculate the values of ApEn and SampEn. N is the length of the time-series (sample number), m is the number of samples used for prediction (embedding dimension), and r is the noise filter level (tolerance parameter) defined as $r = k \times SD$, where SD is the standard deviation of the time series X of N sample number. In this paper, the value of m considered is 3, and the noise filter level, $r = 0.2 \times \mathrm{SD}$, where SD is the standard deviation of the time series X.

Range entropy (RangeEn) is a modification of ApEn and SampEn proposed by Omidvarnia et al. (2018). Both ApEn and SampEn are prone to signal amplitude changes and needed correction of their signal amplitude by its standard deviation. However, the amplitude of

the signal has less effect on RangeEn. For tolerance parameter r, the range entropy (RangeEn) is confined between the intervals 0 (minimum entropy) to 1 (maximum entropy).

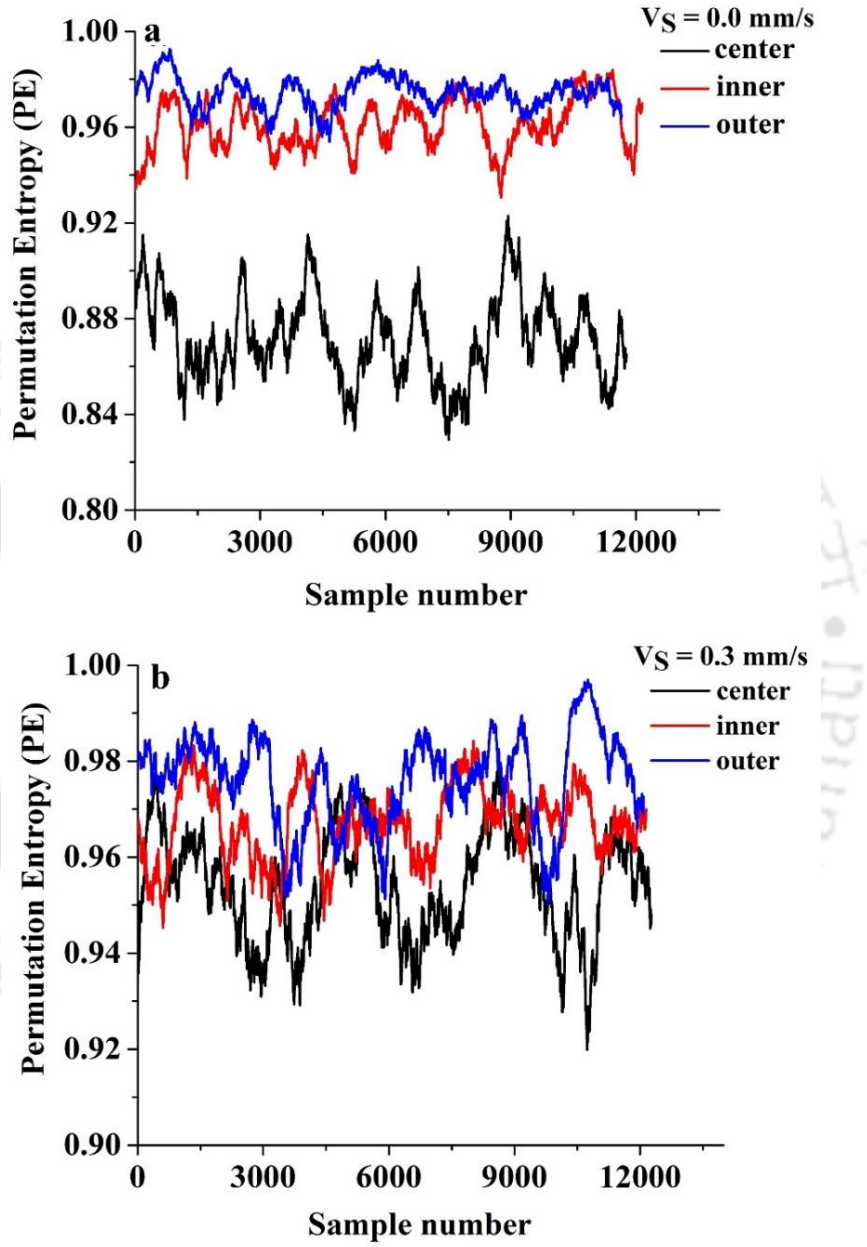

Figure 3.10 Permutation Entropy (PE) of transverse velocity at the center (location 8), inner (location 10), and outer (location 6) flow regions (a) for seepage velocity $V_S = 0.0\,\mathrm{mm/s}$ (b) for seepage velocity $V_S = 0.3\,\mathrm{mm/s}$.

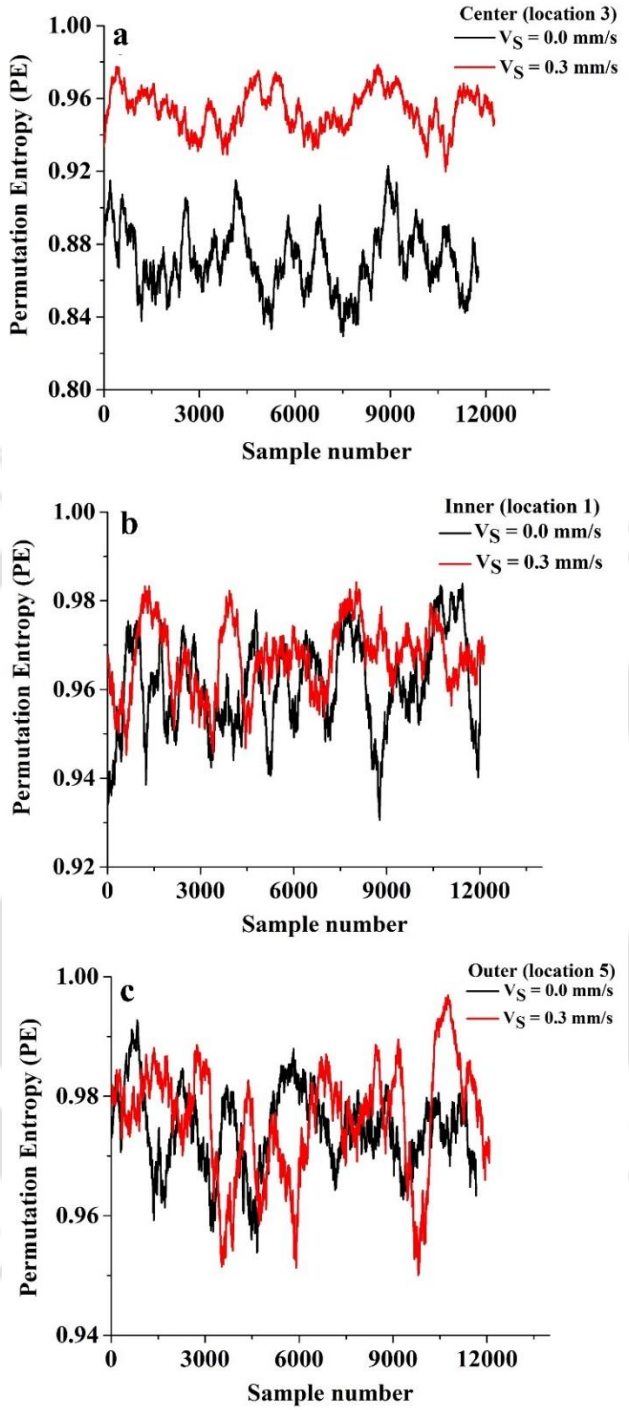

Figure 3.11 Permutation Entropy (PE) of transverse velocity at the (a) center (location 8), (b) inner (location 10), and (c) outer (location 6) flow regions for no seepage ($V_S = 0.0\,\mathrm{mm/s}$) and seepage ($V_S = 0.3\,\mathrm{mm/s}$) flow.

The permutation entropy (PE) for the transverse velocity time-series was examined. The permutation entropy for no seepage and seepage flow at the center (location 8), inner (location 10) and outer (location 6) flow region of the apex is shown in Figure 3.10 and Figure 3.11. Table 3.2 presents the mean of permutation entropy (PE). For seepage and for no seepage flow, in the outer flow region, PE is greater than the inner and central flow region (Figure 3.10 (a,b)). The mean of PE is highest in the outer region (Table 3.2). The higher PE relates to high randomness in the outer region, which may address the transverse velocity fluctuations to be greater in the outer bend apex, eroding the banks.

Table 3.2 Mean of Permutation Entropy (PE) of the transverse velocity at the center (location 8), inner (location 10), and outer (location 6) flow for no seepage ($V_S = 0.0\ mm/s$) and seepage flow ($V_S = 0.3\ mm/s$).

Bend location	**No seepage** ($\boldsymbol{V_S = 0.0\ mm/s}$)	**With seepage** $\boldsymbol{V_S = 0.3\ mm/s}$
Center (location 8)	0.872	0.954
Inner (location 10)	0.961	0.967
Outer (location 6)	0.974	0.976

Table 3.3 Mean of Approximate Entropy (ApEn), Sample Entropy (SampEn), and Range Entropy (RangeEn) of the transverse velocity at the center (location 8), inner (location 10) and outer (location 6) flow regions for no seepage ($V_S = 0.0\ mm/s$) and seepage flow ($V_S = 0.3\ mm/s$).

Location	**Approximate Entropy (ApEn)**		**Sample Entropy (SampEn)**		**Range Entropy (RangeEn)**	
	No seepage	**With seepage**	**No seepage**	**With seepage**	**No seepage**	**With seepage**
Center (location 8)	0.0108	0.0176	0.0137	0.0161	0.1568	0.1694
Inner (location 10)	0.0179	0.027	0.0158	0.0244	0.1681	0.184
Outer (location 6)	0.0214	0.0303	0.0195	0.0283	0.18	0.2103

For seepage flow, PE increases at all the bend locations, indicating higher fluctuations with seepage flow. At the inner (location 10) and outer (location 6) flow, observation reveals no significant difference for no seepage and seepage flow (Figure 3.11(b) and 3.11(c)) and Table 3.2); therefore, approximate entropy, sample entropy and range entropy were also calculated to find more information on it.

From the calculated entropy at the center, inner and outer flow regions (Table 3.3), the complexity or the disorder has increased with seepage flow, which was otherwise not very distinct from permutation entropy (PE). This increase in entropy relates to higher fluctuations with seepage flow.

3.2.8 Summary

Steady flow was passed through a sinuous channel with mobile bed and rigid sides. Due to downward seepage, the main channel water moves out and joins the available groundwater table concerning to which the turbulent flow velocity and stresses experience additional force near the channel bed.

The non-logarithmic distribution of streamwise velocity was however widely studied in bends (Graf and Blanckaert, 2002; Sukhodolov and Kaschtschejewa, 2010). Logarithmic velocity profiles are observed in straight flows or when measured across a straight reach of a channel. The presence of secondary currents in curved channels affect the distribution of the velocity. The maximum mean velocity was observed at the zone of deposition (inner bend). Blanckaert and de Vriend (2005), Constantinescu et al. (2013), da Silva and Ebrahimi (2017) and several researchers observed the maximum velocity to be towards the outer bend. On the other hand, Henderson (1966), Furbish (1988), Esfahani and Keshavarzi (2010) found the maximum velocity towards the inner region of the bend. The results found in this study are well conforming with the maximum mean velocity found towards the inner bend. More than the mean velocity, the fluctuating velocity from the mean is found to be significant in the flow field. The stresses were found higher towards the outer bend, thereby causing erosion. In the outer flow region, streamwise Reynolds shear stresses ($X-Y$ plane) are higher near the bed than the central and inner flow region. The erosion zone (outer region) observes greater stress on account of excess momentum transport due to seepage. In the outer flow region, the near-bed streamwise turbulence intensity is higher.

However, in the central flow region, the near-bed transverse turbulence intensity is higher, where the contributing fluctuations cause circular flow at the bend center.

TKE is dominant in the outer region, corresponding to higher velocity fluctuations. With seepage flow, there were observable changes in the flow with an increase of 30% and 20% of mean velocity and turbulent shear stress ($X-Y$ plane) in the outer flow region. The average turbulence intensity in the outer region of the bend shows a slight 4% of the increase. TKE in the near-bed region of the outer bend has increased with an average rise of 5%. The study also highlights the application of permutation entropy (PE) of transverse velocity time-series, which increased at the center, inner and outer flow region for seepage flow. However, irrespective of seepage condition, PE is maximum at the outer bend, addressing the erosion and maximum sediment transport at the bend apex. Thus, modification in the turbulence parameters due to downward seepage can help understand the complex erosion and deposition patterns in curved channels in which active exchange between surface water and groundwater exists.

3.3 Effect of Downward Seepage on the Near-Bed Flow Turbulence in a Rigid Rectangular Sinuous Channel

3.3.1 Experimental Conditions and Data Recording

The present study was focused at the bed proximity of the channel, since the effect of seepage is maximum near the channel bed. The experiments were done in a rectangular sinuous channel with rigid non-erodible banks, and the channel bed consisted of movable uniform sediment. The results address the effects of downward seepage in the velocity distribution, shear stress distribution and turbulent bursting processes near the channel bed. The bursting events provide information on the bed features along the bend. It was found that no earlier researchers have experimentally observed the condition of downward seepage (suction) at the near-bed of a sinuous channel. The effect of seepage was uniform for the channel length of 15.2 m. In this study, experiments were done in two phases: conditions of no seepage and downward seepage. Two seepage velocities were considered $V_{S1} = 0.05$ mm/s and $V_{S2} = 0.1$ mm/s, which falls in the range of the previous literature.

Table 3.4 Near-bed experimental hydraulic parameters.

Case	Average flow depth, H (m)	Inflow discharge, Q (m^3/s)	Seepage velocity, V_S(mm/s)	Froude number, Fr	Reynolds number, Re
No seepage	0.107	0.00793	0.0 (V_{S0}), 0.05 (V_{S1}), and 0.1 (V_{S2})	0.24	17495
With seepage					

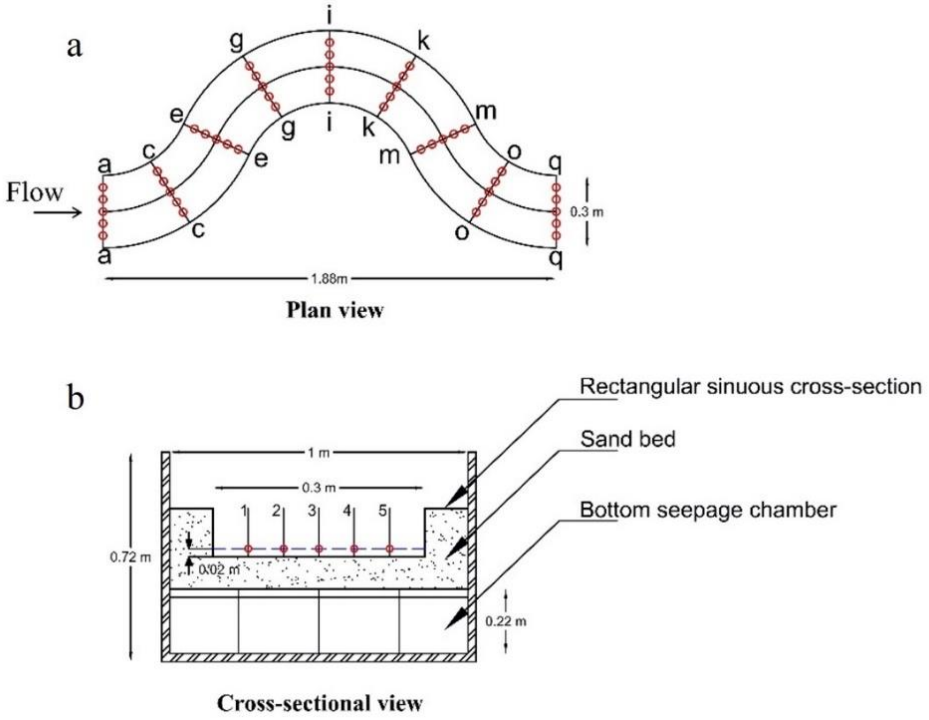

Figure 3.12 Schematic representation of (a) plan view of the test section showing locations of near-bed velocity measurements, and (b) location of near-bed measurement at a distance 0.02 m from the channel bed.

A Nortek (four-beam down-looking probe, Nortek AS, Norway) Vectrino+ velocimeter was used to record the instantaneous velocity. At each location, 6000 samples were collected for 120 s with a sampling rate of 50 Hz (Esfahani and Keshavarzi, 2011). The samples were collected by a cylindrical remote sampling volume located below the central transmitter of the velocimeter at a distance of 0.05 m. The height of the sampling volume

can be adjusted manually. In the present experiments, the sampling volume was set at 2.5 mm, so that the sampling volume did not interact with the bed particles. To study the near-bed interaction between the flow and sediment bed, velocity data were recorded at nine sections $(a, c, e, g, i, k, m, o, q)$ at a distance of 0.02 m above the bed (Figures 3.12). Each section has five locations to capture the flow characteristics thoroughly.

3.3.2 Flow Characteristics

The streamwise flow governs the transfer of momentum of the fluid in straight channels, while in bends, the secondary motion due to curvature leads to transverse and vertical transfer of momentum (Engel and Rhoads, 2017). Therefore, the turbulence structure and momentum transfer in bends differ from that of straight channels. Entering the curve of the channel, when the flow reaches the outer bend, it erodes the outer bank and carries the sediment-laden flow deposits at the inner bank. The secondary flow in meander or sinuous channel is caused by the channel bends or curvature of the channel. Channels with mild curvature have reported only one center-region cell (Hille et al., 1985). There is a weak outer bank circulation along with the center cell in a sharp curvature channel (Blanckaert and Graf, 2004). Figure 3.13 represents the secondary flow at three cross-sections (g, i, and k) of the bend.

The horizontal axis represents the channel width, and the vertical axis represents the flow depth. The flow depth is different along the cross-section, i.e., higher at the zone of erosion and lower at the zone of sedimentation/deposition. The negative sign indicates a decrease in depth from the water level. The vector plots were prepared using the computer software Tecplot 360. For both conditions of no seepage and seepage, almost similar characteristics were noticed. At the bend apex (section i), a clockwise rotation cell at the center of the channel width was observed for both no seepage and seepage condition. In sections g and k, a clockwise rotation cell occurred at the outer half of the bend for no seepage and seepage condition. At the bend upstream (section g) for both no seepage and with seepage condition, an anti-clockwise rotation cell was observed near the inner bend. At bend downstream (section k) with seepage, a very small counter-clockwise rotation was noticed near the inner bend. Hence, the flow vectors reveal the asymmetry in their distribution due to bend curvature.

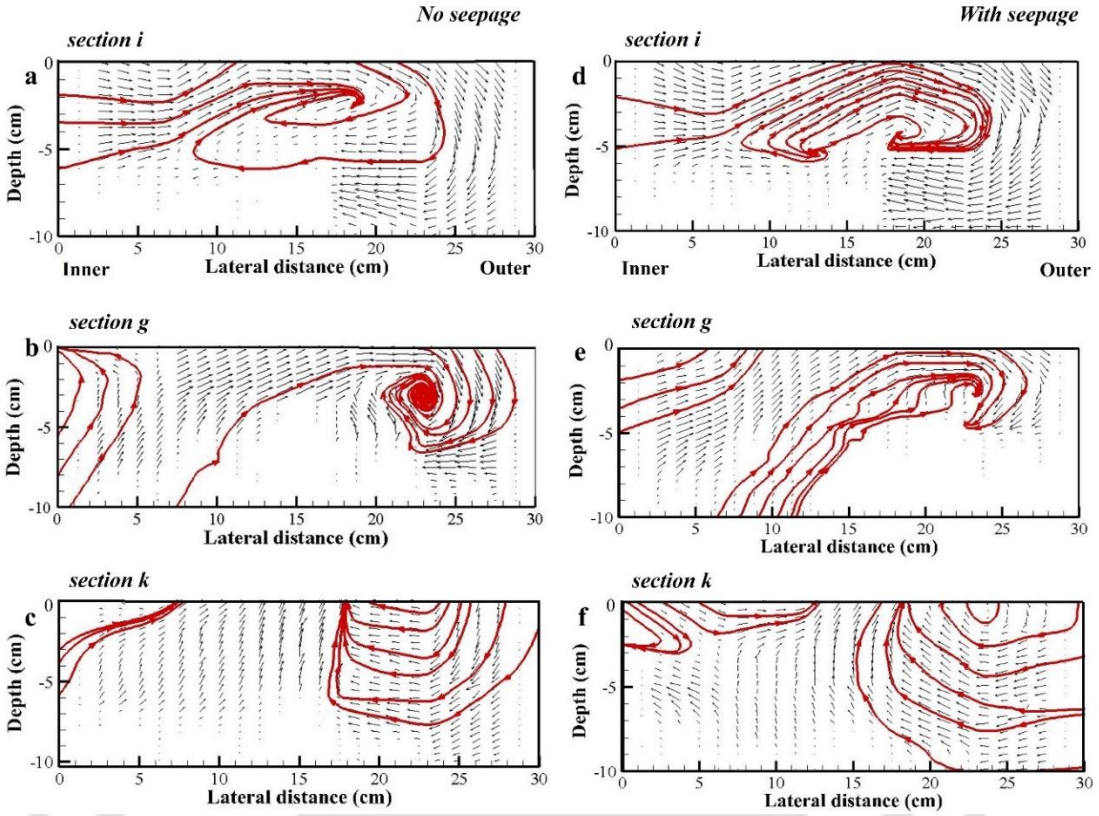

Figure 3.13 Secondary flow for no seepage (a, b, c) and with seepage (d, e, f) at different cross-sections. (a, d) Bend apex (section i), (b, e) Bend upstream (section g) and (c, f) Bend downstream (section k).

The near-bed streamwise velocity is presented in Figure 3.14. The horizontal axis represents the channel wavelength, and the vertical axis denotes the channel width. During the inspection of the velocity distribution throughout the bend, high value of streamwise velocity was found near the deposition region. From this result of the velocity distribution, it is certain that the maximum velocity is not always towards the outer bend, as observed in most cases. de Vriend and Geldof (1983) have mentioned several reasons as to why the maximum velocity is found at the inner bank under different cases. The main velocity may take longer time to reach the outer bend because of the inward skewing; hence, the velocity is mostly redistributed towards the inner bend. Moreover, the potential-vortex effect may be the reason, where sudden transverse tilting of the water surface formed near the bend entrance led to pressure gradients, which caused flow acceleration at the inner part and flow deceleration at the outer part. Further, with the increase in seepage velocity, the

velocity near the bed proximity has increased. With the introduction of downward seepage, the near-bed flow field changes because of the additional force exerted near the boundary of the channel. Kavcar and Wright (2009) found that with downward seepage, the high velocities persist near the channel bed since the low momentum flow near the boundary of the channel is detached from the main flow. With 0.1 mm/s seepage velocity, the velocity increase spread was more near the bed surface than without seepage.

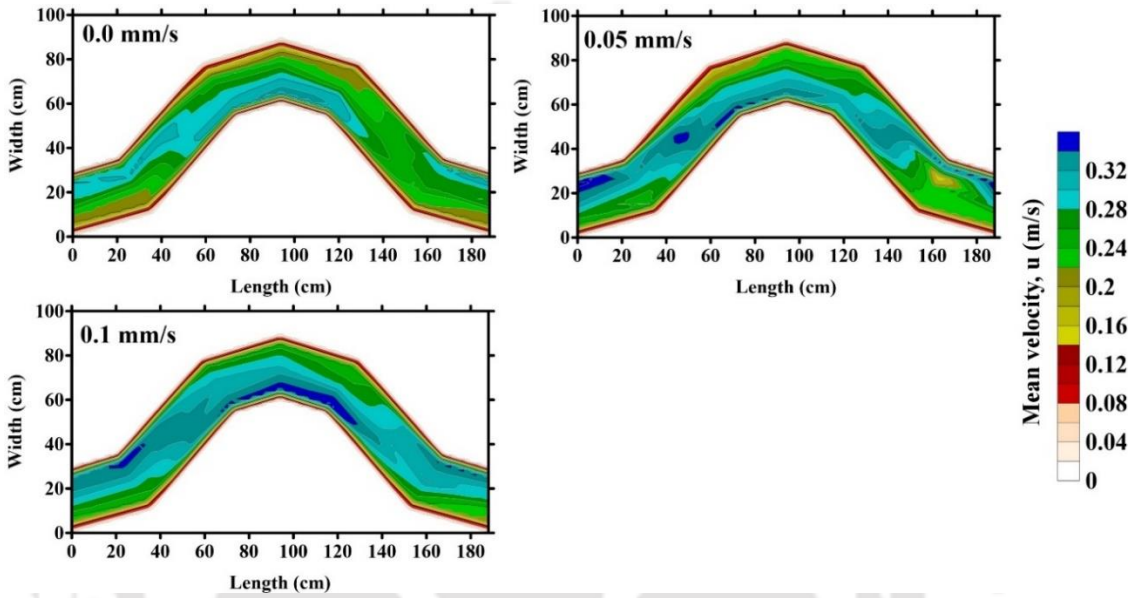

Figure 3.14 Contour plots of near-bed streamwise velocity (m/s) with seepage velocity (a) $V_{s0} = 0.0$ mm/s, (b) $V_{S1} = 0.05$ mm/s, and (c) $V_{S2} = 0.1$ mm/s.

3.3.3 Reynolds Shear Stress (RSS)

The shear stresses acting on the plane of the channel bed is shown in Figure 3.15. Two dominant shear stresses, streamwise and transverse, are prevalent in three-dimensional flow fields as found in curved channels.

The streamwise and the transverse (or radial) Reynolds shear stresses can be defined as:

$$\tau_{zx} = -\rho\overline{u'w'} \tag{3.9}$$

$$\tau_{zy} = -\rho\overline{v'w'} \tag{3.10}$$

$$\overline{u'w'} = \frac{1}{n}\sum_{i=1}^{N}(u-\overline{u})(w-\overline{w}) \tag{3.11}$$

$$\overline{v'w'} = \frac{1}{n}\sum_{i=0}^{N}(v-\overline{v})(w-\overline{w}) \tag{3.12}$$

The Streamwise Reynolds shear stress τ_{zx} is a component of the shear stress acting on the $X-Y$ plane parallel to the flow direction. The transverse Reynolds shear stress τ_{zy} is a component of the shear stress acting in the transverse direction on the plane perpendicular to the vertical direction.

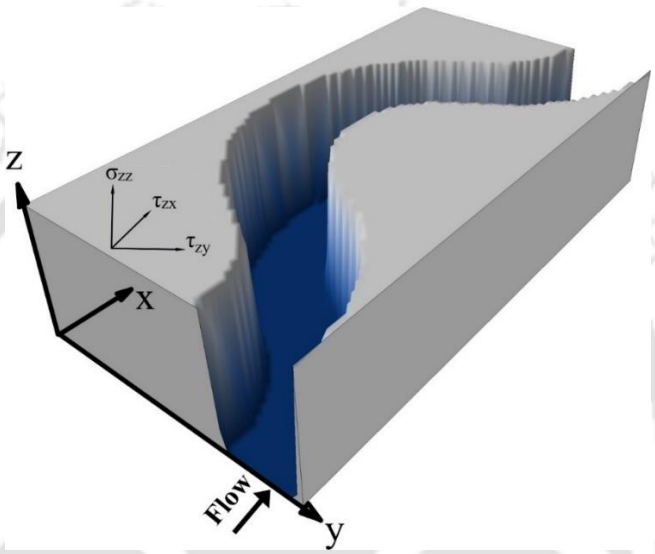

Figure 3.15 Shear stresses acting on the channel bed ($X-Y$ plane).

A contour representation of RSS in transverse direction investigated throughout the bed shows high values in the eroded regions (Figure 3.16). These high values exhibit the motion of sediment in the channel bed, i.e., the flow in bends allows the sediment particles to move in the transverse direction. The flow at the surface is directed towards the outer bend and near the bed surface it is directed towards the inner bend. In this process, the outer bend region was eroded, and the sediment was deposited in the inner bend. This evidence was supported by the secondary flow analysis (Figure 3.13). With the exploration of the RSS at the radial or transverse direction, it is evident that the effects of the transverse velocity fluctuation v' play a vital role in investigating the meander processes. With little seepage application, there is a small increase in the RSS at the eroded regions. The increase in stress would lead to excess momentum transfer in the bed proximity. Esfahani and Keshavarzi

(2011) observed similar characteristics, where they mentioned that the distribution of high velocity is inversely proportional to the transverse Reynolds shear stress at bed proximity.

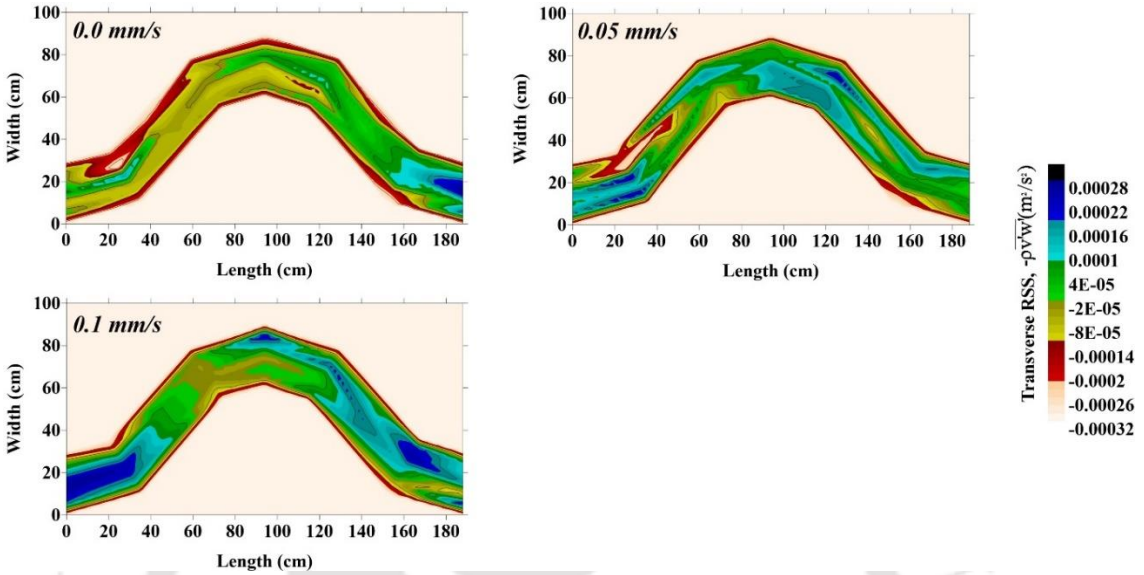

Figure 3.16 Contour plots of near-bed Reynolds shear stress in transverse direction $\tau_{zy} = -\rho\overline{v'w'}(\mathrm{m}^2/\mathrm{s}^2)$ with seepage velocity (a) $V_{S0} = 0.0$ mm/s, (b) $V_{S1} = 0.05$ mm/s, and (c) $V_{S2} = 0.1$ mm/s.

3.3.4 Bed Shear Stress

The bed shear stress $(\tau_\circ)$ was calculated to inspect the transport of sediment in the sinuous channel. It is defined in the form of shear velocity (u_*) as:

$$u_* = \sqrt{\tau_o/\rho} \tag{3.13}$$

where ρ is the mass density of water. The bed shear stress was evaluated by the turbulent kinetic energy (TKE) method, which states that TKE is proportional to the bed shear stress (Soulsby and Dyer, 1981). Biron et al. (2004) estimated the bed shear stress in simple and complex flow fields with different methods. They found that the Reynolds shear stress method was appropriate to use in a simple flow field, whereas in a complex flow field, the TKE method gave a good result.

$$\tau_o = C_1 \times \rho \times TKE \tag{3.14}$$

$$TKE = \frac{1}{2}\left(\overline{u'u'} + \overline{v'v'} + \overline{w'w'}\right) \tag{3.15}$$

where u', v' and w' are the fluctuating components of velocity in the streamwise, transverse and vertical directions, respectively. The value C_1 was adopted as 0.19 for a variety of flows (Stapleton and Huntley, 1995; Thompson et al., 2003). In the present study, the TKE method was used because it is reliable and robust.

The bed shear stress at the outer region of the bend was higher in both the case of no seepage or with seepage. This implies that sand bed movement in the outer region is more than the center or the inner region of the bend. The bed shear stress at the outer region was subjected to 46% of bed shear with seepage application V_{S1} and further 27% higher with seepage application V_{S2}. With downward seepage, the shear velocity and the bed shear stress at all locations were higher, which reports that the flow exerts greater shear on the channel bed.

Table 3.5 Bed shear stress and shear velocity estimated at the inner, center, and outer regions of the bend.

	Bed shear stress (τ_o, N/m^2)			**Shear velocity (u_*, m/s)**		
Seepage velocity →	V_{S0}	V_{S1}	V_{S2}	V_{S0}	V_{S1}	V_{S2}
Location ↓						
Inner	0.842	1.563	1.813	0.029	0.039	0.043
Center	1.933	2.776	2.964	0.044	0.053	0.054
Outer	2.011	2.915	3.714	0.045	0.054	0.061

3.3.5 Three-dimensional Bursting Phenomenon (Octant Analysis)

Kline et al. (1967) introduced the bursting phenomenon in two-dimensional flow as in straight channels. In studies, such as flow in bends (Tilston et al., 2009), in a vortex chamber (Keshavarzi and Gheisi, 2006), and flow over ripples (Mianaei and Keshavarzi, 2008), the flow field is three-dimensional. The two-dimensional quadrant analysis seems insufficient in such studies. This new method of bursting process, also called octant

analysis, is divided into two classes A and B, where each of this class comprises of four events. In a sinuous channel, the flow velocity across the channel width (transverse velocity) is significant, and hence the two-dimensional quadrant analysis is inadequate to study the flow in a bend. The flow in bend is the key factor concerning erosion at the outer bank and the development of river meanders (Camporeale et al., 2007; Crosato, 2008).

Depending on the sign of the fluctuating velocities u' and w', they classified the bursting events into four quadrants q_i (i = 1, 2, 3 and 4). The quadrants are classified as $q_1(u' > 0 \text{ and } w' > 0)$ as outward interaction events, $q_2(u' < 0 \text{ and } w' > 0)$ as ejection events, $q_3(u' < 0 \text{ and } w' < 0)$ as inward interaction events and $q_4(u' > 0 \text{ and } w' < 0)$ as sweep events. In channels with loops and bends, the transverse velocity and its fluctuations are significant, which are otherwise neglected in straight flow analysis. Thus, in a sinuous channel bend, the flow characteristics are three-dimensional. Keshavarzi and Gheisi (2006) proposed three-dimensional bursting events.

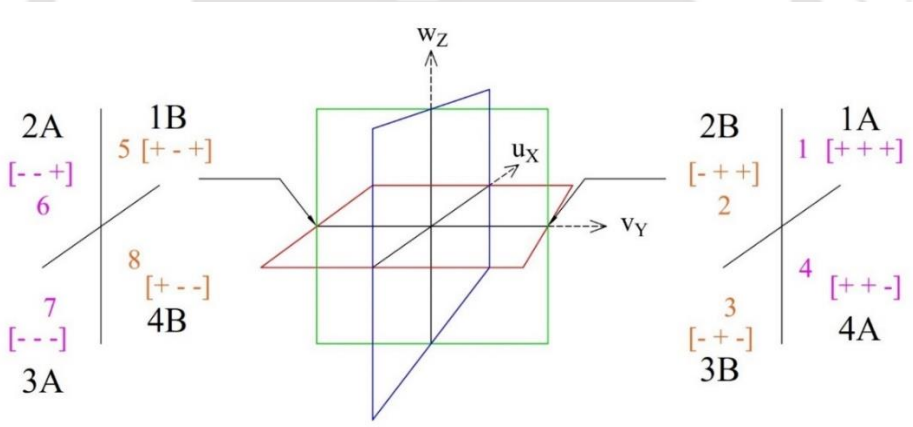

Figure 3.17 Quadrants showing bursting events in a 3-dimensional flow field.

Depending on the sign of the three-dimensional fluctuating velocities u', v' and w', they classified the events into two groups: Class A and Class B. Class A indicates a group of four events that move towards the inner bank, and Class B indicates another group of four events that move towards the outer bank. They are defined as follows:

Class 1A: Internal outward interaction $(u' > 0, v' > 0, w' > 0)$

Class 2A: Internal ejection $(u' < 0, v' < 0, w' > 0)$

Class 3A: Internal inward interaction $(u' < 0, v' < 0, w' < 0)$

Class 4A: Internal sweep $(u' > 0, v' > 0, w' < 0)$

Class 1B: External outward interaction $(u' > 0, v' < 0, w' > 0)$

Class 2B: External ejection $(u' < 0, v' > 0, w' > 0)$

Class 3B: External inward interaction $(u' < 0, v' > 0, w' < 0)$

Class 4B: External sweep $(u' > 0, v' < 0, w' < 0)$

A conceptual sketch of the bursting events in a three-dimensional flow field is shown in Figure 3.17. The classifications indicate the transfer of momentum between the water layers, which further generates turbulent shear stresses along with the streamwise and transverse directions (Liu and Bai, 2013). The contribution probability *P* of each event can be defined as:

$$P_k = n_k / N \tag{3.16}$$

$$N = \sum_{k=1}^{8} n_k \tag{3.17}$$

where, n_k is the number of occurrences of each event, *N* is the total number of events (total number of instantaneous velocity samples), and subscript k changes from 1 to 8 for the eight events. The bursting phenomena signify the momentum transfer between the water layer and the sediment channel bed. This instantaneous momentum transport exerts streamwise and transverse turbulent stresses on the sediment bed $(X - Y)$ plane, which is responsible for the movement of sediment in the sinuous channel. Therefore, the velocity data was collected at a distance of 0.02 m from the channel bed. On these lines, considering the near-bed flow interaction with the seepage flow underneath the main channel, the octant analysis (bursting phenomena in three-dimensional flow field) was conducted near the channel bed and not throughout the water column. Figures 3.18, 3.19 and 3.20 present the bursting events for seepage velocity 0.0 mm/s, 0.05 mm/s and 0.1 mm/s, respectively. In these figures, the x-axis represents the length of a bend, and the y-axis represents the channel width in centimeters. From the calculated contribution probability, the direction of sediment motion can be predicted. Hence, the analysis of the bursting events is explained

parallel to the morphological features observed in this study. The morphology of the channel bed is given in Appendix A (Figure A.1).

The events 3A (internal inward interaction) and 1B (external outward interaction) are maximum at the entrance (cross-section a, c, and e). These events have negative radial velocity, and hence they move the sediment towards the outer bend. A patch of deposit near the outer wall at the entrance is visible from the morphology investigation (refer Figure A.1). The events 4A (internal sweep), 2B (external ejection), and 1A (internal outward interaction) with positive radial velocity push the sediments particles towards the inner bend. Moreover, the internal events induce the bed material to move from the outer region towards the inner region of the bend, which highlights the outer bend erosion and inner bend deposition. Also, at the bend apex (refer Figure 3.11) a clockwise rotation cell was observed near the outer bend, which supplements the erosion process.

Analyzing the contribution probability for no seepage condition (0.0 mm/s), the contribution of the events 2B (external ejection), 4B (external sweep), 4A (internal sweep) and 2A (internal ejection) are highest from cross-section $'g'$ to cross-section $'q'$ (Figure 3.18). 4A and 2B act towards the inner bend, whereas 4B and 2A act towards the outer bend. From the above analysis, it was observed that the sweep and ejection events are dominant, which could be related to bed level changes along the channel (Refer Figure A.1). The aim is to find how downward seepage has an impact on momentum transfer. For downward seepage condition (0.05 mm/s and 0.1 mm/s), the ejection and sweep events of both internal and external class have increased (Figure 3.19 and 3.20). To quantify the increase in downward seepage, the percentage increase was estimated for internal sweep (4A) and external ejection (2B).

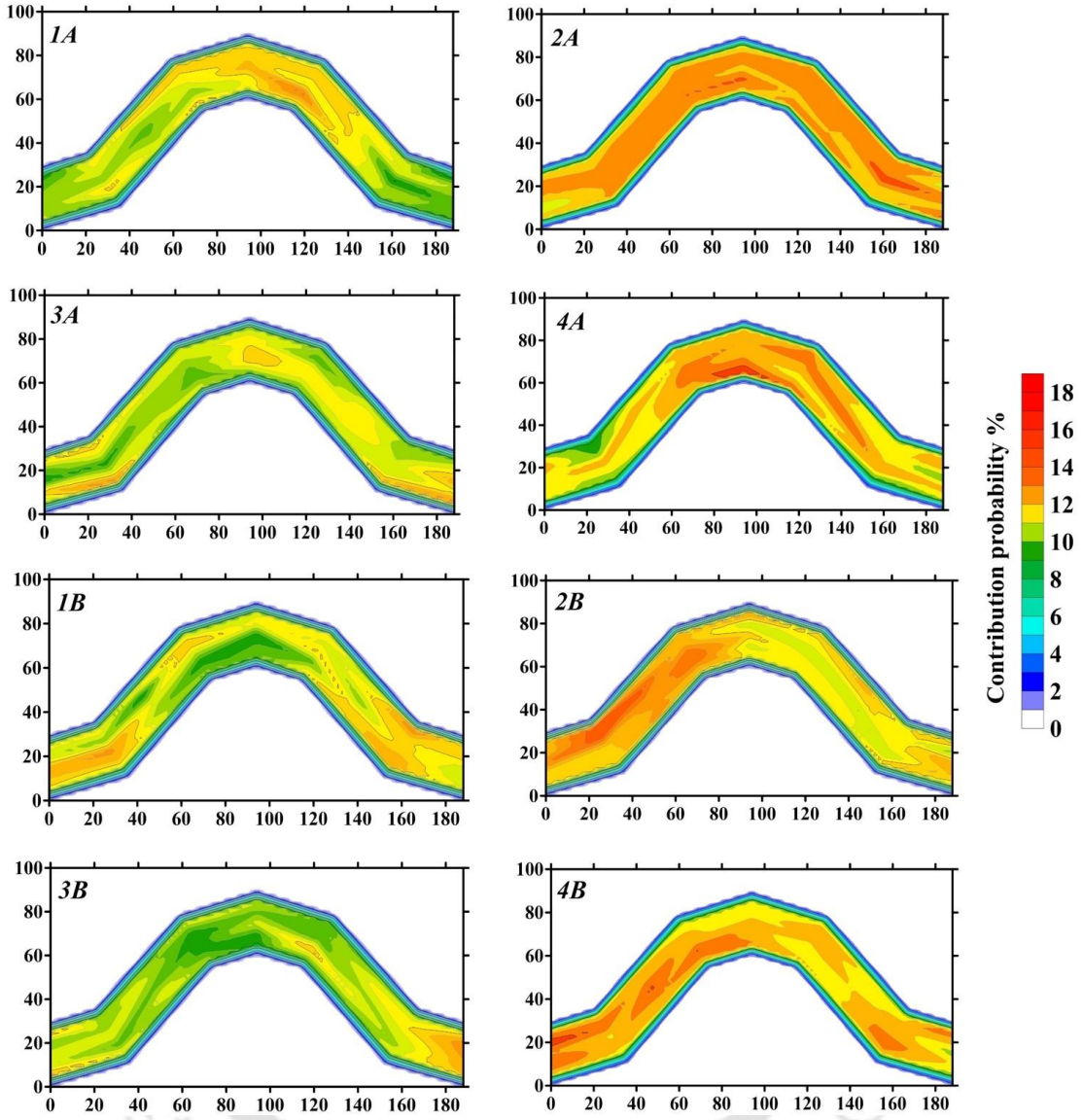

Figure 3.18 Contours of contribution probability (%) of bursting events with seepage velocity $V_{S0} = 0.0$ mm/s.

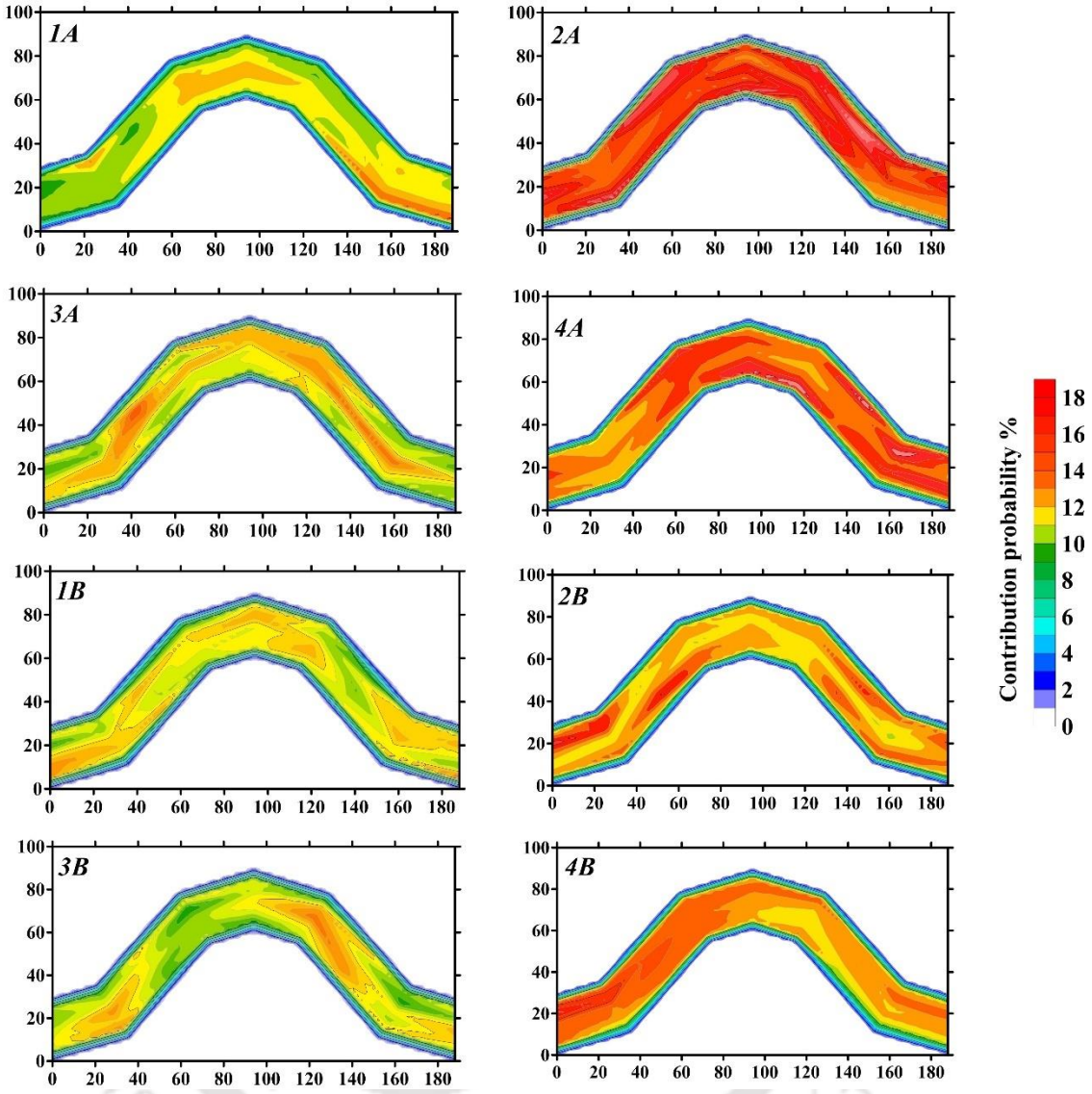

Figure 3.19 Contours of contribution probability (%) of bursting events with seepage velocity $V_{S1} = 0.05$ mm/s.

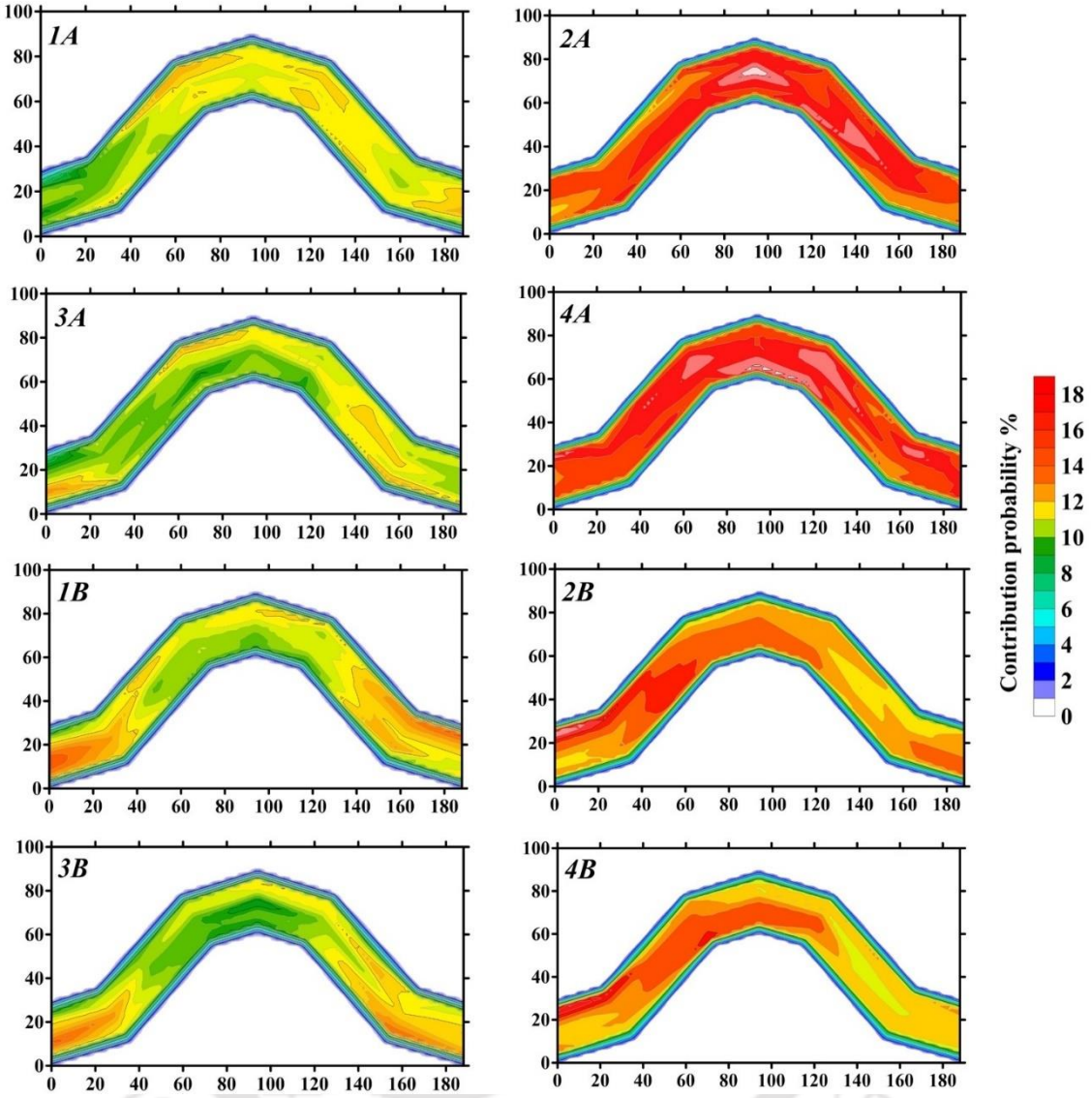

Figure 3.20 Contours of contribution probability (%) of bursting events with seepage velocity $V_{S2} = 0.1$ mm/s.

The contribution probability for internal sweep (4A) and external ejection (2B) increased by 5.16% and 3.72%, respectively, with the application of downward seepage (0.05 mm/s seepage velocity). With further increase in seepage velocity from 0.05 mm/s to 0.1 mm/s, the contribution probability increased 11.04% for event 4A and 8.21% for event 2B. The quantification of the bursting events with downward seepage indicates a surge in sediment transport. The focus of the study was to explore seepage effects on the three-dimensional near-bed bursting events using the octant analysis. Results reveal that downward seepage

causes excess near-bed momentum transfer, and the contribution probability has increased. This alternation in the near-bed flow structure significantly affects the morphological behavior of a sinuous channel with active downward seepage.

3.3.6 Summary

The secondary flow in bends has shown the presence of helical flow with seepage and no seepage flow. This confirms the potential of the flow to change the channel bed configuration. The flow at the surface approaching the bend moves towards the outer bend, which exerts substantial shear on the streambed near the bank of the channel. This leads to erosion at the outer bend. Therefore, eroded sediments are eventually carried towards the inner region of the bend by the flow near the channel bottom in radial (transverse) direction. The current study demonstrates the turbulent flow behavior of a sinuous alluvial channel affected by downward seepage. Despite the low magnitude of seepage velocity, there were noticeable changes in bed morphology and turbulent parameters in the sinuous channel. The sediment transport across the bend can be ascertained from the RSS contour plots, indicating that the flow allows the sediment to move in a transverse or radial direction. For downward seepage, the velocity and RSS were observed to increase with the increase in seepage velocity. From the bursting phenomenon, the contribution probability of each of the bursting events was determined, and it provides better understanding of the momentum transfer occurring in between the water layer and the sediment. The analysis of the bursting phenomenon highlights the erosional and depositional features along the bend. The contribution probability increased with the application of downward seepage.

3.4 Effect of Downward Seepage on the Flow Turbulence in Mobile Boundary Sinuous Channel

3.4.1 Experimental Conditions and Data Recording

In this study, flow turbulence was analyzed in mobile boundary sinuous channel of rectangular and trapezoidal cross-section under two conditions: (1) without seepage and (2) with downward seepage. The channel had mobile erodible banks and sand bed. The three-dimensional instantaneous flow velocity was investigated along the center of the channel at five locations of the second bend. The planform and the cross-sectional view are

shown in Figure 3.21. The flow was restricted to the main channel, i.e., the sinuous channel. There was no overbank flow in the sinuous channel, i.e., the bed was fully saturated and the banks were not fully saturated. The hydraulic conditions of the experiments are presented in Table 3.6. The flow turbulence for the discharge $Q = 0.00629$ m^3/s are shown only to avoid repetition of work.

Table 3.6 Hydraulic conditions of the mobile boundary experiments.

Channel	**Inflow Discharge, $Q(\mathrm{m^3/s})$**	**Seepage condition**	**Average flow depth (m)**	**Froude number, Fr**	**Reynolds number, Re**	**Seepage velocity, $V_S(\mathrm{mm/s})$**
Mobile Rectangular	0.00629	No seepage	0.102	0.20	13978	-
		With seepage	0.100	0.21	14130	0.12
Mobile Trapezoidal	0.00629	No seepage	0.109	0.28	14635	-
		With seepage	0.099	0.33	15866	0.14

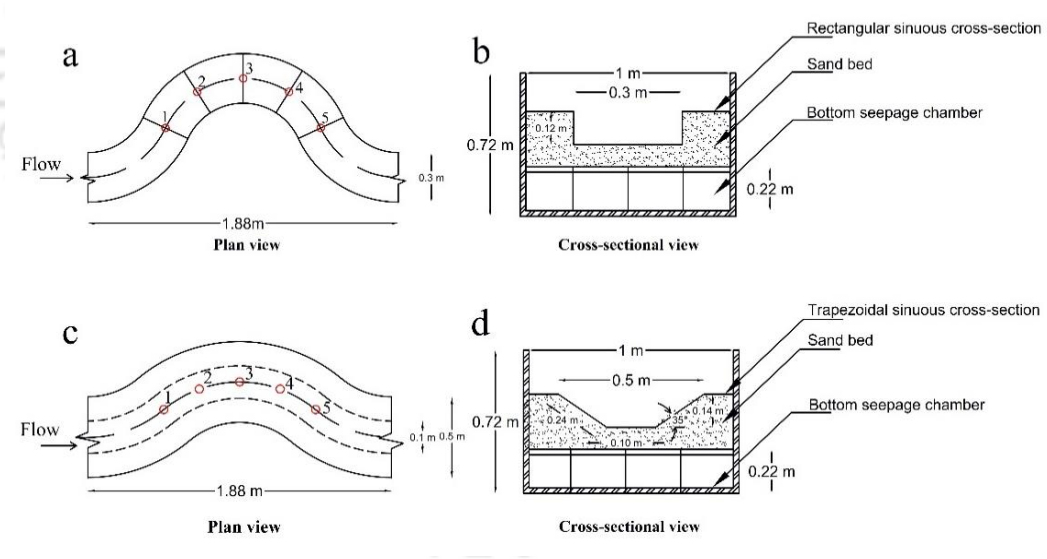

Figure 3.21 Experimental setup (a) Planform of rectangular channel, (b) cross-sectional view of rectangular channel, (c) Planform of trapezoidal channel, and (d) cross-sectional view of trapezoidal channel.

3.4.2 Mean Streamwise Velocity

The flow velocity at the center of the sinuous channel was measured to quantify the effect of seepage. On account of the interaction between the surface and sub-surface flow, the flow distribution may be modified. Figure 3.22 and Figure 3.23 present the streamwise flow distribution at five locations in a rectangular and trapezoidal sinuous bend, respectively.

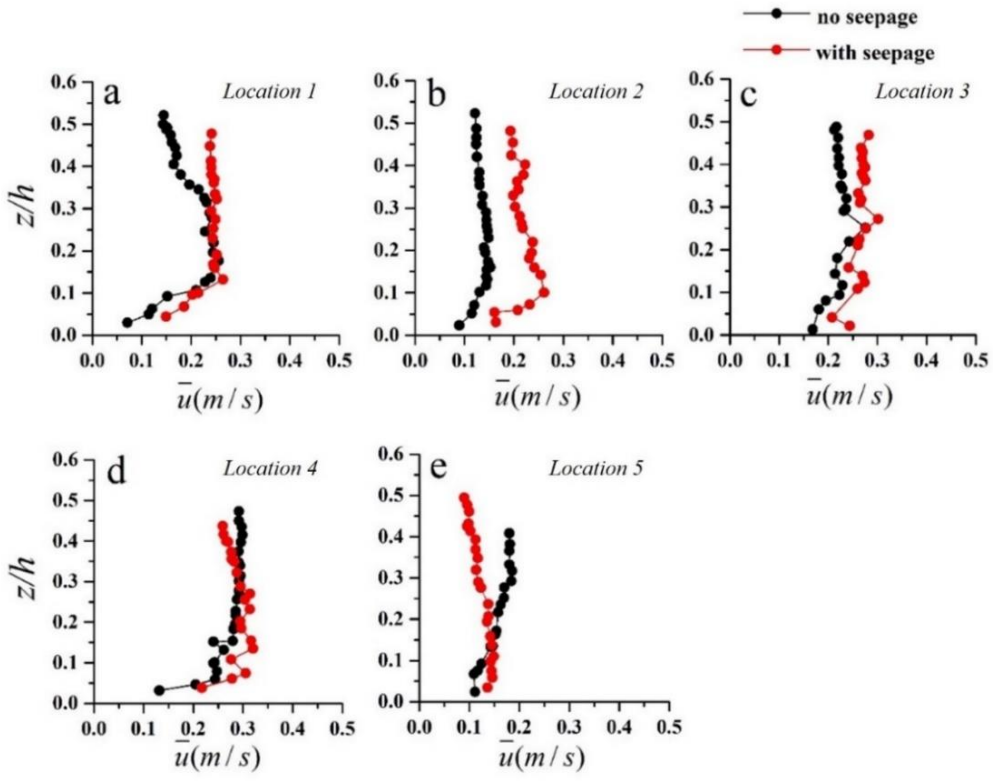

Figure 3.22 Streamwise velocity distribution in mobile rectangular sinuous channel.

At all the locations of measurement, the flow distribution has shifted with the application of downward seepage. Seepage is dominant at the channel bed, and therefore it is important to address the modification near the bed. The measurement of the flow was taken at the initial centerline of the sinuous channel. The banks of the channel were evolving continuously, which limited the measurements near the channel banks. The non-logarithmic velocity distribution in the sinuous bend depicts the altered flow in the presence of curves in the channel. In the present study, the percentage increase in flow velocity was calculated for $z/h < 0.2$ at all locations of both the sinuous channel, where z is the point

of velocity measurement (positive upwards) and h is the total depth. The percentage increase in the rectangular sinuous channel near the channel bed was 17% (location 1), 65% (location 2), 22% (location 3), 19% (location 4) and 8% (location 5).

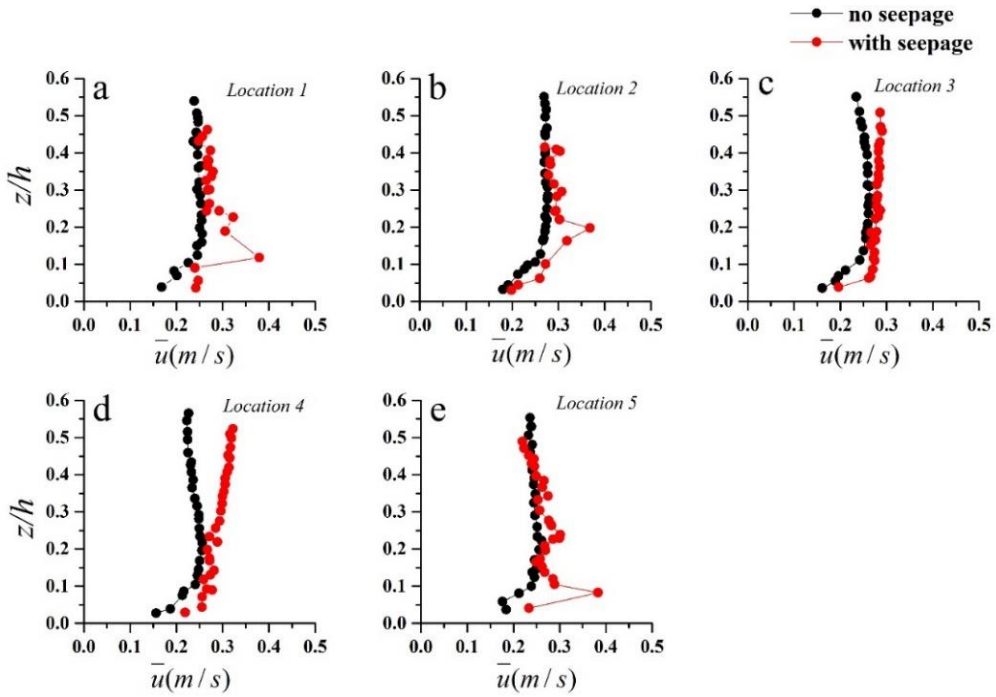

Figure 3.23 Streamwise velocity distribution in a mobile trapezoidal sinuous channel.

In trapezoidal sinuous channel, the percentage increase near the channel bed was 25% (location 1), 15% (location 2), 18% (location 3), 18% (location 4) and 22% (location 5). It was observed that downward seepage modifies the flow field in a channel bend at all these locations. Kavcar and Wright (2009) observed alteration in velocity distribution near the channel bed of straight flow in the presence of downward seepage.

3.4.3 Reynolds Shear Stress (RSS)

The Reynolds shear stress depicts the flow distribution within a sinuous bend. In sinuous bend, the flow is dominated by both primary and secondary flow due to channel curvature. The bend flow is subjected to a helical flow pattern, which results in cross circulation cells within the sinuous bend. The centrifugal force causes the surface flow to move towards the outer bend, and the bottom flow near the bed is deflected towards the inner bend due to the

radial pressure gradient. In a straight curved channel (Deshpande and Kumar, 2016), the Reynolds shear stress (RSS) distribution showed a typical triangular distribution where the RSS increased with a decrease in the distance from the boundary of the channel. However, the RSS distribution in curved sinuous channels depicts discontinuity in its distribution. The streamwise RSS $\tau_{zx} = -\rho\overline{u'w'}$ acting on the plane $X - Y$ and parallel to the flow direction is shown in Figures 3.24 and 3.25 for the rectangular and trapezoidal sinuous channels, respectively. The RSS distribution is both positive and negative, which depicts the helical flow in bends. The results infer the high momentum flux near the channel streambed due to downward seepage.

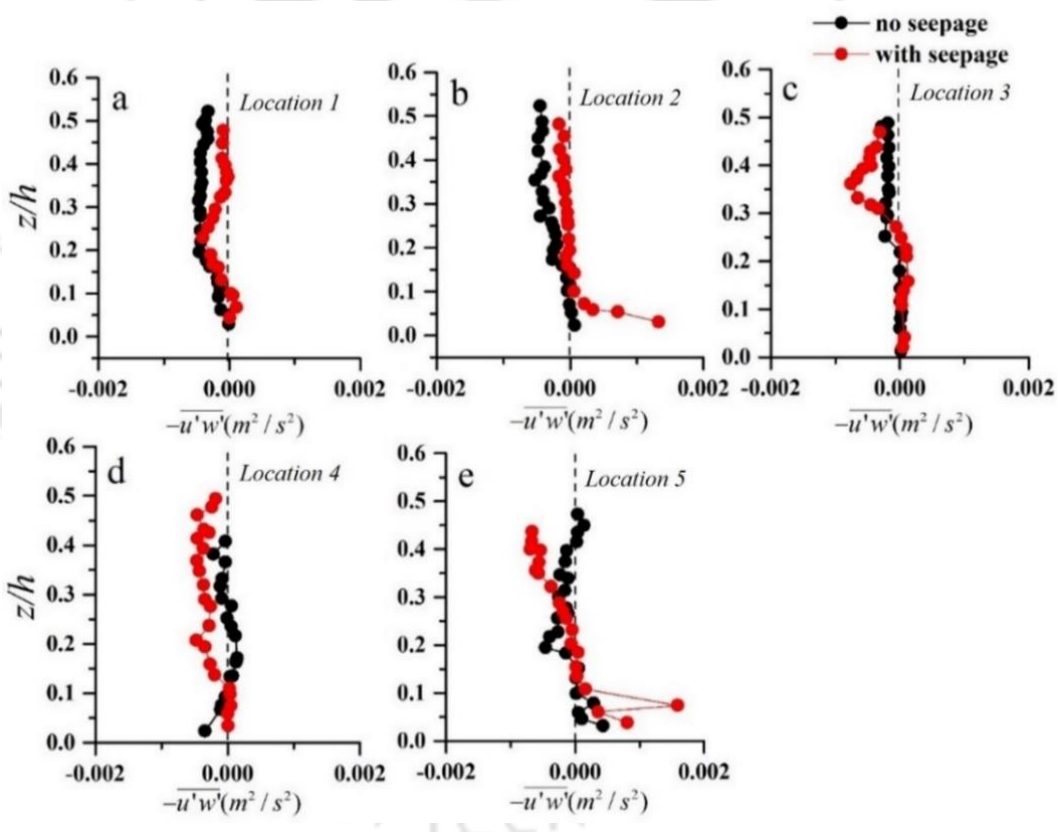

Figure 3.24 Streamwise Reynolds shear stress distribution in mobile rectangular sinuous channel.

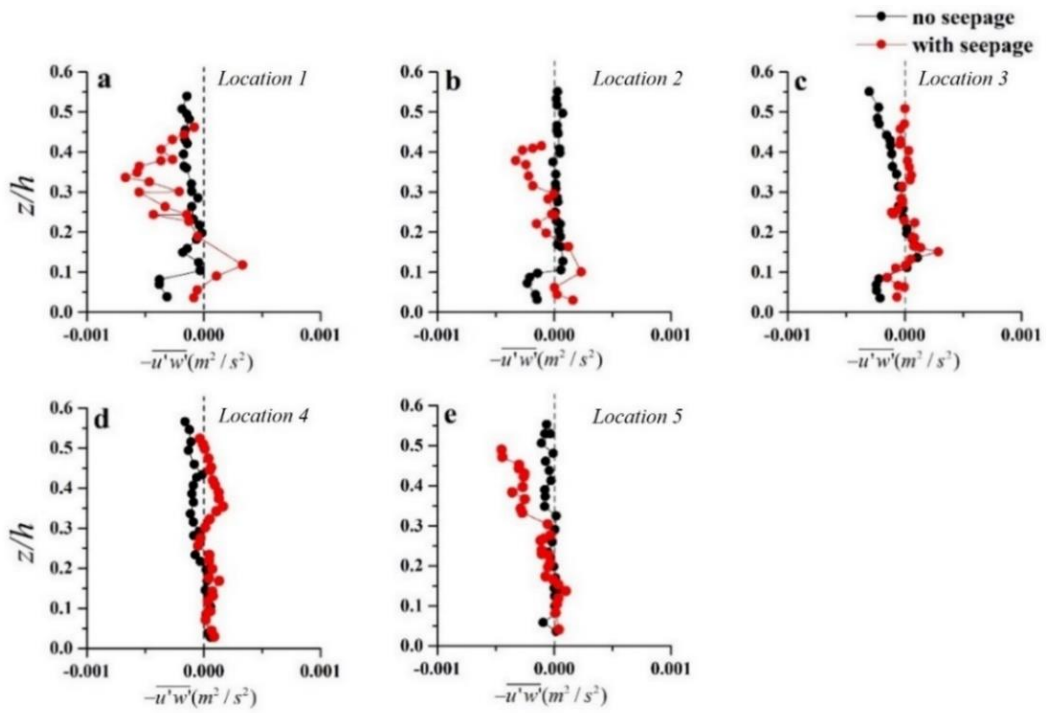

Figure 3.25 Streamwise Reynolds shear stress distribution in mobile trapezoidal sinuous channel.

3.4.4 Reynolds Normal Stress (RNS)

The streamwise, transverse and vertical turbulence intensities have been plotted for rectangular and trapezoidal mobile sinuous channels in Figure 3.26 and Figure 3.27. The vertical turbulent intensity $\left(\sqrt{\overline{w'w'}}\right)$ over the channel bed is lower throughout the flow depth, which indicates the dominance of the streamwise and transverse fluctuations. Within the sinuous bend, the magnitude of streamwise and transverse turbulence intensities is higher at all locations, which was also confirmed by Blanckaert and Graf (2001) and Engel and Rhoads (2017).

When the flow approaches the bend, high fluctuations prevail in the case of seepage flow, predominantly near the channel bed $(z/h < 0.2)$. Along the bend, the transverse turbulence intensity increased about 40% at average with seepage flow near the bed. For streamwise turbulence intensity, around 45% increase was observed near bed with seepage (Figure 3.26).

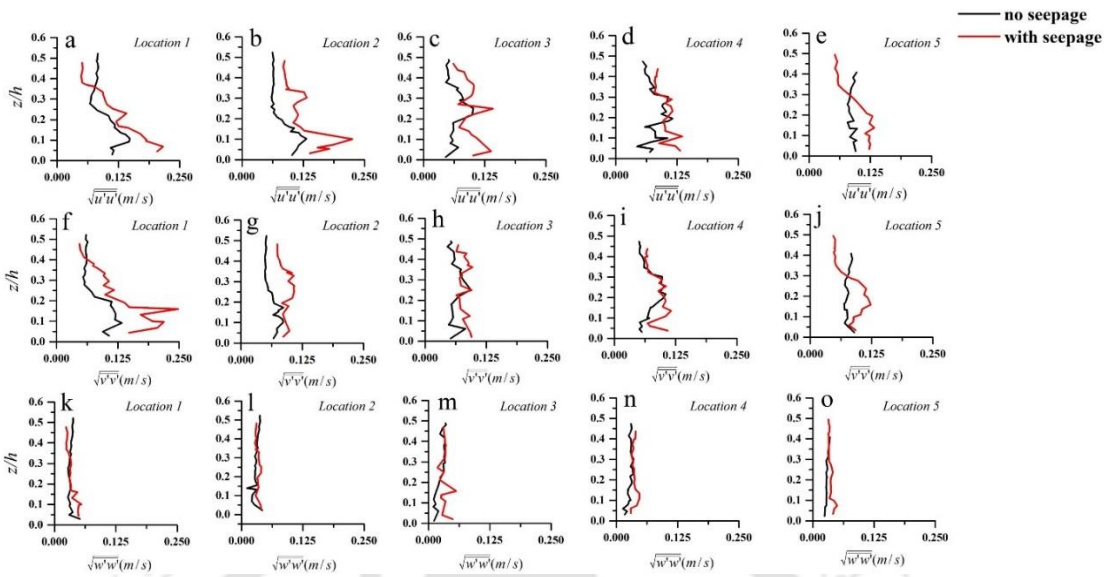

Figure 3.26 Turbulence intensity of mobile rectangular sinuous channel in streamwise direction ($a\ to\ e$), transverse direction ($f\ to\ j$), and vertical direction ($k\ to\ o$).

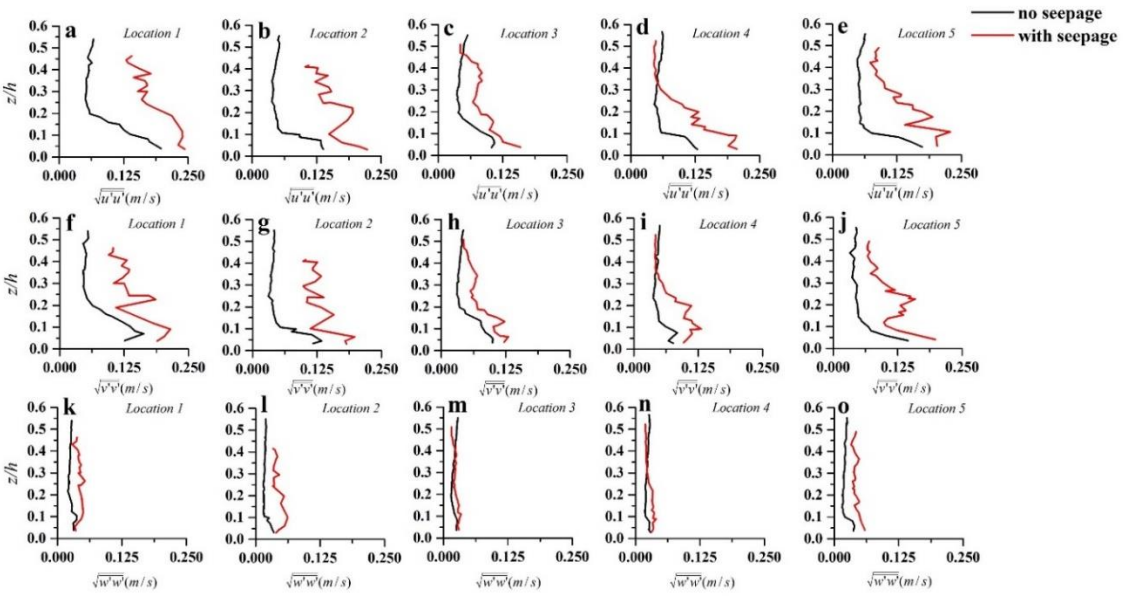

Figure 3.27 Turbulence intensity of mobile trapezoidal sinuous channel in streamwise direction ($a\ to\ e$), transverse direction ($f\ to\ j$), and vertical direction ($k\ to\ o$).

The trapezoidal sinuous channel flow is also characterized by an increase in streamwise and transverse turbulence intensities. At all the locations with downward seepage, the magnitude of the intensities has increased. There is an increase in streamwise turbulence intensity and transverse turbulence intensity with seepage (Figure 3.27).

3.4.5 Bed Shear Stress

Bed shear stress is an essential parameter in the study of fluvial processes. The channel materials are kept in motion by the shear stress acting at the boundary of the channel. Therefore, the movement of sediment particles can be associated with the bed shear stress (τ_o). Sediment motion occurs when the bed shear stress (τ_o) is greater than the critical bed shear stress (τ_c). There are many methods to calculate bed shear stress, but it has been a challenging to estimate in a bend (3-dimensional flow) because of its complexity. Generally, one of the widely used approaches to compute bed shear stress or shear velocity is by measuring the water surface slope under uniform flow conditions. However, the uniform flow condition with seepage is invalid. Recently, with the advancement in velocity measurements, bed shear stress can be calculated by measuring flow velocity. In a complex three-dimensional flow field, the estimation of bed shear stress by TKE is found to be robust and resilient, considering the velocity fluctuations in all three directions of flow. Yu et al. (2019) measured the shear stress on the cohesive bank of a sinuous bend by the turbulent kinetic energy (TKE) approach. Zhang et al. (2020) estimated the bed shear stress in a bend using the log-law method, Reynolds methods, turbulent kinetic energy (TKE) method, and TKE-w' method. They found the TKE-w' method to be more suitable than the TKE method. Biron et al. (2004) found the TKE method the best match with bed topography in complex flows. With the flow velocity measurements by ADV, the bed shear stress can be calculated by the TKE method (Section 3.3.4).

The turbulent kinetic energy was plotted against the normalized water depth ($\hat{z} = z/h$). The turbulent kinetic energy (TKE) profiles at all the five locations of the rectangular and trapezoidal bend are presented in Figure 3.28 and Figure 3.29. In all the profiles, TKE is found to be high, particularly near the channel bed ($z/h < 0.2$) with downward seepage.

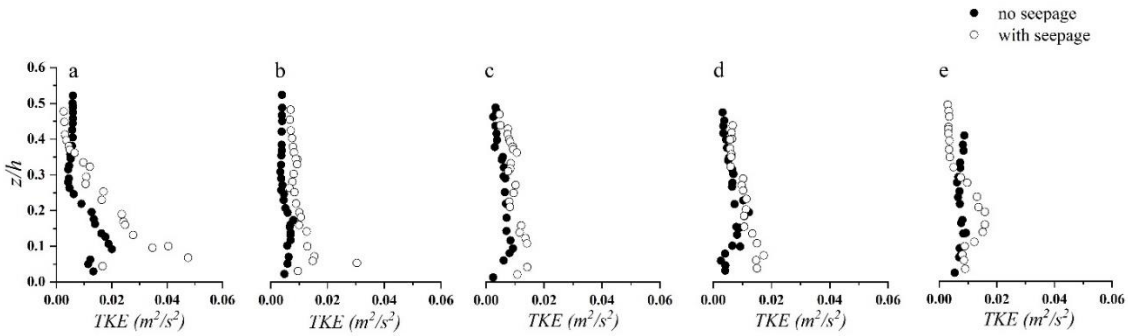

Figure 3.28. Turbulent Kinetic Energy (TKE) profiles in rectangular sinuous channel at (a) Location 1, (b) Location 2, (c) Location 3, (d) Location 4, and (e) Location 5.

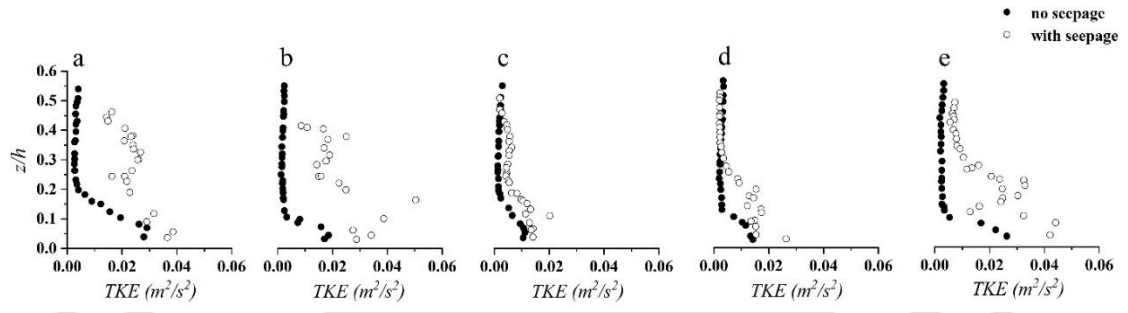

Figure 3.29. Turbulent Kinetic Energy (TKE) profiles in trapezoidal sinuous channel at (a) Location 1, (b) Location 2, (c) Location 3, (d) Location 4, and (e) Location 5.

The average bed shear stress near the channel bed at a non-dimensional height of 0.1 was computed for no seepage and with seepage, as shown in Table 3.7 and Table 3.8. The calculated bed shear stress at all the locations with seepage and without seepage was higher than the critical bed shear stress ($\tau_c = 0.686\ N/m^2$). An increment in bed shear stress in the case of downward seepage was observed. This increase in bed shear stress infers extra shear on the streambed of the sinuous channel. The higher bed shear stress links to the downstream migration of sediment with downward seepage, as noticed from the contour representation of morphological changes. At the bend upstream (location 1 and 2), the bed shear is high near the channel bed in the case of the trapezoidal sinuous channel (Table 3.8). This can be inferred from the high turbulence intensity fluctuations at the bend entrance.

Table 3.7 Bed shear stress (τ_o) in mobile rectangular sinuous channel ($z/h < 0.2$) for no Seepage (NS) and with seepage (WS) condition.

	Location 1		***Location 2***		***Location 3***		***Location 4***		***Location 5***	
Seepage condition	**NS**	**WS**	**NS**	**WS**	**NS**	**WS**	**NS**	**WS**	**NS**	**WS**
$\boldsymbol{\tau_o}$ *(N/m²)*	2.851	4.409	1.229	2.279	1.314	2.422	1.178	2.708	1.435	2.225

Table 3.8 Bed shear stress (τ_o) in mobile trapezoidal sinuous channel ($z/h < 0.2$) for no seepage (NS) and with seepage (WS) condition.

	Location 1		***Location 2***		***Location 3***		***Location 4***		***Location 5***	
Seepage condition	**NS**	**WS**	**NS**	**WS**	**NS**	**WS**	**NS**	**WS**	**NS**	**WS**
$\boldsymbol{\tau_o}$ *(N/m²)*	3.166	6.483	1.50	6.639	1.256	2.220	1.359	3.146	1.810	6.096

3.4.6 Summary

Seepage with high flow rate has shown much difference in the channel planform. With the application of low seepage velocity, noticeable changes were observed in the flow behavior. The Reynolds shear stress estimated with downward seepage has increased near the channel bed, indicating high momentum flux. The bed shear stress quantifies sediment transport rate, which was found to be high near the channel bed with seepage flows. As the flow interacts with the porous boundary of the channel, additional force is exerted on the sediment that results in excess sediment transport. The high bed shear on the streambed of the channel can be attributed to the morphological changes in the channel. Addressing the results, the study can be implemented to solve real problems of river engineering such as bank stability and failure of hydraulic structures.

4

Morphological Characteristics in a Sinuous Channel with and without Downward Seepage

4.1 Introduction

In this chapter, the morphological changes under the influence of downward seepage are discussed. The effect of downward seepage on the morphological changes was observed in three different types of sinuous channel. Bed features in a sinuous bend are intrinsically associated with the hydraulic and geometric conditions of the channel. In a sinuous channel, the banks are vulnerable, and with the application of downward seepage, excess momentum is generated at the proximity of the channel bed. Therefore, these changes in the hydraulic conditions may influence the morphology in a sinuous bend.

The morphological changes were analyzed along a bend of sinuous channel. Experiments were performed for different sinuous channels (Figure 2.17). For each of the sinuous channel, test was run for two discharge values. For one discharge, there was two set of experiments, no seepage and with seepage experiments.

Morphology investigation was conducted in three sinuous channels (Table 2.2); Case I rigid rectangular channel (a rectangular sinuous channel with rigid banks), Case III mobile rectangular channel (a rectangular sinuous channel with mobile bank and bed), and Case IV mobile trapezoidal channel (a trapezoidal sinuous channel with mobile bank and bed). The flow was gradually released from the overhead tank for each experimental run and entered the channel smoothly. The flow increased slowly until the channel achieved the steady flow conditions. For all the runs, the fully turbulent flow was achieved with a high Reynolds number greater than 10 000, and the flow was maintained at the sub-critical condition with Froude number less than 1.

A physical model of a sinuous channel was prepared in the laboratory flume. Scale effects may arise in physical modeling of sediment transport processes when all the forces in the model and the real field river are non-identical. As gravity is the primary driving force in open-channel flows, the Froude number similar to field conditions was attempted. In the field study by Engel and Rhoads (2012), the onsite Froude number (Fr) was about 0.3 (subcritical flow). The Froude number obtained in this study is very close to the field conditions. Most of the river flows are turbulent and in the hydraulic rough regime, where losses are independent of the Reynolds number. Therefore, the Reynolds number (Re) of the laboratory flows were greater than 10 000 and the shear Reynolds number (R_*) was achieved greater than 70 so that the laboratory flow was in the fully turbulent hydraulic rough regime to better account for the losses (Heller, 2011).

4.2 Morphological Changes in Rigid Rectangular Sinuous Channel

4.2.1 Experimental Conditions and Data Recording

Four experimental runs were conducted for this study, two for each flow discharge $Q = 0.0135\ \mathrm{m^3/s}$ and $Q = 0.0156\ \mathrm{m^3/s}$. No seepage and with seepage experiments were conducted for each discharge. In this study, the sides or banks of the channel were made rigid and the bed comprised of movable sediment of D_{50} 1.1 mm. The morphology observation was only at the bed of the sinuous channel. The measurement of bed changes was recorded at the second bend of the sinuous channel from the upstream to eliminate the entry and exit effects. At the inlet of the flume, sediment supply was not considered. In the rigid rectangular sinuous channel, smooth entry of the flow into the channel as well as smooth exit from the channel was ensured by providing guide vanes. The bed elevation along the sinuous bend was recorded with the Ultrasonic Ranging System (URS).

In this section, the results of Case 1 are presented for both no seepage and with seepage condition. To inspect the morphological changes along a bend, the experiments were run for a duration of $10 - 12$ h with bed materials in the state of motion. The main channel discharge was kept constant throughout the run. After 12 h, the bed materials were observed to be in the state of quasi-equilibrium (very slow bed movement with minimum change), after which the experiments were stopped. The Ultrasonic Ranging System (URS)

measured the geometry of the channel bed along the bend at 17 sections $(a, b, c, d, e, f, g, h, i, j, k, l, m, n, o, p, q)$ as shown in Figure 4.1. The transducers were mounted on a trolley and were aligned carefully to track the changes.

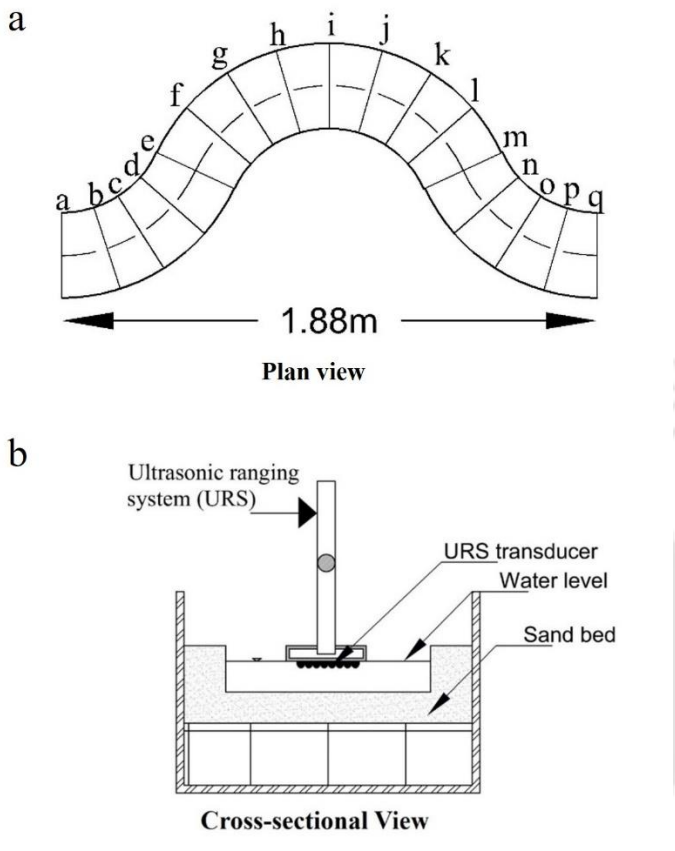

Figure 4.1 Sections $'a'$ to $'q'$ in the test section of the channel where bed elevation readings were made to track the morphological changes.

The URS provided the elevation (in centimeters) of the channel bed from the water surface. After desired discharge was achieved in the channel, the morphology readings were taken at every 2 h time interval without draining the water. The contour representations of the channel bed at 2 h, 4 h, 6 h, 8 h, and 10 h are shown with no seepage and seepage condition for two discharge values (Figure 4.3 to 4.6). The x-axis and y-axis denote the channel length (cm) and the channel width (cm), respectively. The colour scale presents the bed elevation in centimeters. The negative values signify the depth to the bed surface measured from the water surface. High values denote the maximum depth measured on the channel bed. The development of the bed surface in the channel is visible in the representation

(Figure 4.2). Without sediment feed at the upstream of the channel, both deposition and erosion in the channel bend were observed (from section $'a'$ to section $'q'$).

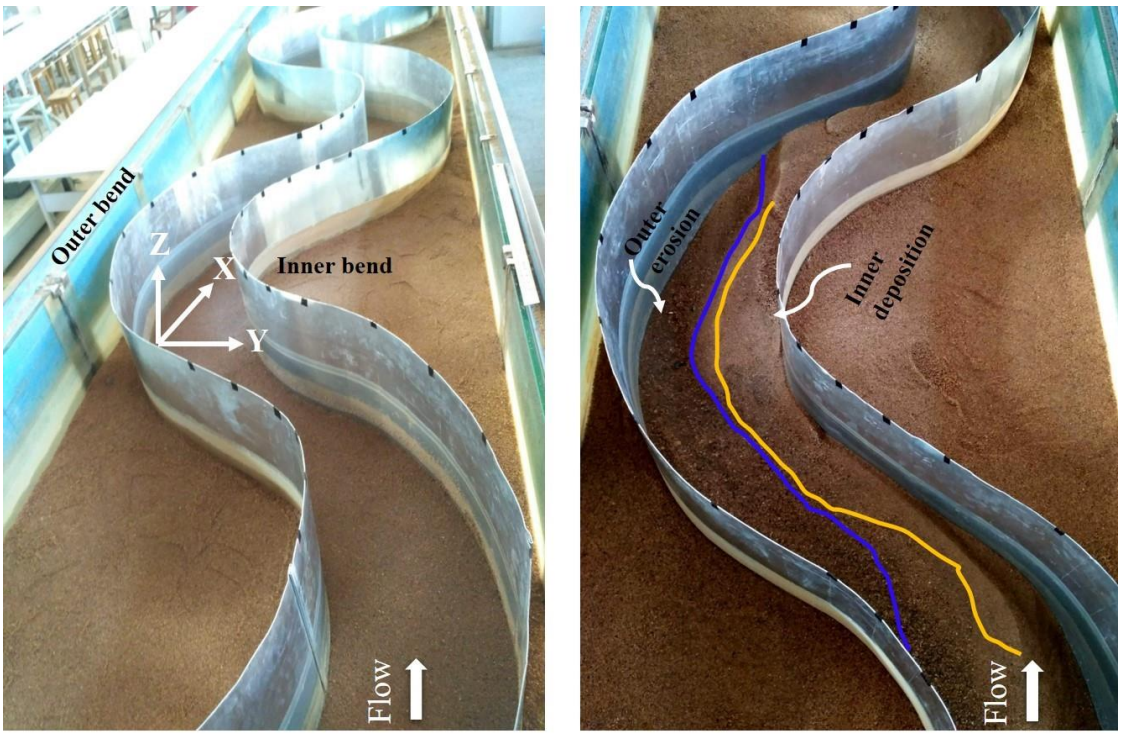

Figure 4.2 Photographs of morphological changes in rigid rectangular sinuous channel.

The erosion is a result of the transport of sediment particles. From a granular perspective, the motion of a sediment particle depends upon the balance of drag force exerted by the fluid flow and submerged weight of the particle. Classical turbulence parameter associated with transport is the average bed shear stress τ_o. When τ_o exceeds the critical bed shear stress value τ_c, erosion is expected. In our study, the critical or threshold shear stress (τ_o) for 1.1 mm sand size is 0.686 $\mathrm{N/m^2}$ from Shields' curve. Therefore, in our experiment, the sand particles were in motion, as the bed shear stress was higher than the critical shear.

4.2.2 Effect of Downward Seepage on the Morphological Changes in Rigid Rectangular Sinuous Channel

The erosion and deposition patches are visible in all the figures. With the acquired flow discharge, visible transport of sediment took place. The main highlight is the effect of

downward seepage. In Figures 4.3, 4.4, 4.5, and 4.6, the development of the channel bed was observed to change with time and downward seepage.

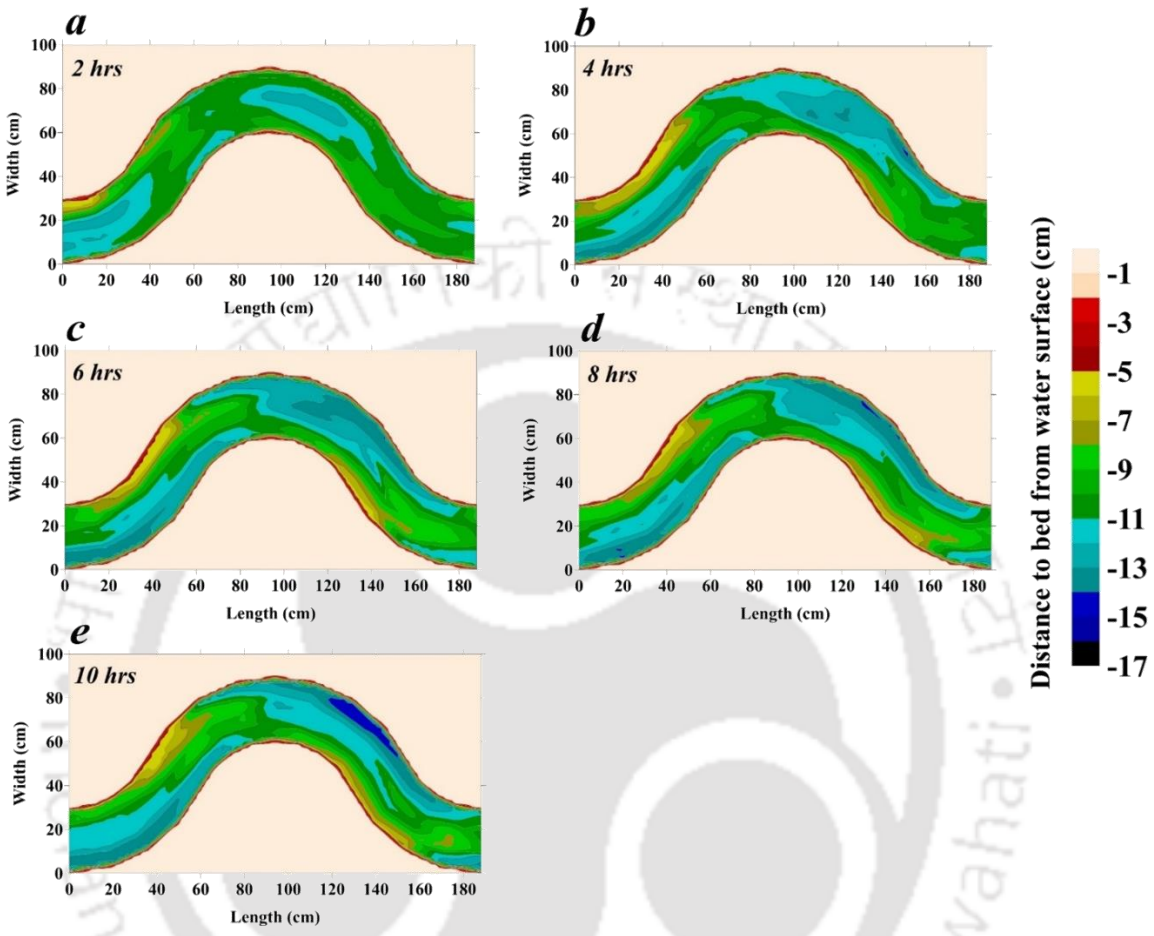

Figure 4.3 Contour representation of morphological changes along rigid rectangular sinuous bend for seepage velocity 0.0 mm/s ($Q = 0.0135\ \mathrm{m}^3/\mathrm{s}$).

The development of the channel bed without seepage and with discharge $Q = 0.0135\ \mathrm{m}^3/\mathrm{s}$ was nominal. Distinguished zones of deformation were not significantly noticed. With the same discharge rate and downward seepage application, few deeper scour zones were observed along the streambed. Investigation with seepage $(4\mathrm{h}, 6\mathrm{h}, 8\mathrm{h}, 10\mathrm{h})$ shows initial development of variation in bed along the outer and inner bend (Figure 4.4). With time, the scour depth at the outer bend is prominent. Under the condition of no seepage, minimum scour $(10\mathrm{h})$ at the outer region of the bend was observed (Figure 4.3). With the increase in seepage velocity, the scour at the outer zone increased due to the excess momentum at the bed proximity. Also, there were changes in the bed surface with

time until the sediment reached a condition of quasi-equilibrium, where minimum changes occurred.

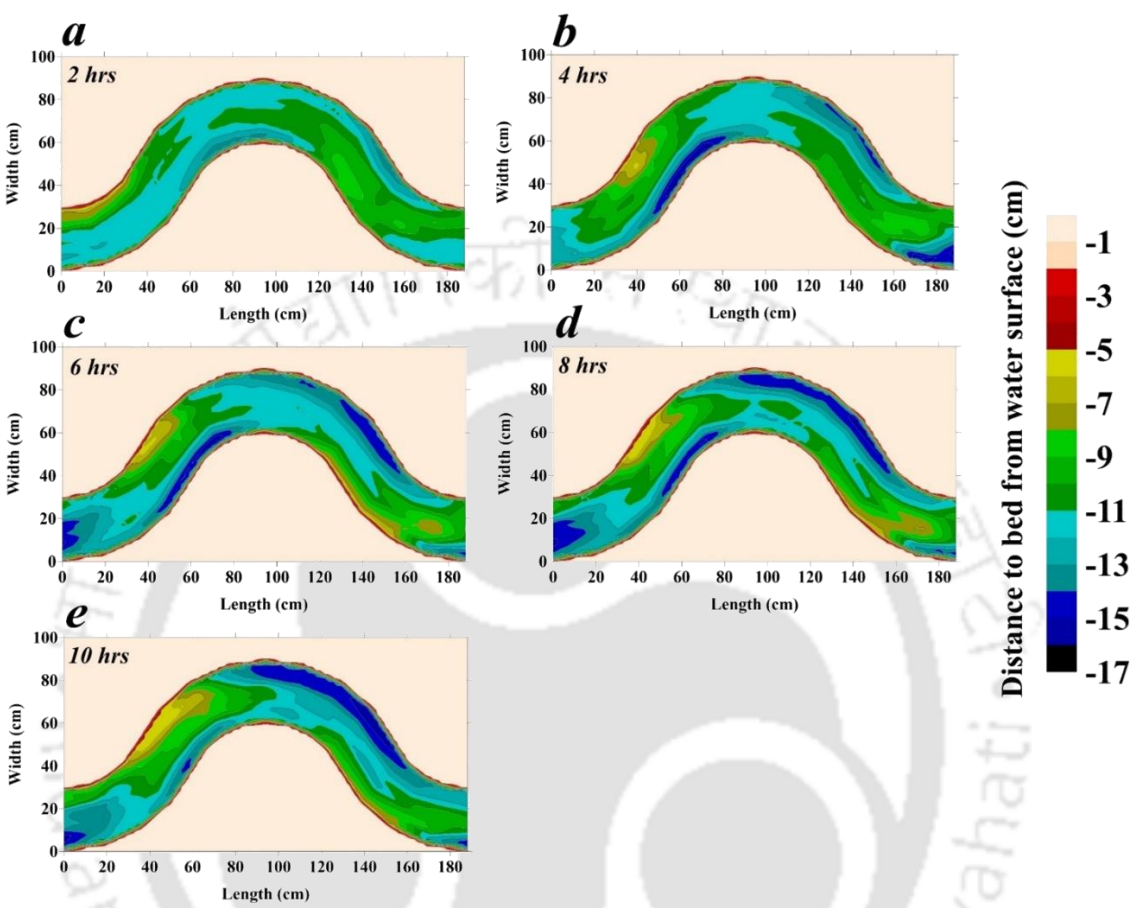

Figure 4.4 Contour representation of morphological changes along rigid rectangular sinuous bend for seepage velocity 0.3 mm/s ($Q = 0.0135\ \mathrm{m}^3/\mathrm{s}$).

With the increase in discharge rate $Q = 0.0156\,\mathrm{m}^3/\mathrm{s}$, the streambed was subjected to change without seepage (Figure 4.5). The erosion was mainly located near the bend apex. At the far upstream of the bend apex, a patch of deposited sand settled. This sand bar developed at the downstream of the previous inner bend. Just after the deposition zone, flow circulation takes place, thus referring to erosion presented in Figure 3.13. Keeping the discharge rate unchanged and with downward seepage, streambed development was distinct with scour zones at the outer region of the bend (Figure 4.6).

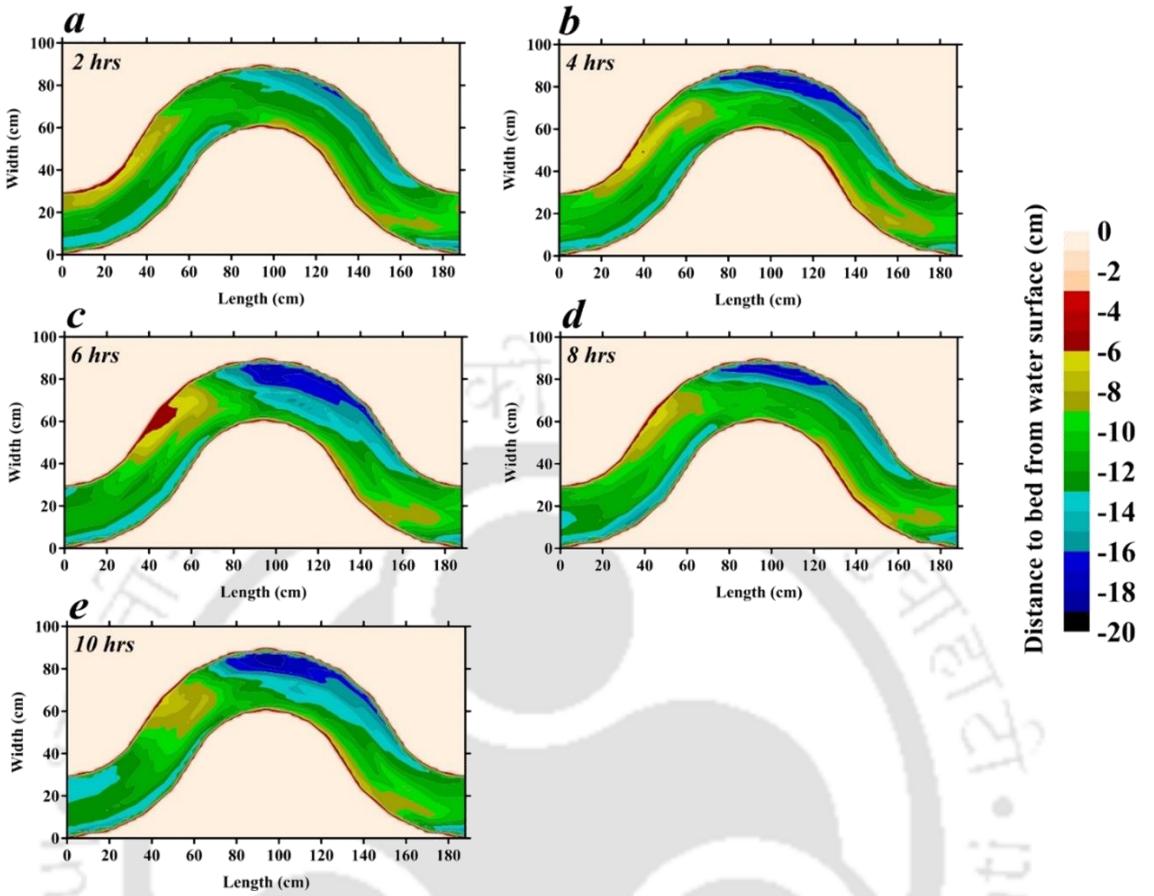

Figure 4.5 Contour representation of morphological changes along rigid rectangular sinuous bend for seepage velocity 0.0 mm/s ($Q = 0.0156\ \mathrm{m}^3/\mathrm{s}$).

The cross-sectional bed elevation across bend apex (section i) is shown in Figures 4.7, 4.8, 4.9, and 4.10 for all the cases in a rigid rectangular channel. Considering the initial level as the datum, the outer bend experiences erosion, which has increased with time. The flow characteristics and the channel planform play significant role in the development of morphological changes in a channel. With the scour in the outer part of the channel, the phenomenon cannot be attributed to the maximum velocity. In this study, the reported maximum mean velocity was observed at the inner region of the bend. Therefore, the observed morphological changes in the sinuous channel do not conform to the maximum velocity distribution. The outer bend of the sinuous channel possesses high fluctuating velocity as noticed from the flow stresses analyzed in the bend. Therefore, the outer bend erosion mostly depends on the velocity fluctuation or deviation from mean velocity rather than the mean velocity.

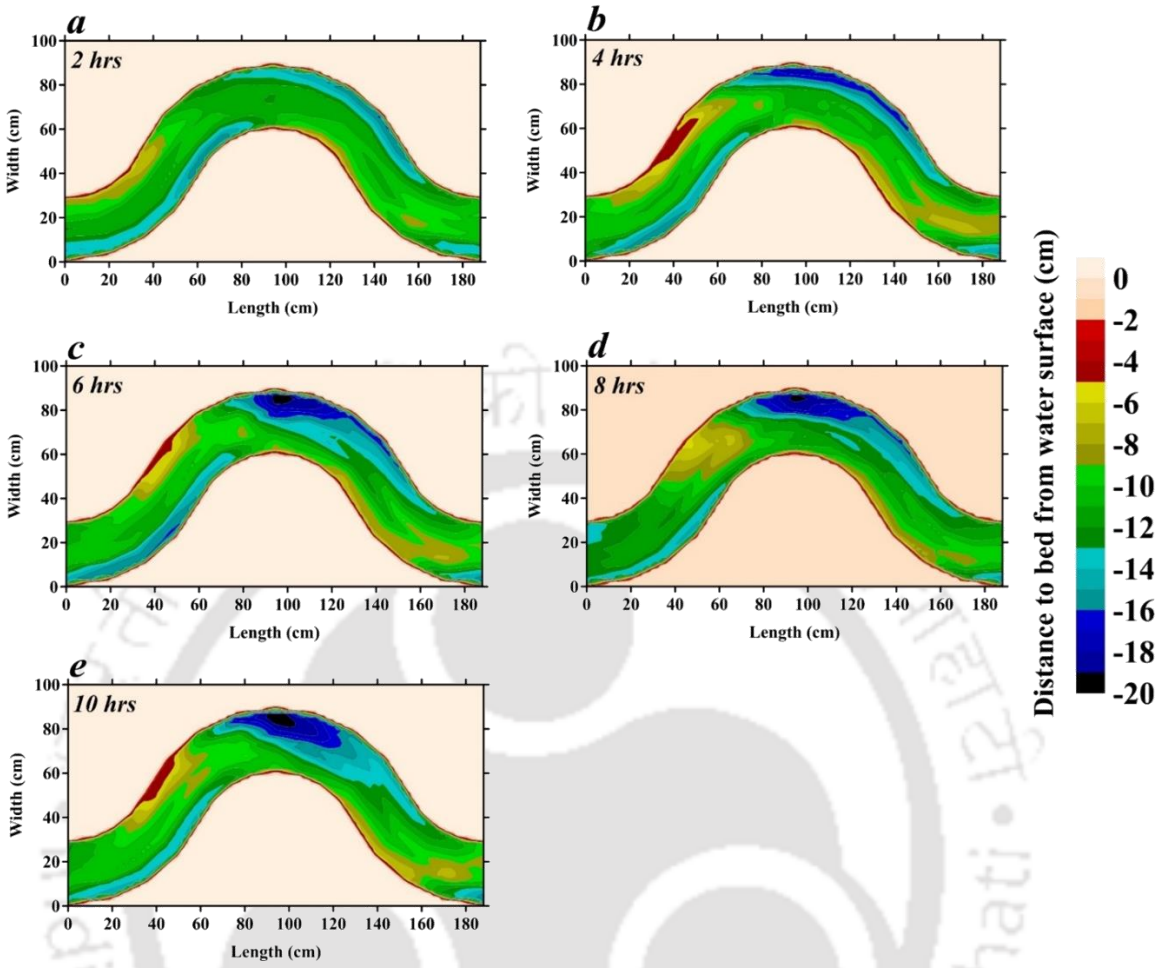

Figure 4.6 Contour representation of morphological changes along rigid rectangular sinuous bend for seepage velocity 0.3 mm/s ($Q = 0.0156\ \mathrm{m}^3/\mathrm{s}$).

It is evident from the cross-sectional profile that downward seepage is significant in the eroded region of the bend. The bed elevation near the outer zone has lowered with the application of downward seepage (Figure 4.8 and 4.10). From Figure 4.9 and 4.10, bed level has lowered with the increase in discharge ($Q = 0.0156\ \mathrm{m}^3/\mathrm{s}$). Both discharge and downward seepage influence the channel morphology. This refers to the point that when the discharge is high, the bed elevation is well defined due to downward seepage. The sediment transport increased with downward seepage since seepage generates excess momentum transfer at the bed proximity.

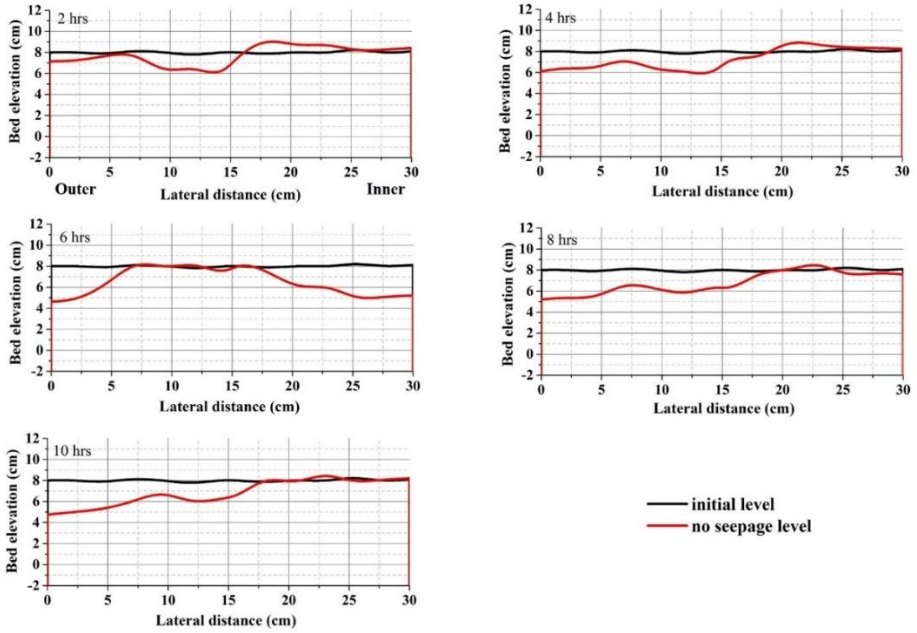

Figure 4.7 Cross-sectional profiles at the bend apex (section i) of the rigid rectangular channel for seepage velocity 0.0 mm/s ($Q = 0.0135\ m^3/s$).

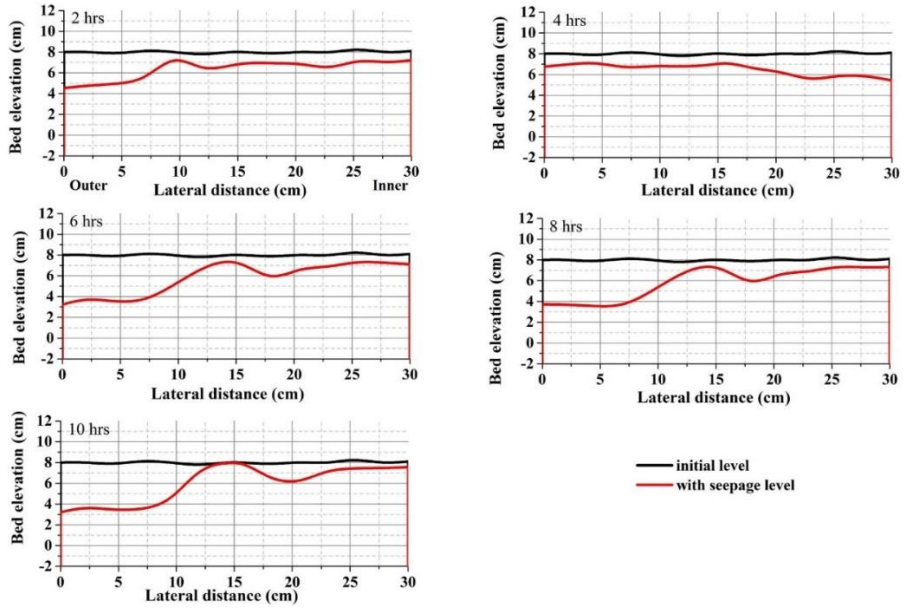

Figure 4.8 Cross-sectional profiles at the bend apex (section i) of the rigid rectangular channel for seepage velocity 0.3 mm/s ($Q = 0.0135\ m^3/s$).

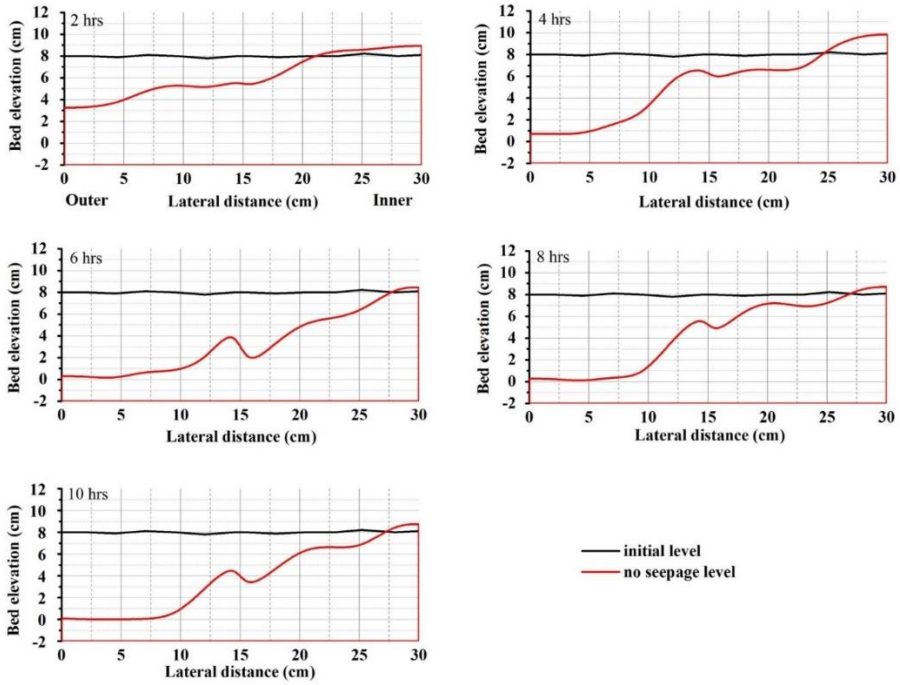

Figure 4.9 Cross-sectional profiles at the bend apex (section i) of the rigid rectangular channel for seepage velocity 0.0 mm/s ($Q = 0.0156\ m^3/s$).

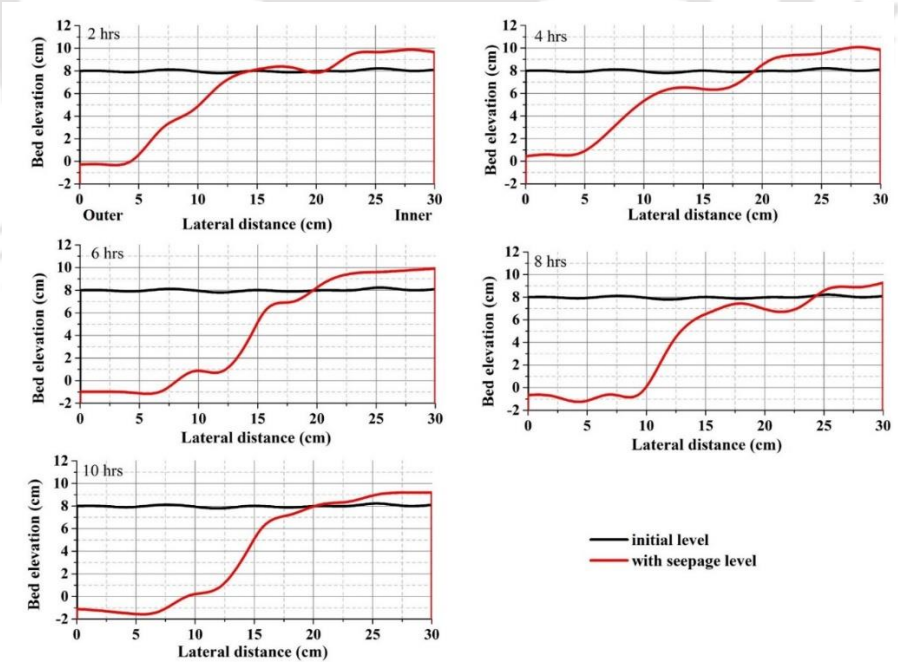

Figure 4.10 Cross-sectional profiles at the bend apex (section i) of the rigid rectangular channel for seepage velocity 0.3 mm/s ($Q = 0.0156\ m^3/s$).

4.2.3 Time – dependent Celerity

Wavelet Transform

Sediment transport in a bend is a continuous process leading to morpho-dynamical changes in the channel bed in the form of erosion and sedimentation. The migration speed of the channel bed was statistically estimated by wavelet analysis. To evaluate the time-dependent celerity in bend, the bed elevation was recorded by ultrasonic ranging system for every 3 sec at different time intervals in a single experimental run, each for no seepage and with seepage. The measurements were made at the bend apex (section i) and at the bend upstream (section f). The flow in bends erodes the bed material from the outer bank and deposits at the inner. With seepage, lateral flow occurs from the channel bed, which impacts the flow behavior and sediment transport rate.

Various researchers investigated morpho-dynamic changes of bedforms from initial to an equilibrium state to explain the complex configuration of bedforms developed under the action of open channel flow (Coleman and Melville, 1994; Jerolmack and Mohrig, 2005). Recent works have shown bedform characterization (temporal and spatial) statistically at multiple scales (Nikora and Goring, 2001; Sharma et al., 2017; Barman et al., 2017). Previous researches have exposed the existence of multi-scale dynamic properties in migrating natural bedforms. Singh et al. (2011) have extensively analyzed the multi-scale dynamic properties of bedform configuration. This study focuses on evaluating the migration of bed materials under the effect of seepage in a steady-state flume experiment. Scale-dependent celerity of bedform development at the bend is evaluated over a different range of temporal scales. To assess this event, wavelet analysis provides valuable insights and a clear understanding. The bed elevation time series at the bend center (section i) and at the bend upstream (section f) were treated as a discrete signal over the time domain. The bed elevation time series at these two locations were denoted as two signals $f_1(t)$ and $f_2(t)$, respectively. For a function $f(t)$, the wavelet transform is defined as an integral transform with a series of functions $\psi_{a,b}(t)$, that is,

$$W_{f(t)}(a,b) = \int_{-\infty}^{+\infty} f(t)\psi_{a,b}(t)dt \qquad (4.1)$$

where $\psi_{a,b}$ is a wavelet function which comes from a mother wavelet called $\psi(t)$, given by:

$$\psi_{a,b}(t) = \frac{1}{\sqrt{a}}\psi\left(\frac{t-b}{a}\right) \tag{4.2}$$

where a and b are known as scaling and translation (i.e., location along with the signal) parameter, respectively. $1/\sqrt{a}$ is a multiplying factor used to normalize the variance (Mallat, 1999). The admissibility condition must be satisfied for wavelet transform is that the wavelet function should be zero i.e., $\int_{-\infty}^{+\infty}\psi(t)dt = 0$. The frequently used mother wavelet belongs to the family of Gaussian-based wavelets, which are classified as the Nth-order derivatives of a Gaussian function $g_o(t)$, i.e., $g_N(t) = (d^N/dt^N)g_0(t)$ where $N = (1,2,3,\dots)$. In the present study, a Mexican hat wavelet $g_2(t)$ was used which has a number of vanishing moments of $N = 2$. More details on wavelets can be found in previous literature (Kumar and Foufoula-Georgiou, 1997).

$$g_2(t) = \frac{2}{\sqrt{3}}\pi^{-1/4}(1-t^2)e^{-t^2/2} \tag{4.3}$$

The wavelet coefficients of the bed elevation time series of both the locations at various scales and translation are obtained by the expression:

$$WC(a,b) = \frac{1}{\sqrt{a}}f(t)g_2\left(\frac{t-b}{a}\right)dt \tag{4.4}$$

Wavelet Cross-correlation

Analysis of cross-correlation facilitates the statistical solution of the measure of waveform relationship between the stationary time series of two data sets. A quantitative measure of the linear dependence between two signals when it travels with time with respect to each other can be estimated with the cross-correlation coefficient. WCC is the wavelet cross-correlation between two signals $f_1(t)$ and $f_2(t)$. It is calculated as:

$$WCC_{f_{1(t)},f_{2(t)}}(a,\Delta t) = \int_{-\infty}^{+\infty} WC_{f_1}(a,b)WC_{f_2}(a,b+\Delta t)db \tag{4.5}$$

where, $WC_{f_1}(a,b)$ and $WC_{f_2}(a,b+\Delta t)$ are the wavelet coefficients of bed elevation time series $f_1(t)$ and $f_2(t)$, respectively at scale a and two consecutive locations b and $b+\Delta t$

along with the signals. For a particular scale a, the standard cross-correlation analysis corresponding to the time lag Δt_{max}, which resulted in maximum cross-correlation between the two signals $f_1(t)$ and $f_2(t)$, was used to estimate the average bedform celerity. The celerity at scale a can be calculated as $V_c(a, \Delta t) = L/\Delta t_{max}$, where L is the spatial distance, i.e., the distance between the two measuring locations of bed elevation.

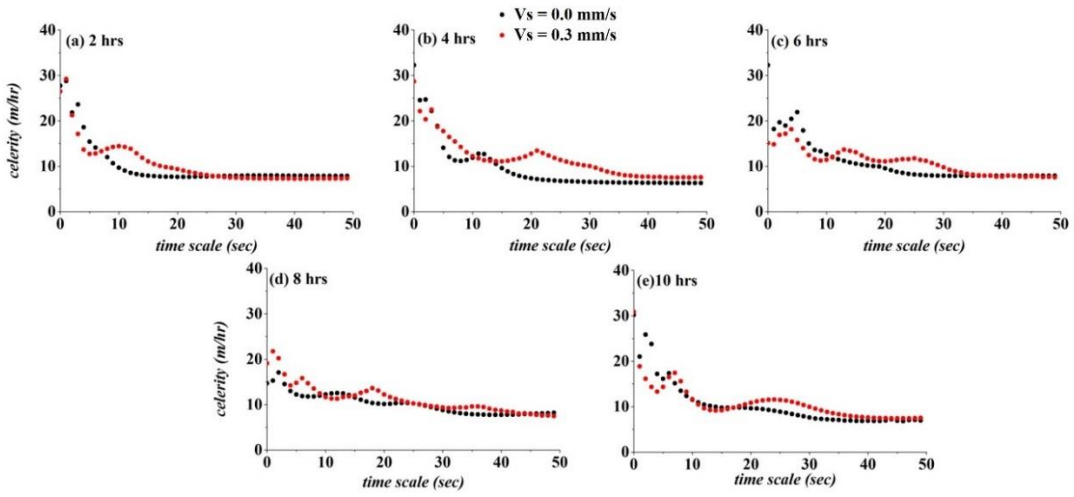

Figure 4.11 Time scale celerity at bend upstream and bend apex (section f and i) of the rigid rectangular channel.

The time scale dependent celerity was calculated for two locations, section f and i, for both seepage and no seepage condition with discharge $Q = 0.0156$ m^3/s at various time scale. The celerity plots at different run time of the experiment (2 h to 10 h) are presented in Figure 4.11. The statistical values of bed celerity at various time scale are given in Table 4.1.

The celerity gradually decreases with the increase in scale and becomes constant after a certain time scale. The celerity is high at lower time scale. The celerity becomes constant at about 15s for no seepage, and at about 25s for with seepage. For time scale less than 30s, the celerity is faster with seepage. The average celerity or speed of the evolution of bedforms is found to be high with seepage in comparison to no seepage (Table 4.1). Thus, the celerity has increased with downward seepage, that is, a higher rate of sediment transport under the action of seepage. As the rate of transport has increased with seepage, the erosion at the outer bank of the bend has increased as observed from the morphological

study. In this line, the analysis confirmed that the change or evolution of bedforms has increased with downward seepage.

Table 4.1 Time-dependent celerity at different time scale for no seepage and with seepage.

Time scale (sec)	Celerity (m/h)									
	$V_S = 0.0$ mm/s					$V_S = 0.3$ mm/s				
	2 h	4 h	6 h	8 h	10 h	2 h	4 h	6 h	8 h	10 h
1	27.711	32.248	32.244	14.672	30.192	26.466	28.666	15.083	19.095	30.881
2	28.744	24.556	18.181	15.291	21.003	29.199	22.122	14.820	21.721	18.837
3	21.809	24.691	19.665	17.053	25.853	21.242	20.334	16.864	20.211	16.143
4	23.617	22.179	18.961	14.532	23.781	17.127	22.421	17.151	16.656	14.323
5	18.605	18.845	20.446	12.992	17.205	13.667	18.681	18.141	14.188	13.292
6	15.391	14.062	21.905	12.217	16.123	12.704	17.736	15.754	14.778	14.347
7	14.095	12.061	17.874	11.879	17.335	12.811	16.434	13.964	15.787	16.479
8	13.289	11.287	15.015	11.774	15.149	13.290	15.452	12.465	14.694	17.415
9	11.978	11.162	13.560	11.796	13.498	13.844	14.233	11.568	13.501	15.572
10	10.638	11.385	13.299	11.959	12.350	14.244	13.098	11.259	12.432	13.269
11	9.680	11.885	12.602	12.203	11.511	14.406	12.238	11.403	11.655	11.657
12	9.034	12.749	12.057	12.441	10.935	14.262	11.713	11.947	11.312	10.457
13	8.570	12.652	11.568	12.536	10.442	13.841	11.321	12.965	11.280	9.622
14	8.263	11.565	11.196	12.453	10.160	12.863	11.183	13.677	11.643	9.213
15	8.055	10.525	10.857	12.104	9.926	11.849	11.113	13.400	11.783	9.110
16	7.907	9.578	10.557	11.559	9.769	11.065	11.065	13.063	12.021	9.192
17	7.819	8.843	10.322	11.079	9.773	10.484	11.214	12.379	12.575	9.430
18	7.751	8.282	10.142	10.657	9.778	10.078	11.456	11.671	13.004	9.744
19	7.709	7.878	10.008	10.354	9.791	9.792	11.741	11.272	13.607	10.109
20	7.677	7.564	9.917	10.186	9.737	9.609	12.135	11.109	13.067	10.489
21	7.661	7.332	9.537	10.105	9.638	9.369	12.740	11.043	12.204	10.842
22	7.661	7.171	9.114	10.166	9.562	9.045	13.442	11.187	11.635	11.149
23	7.673	7.044	8.787	10.288	9.463	8.747	12.888	11.384	11.217	11.379
24	7.692	6.940	8.538	10.356	9.279	8.486	12.378	11.533	10.843	11.503
25	7.724	6.845	8.336	10.359	9.097	8.244	11.818	11.545	10.536	11.535
26	7.759	6.776	8.191	10.269	8.864	8.043	11.378	11.711	10.253	11.475
27	7.793	6.717	8.101	10.073	8.623	7.869	11.023	11.374	10.050	11.314
28	7.828	6.654	8.005	9.774	8.385	7.724	10.647	11.199	9.887	11.065
29	7.864	6.607	7.957	9.439	8.111	7.614	10.443	10.716	9.679	10.742
30	7.894	6.561	7.926	9.091	7.885	7.528	10.207	10.274	9.550	10.355
31	7.921	6.523	7.911	8.771	7.617	7.457	10.027	9.775	9.357	9.945
32	7.939	6.488	7.896	8.498	7.397	7.405	9.648	9.243	9.243	9.543
33	7.958	6.470	7.898	8.285	7.276	7.368	9.202	8.901	9.263	9.156
34	7.968	6.453	7.905	8.118	7.193	7.335	8.800	8.625	9.348	8.828
35	7.976	6.436	7.912	7.985	7.117	7.315	8.488	8.318	9.366	8.545
36	7.973	6.417	7.917	7.890	7.061	7.300	8.214	8.153	9.568	8.310
37	7.967	6.404	7.919	7.811	6.932	7.288	8.010	8.025	9.563	8.106
38	7.955	6.401	7.933	7.771	6.926	7.275	7.904	7.914	9.432	7.937
39	7.942	6.395	7.927	7.754	6.864	7.273	7.791	7.946	9.102	7.798
40	7.934	6.366	7.922	7.736	6.848	7.275	7.686	7.715	8.827	7.686
41	7.914	6.369	7.936	7.753	6.874	7.269	7.684	7.715	8.682	7.600
42	7.903	6.355	7.920	7.776	6.836	7.270	7.624	7.948	8.471	7.529
43	7.885	6.344	7.916	7.798	6.825	7.265	7.635	7.923	8.370	7.485

44	7.882	6.351	7.922	7.842	6.925	7.272	7.508	7.761	8.020	7.451
45	7.869	6.322	7.915	7.901	7.212	7.276	7.528	7.622	8.048	7.432
46	7.864	6.328	7.916	7.944	6.900	7.285	7.515	7.779	7.879	7.428
47	7.857	6.326	7.908	8.002	6.807	7.288	7.584	7.784	7.739	7.436
48	7.856	6.328	7.906	8.047	7.016	7.300	7.530	7.590	7.620	7.450
49	7.864	6.315	7.906	8.119	7.058	7.310	7.562	7.663	7.600	7.469
50	7.870	6.295	7.911	8.172	6.928	7.322	7.550	7.576	7.459	7.498
Average Celerity (m/h)										
	10.084	9.607	10.863	10.193	10.477	10.433	11.656	10.878	11.276	10.831

4.2.4 Summary

The presence of downward seepage caused morphological instabilities along the sinuous bend. The streambed development in the channel bed was a function of fluctuating velocity and the active seepage present near the channel bed. At the outer bend region, the magnitude of the velocity fluctuation moment is significant, indicating erosion, even without downward seepage. The altered flow with seepage affected the transport of sediment and caused noticeable modifications along the channel bed. With seepage, the erosion rate enhanced along the outer bend of the channel. With time scale, the celerity was observed to increase with downward seepage. The increase in the average bed celerity can be attributed to a high rate of sediment transport.

4.3 Morphological Changes in Mobile Boundary Sinuous Channel

4.3.1 Experimental conditions and Data Recording

To examine the effect of downward seepage on the morphology of the sinuous channel, the bed morphology was measured with the help of a digital point gauge. The readings were taken at the second bend of the sinuous channel after the water was drained completely from the main channel at the end of the experiment. At the initiation of the experiments, the sediment transport was rapid, therefore, the recording of bed elevation with the Ultrasonic Ranging System during the experiments was not feasible. After 12 h, the channel achieved a quasi-equilibrium state, showing no or very little change along the channel. The experiment was stopped after 12 h run, and the water was drained from the main channel. Then the exposed bed surface was measured by the digital point gauge (least

count 0.01 mm), which displayed the elevation from a reference datum on the channel bed, which was set to zero on the channel bed before the start of the experiment. The point gauge was mounted on a trolley and recorded the bed deformation along the longitudinal and transverse direction of the sinuous bend. Based on the above procedure, the no seepage experiments were conducted first for each discharge, following seepage experiments This section aims to inspect the morphological changes in an active seepage alluvial channel.

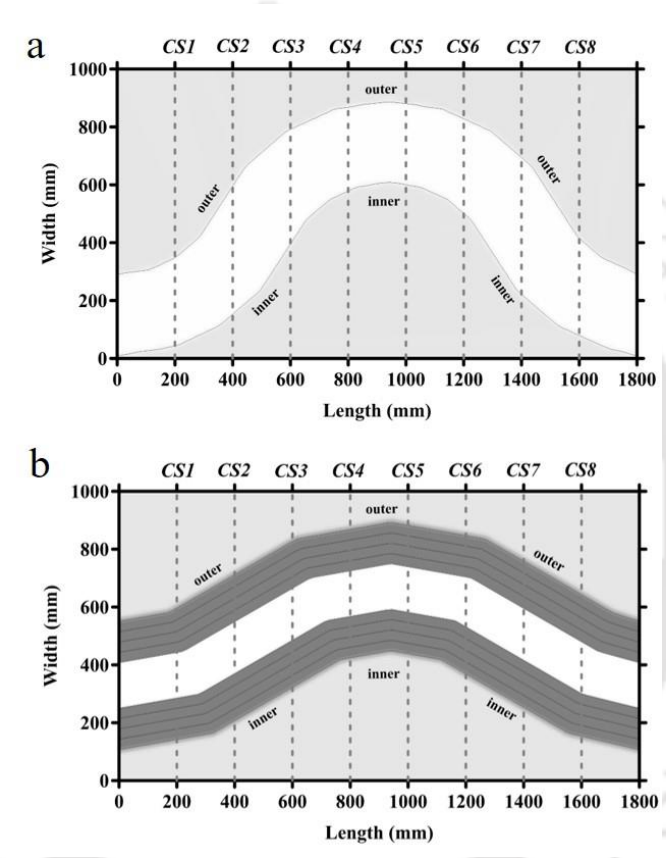

Figure 4.12 Morphological measurements across the cross-sections in (a) mobile rectangular sinuous bend, and (b) mobile trapezoidal sinuous bend.

Cross-sectional profiles, contour representation, and 3-dimensional surface plots are presented for two discharges, 0.00629 m^3/s, and 0.00793 m^3/s. For each discharge, the changes were observed with the effect of downward seepage with respect to without seepage experiments. The cross-sectional profiles are shown for eight cross-sections (*CS1* to *CS8*) of the sinuous bend given in Figure 4.12. Along these eight sections, the bed elevation was measured. For the bend morphology, the data points were recorded in the x-

direction (along the channel length) for every 200 mm and in the y-direction (along the channel width) every 20 mm. Approximately, 300 to 350 data points were collected for fine contouring of the bed elevation. The deformation along the streambed and bank of the sinuous channels showed remarkable alteration as shown in Figure 4.13. Bank erosion in a sinuous alluvial channel is a continuous phenomenon resulting in bank instability and sediment migration.

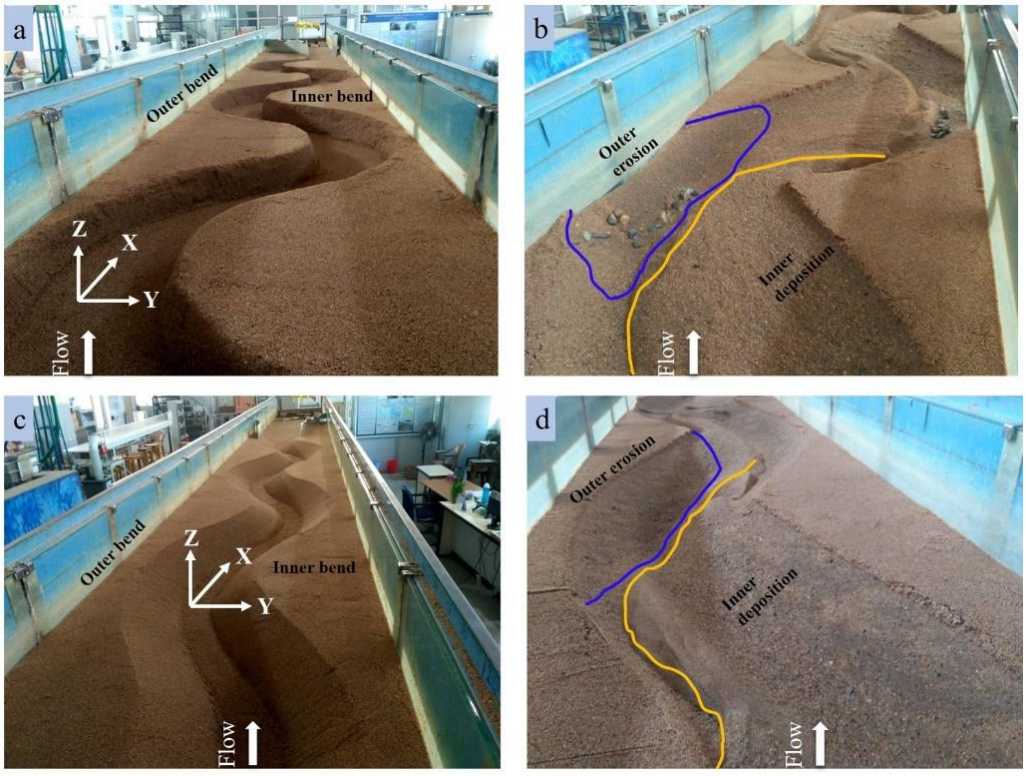

Figure 4.13 Photographs of morphological changes in (a, b) mobile rectangular sinuous channel and (c, d) mobile trapezoidal sinuous channel.

4.3.2 Effect of Downward Seepage on the Morphological Changes in Mobile Rectangular Sinuous Channel

In the experiments, sediment transport was noticed in the channel with the development of sand bars and pools at the bends. Sediment migration to the downstream of the channel was found in the channel, until it achieved a quasi-equilibrium state (no change or very little change in the bed surface elevation). The channel evolved with time, and the banks were continuously changing with the flow.

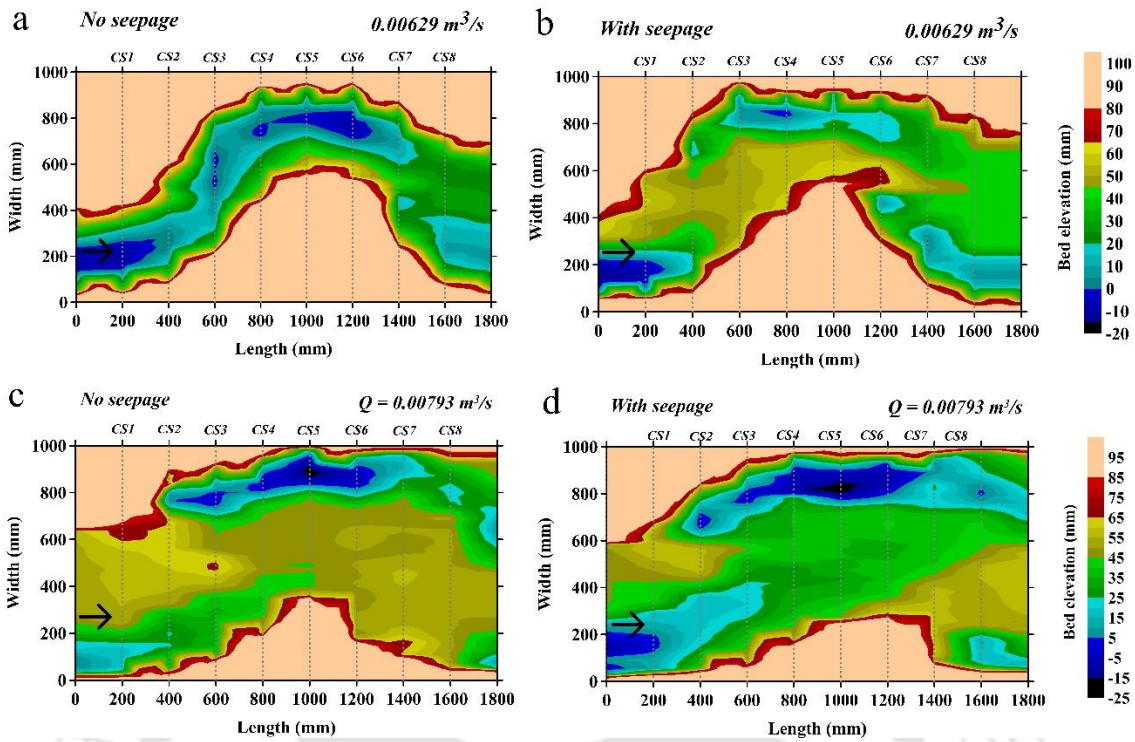

Figure 4.14 Contour plots of the morphological changes in mobile rectangular sinuous bend (a, c) no seepage and (b, d) with seepage flow.

The contour plots of the morphological changes are presented in Figure 4.14 for two discharge rates. The arrows denote the flow direction. The increase in inflow discharge showed different morphological changes along the channel. The erosion at the outer region and deposition at the inner region of the bend became prominent with the increase in discharge. Comparing the no seepage and with seepage cases [Figure 4.14(a) and Figure 4.14(b)], changes were observed, which indicates an increase in the transport of sediment. At the inner region of the bend, a huge sediment deposition occurred, although the erosion has reduced at the outer bend with seepage. This change along the bend with seepage translates the potential of the seepage activity to assist in the sediment transport. However, the small flow rate in the channel has hindered the sediment from moving further downstream. The flow rate is one of the factors in the development of morphological features of a channel. The other factors are the channel shape, groundwater flow and nature of sediment. Widening of the channel at the downstream end was associated mainly with erosion along the bankline.

Figure 4.14(c) and Figure 4.14(d) present the contour plots for no seepage and seepage cases with a higher flow discharge of 0.00793 m^3/s. In both the plots, prominent deposition and erosion zone was observed. With downward seepage, the area of erosion has increased at the outer bend location. As well, at the inner bend location, the deposition has reduced. This indicates sediment migration downstream with seepage at the inner bank and shifting of the channel planform in the downstream direction.

Representation of the 3-dimensional surface plots indicates that with increase in flow rate, seepage activity can cause significant modification across the sinuous bend (Figure 4.15 and 4.16). High bed shear stress estimated at the center of the sinuous bend provides evidence on sediment transport. The flow passing along the channel approaches the outer bend channel bed with higher fluctuating velocities compared to no seepage condition. The increased flow rate and downward seepage caused greater streambed modifications.

In Figure 4.17, for discharge 0.00629 m^3/s, the cross-sectional profiles represent the bed elevation for no seepage and with seepage cases. with seepage condition, the banks of the sinuous bend have shifted as compared to the no seepage. In *CS1* to *CS3*, towards the outer region, and in *CS6* to *CS8*, towards the inner region, the banks are found to shift for with seepage cases. However, at the bend apex (*CS4* and *CS5*), the change was found to be minimum. One distinctive observation in these profiles is the raised bed elevation with seepage. Sediments from the upstream moved downstream, showing higher bed elevation due to increased sediment transport with downward seepage. In Figure 4.18, with increased flow discharge rate (0.00793 m^3/s), the morphological changes in the channel were observed. Without downward seepage, the channel has widened eroding the banks of the channel with the increase in flow rate. With downward seepage, the bed elevation has lowered, which indicate washing away of sediment further downstream of the channel.

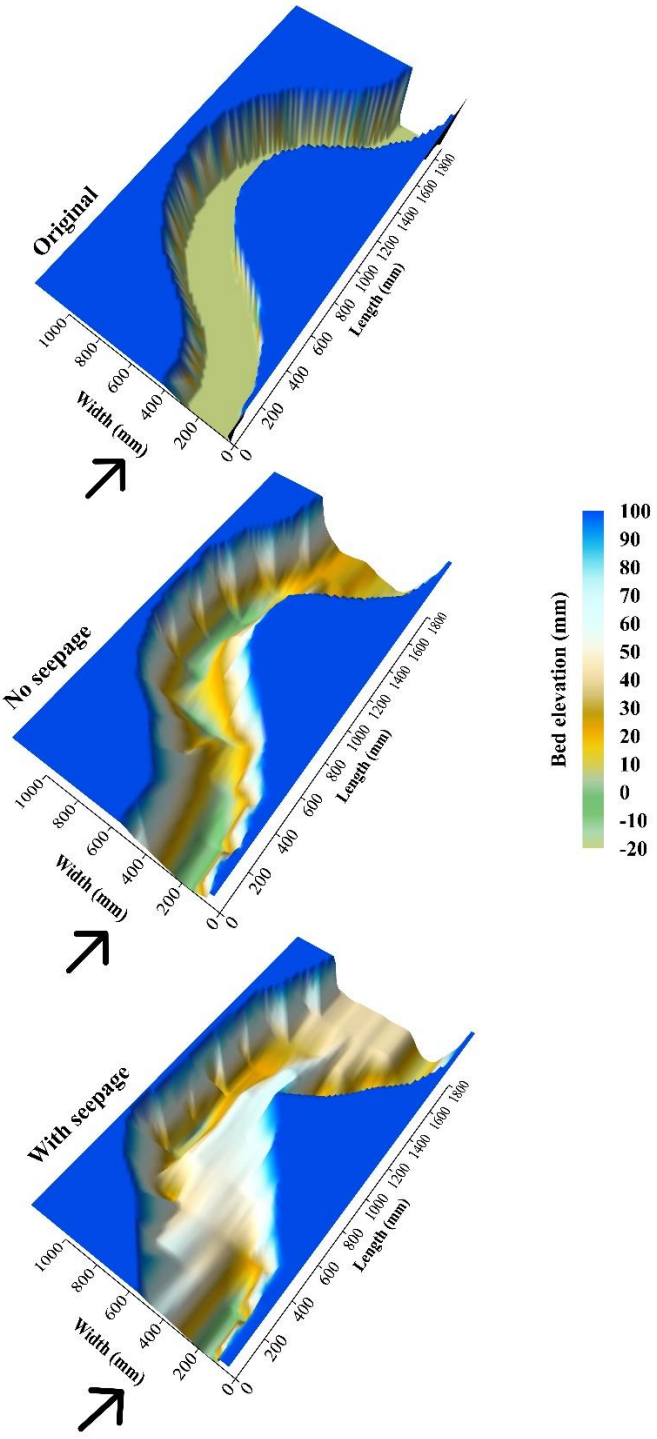

Figure 4.15 3-dimensional surface plots of the morphology along the mobile rectangular sinuous bend at $Q = 0.00629\ \mathrm{m}^3/\mathrm{s}$.

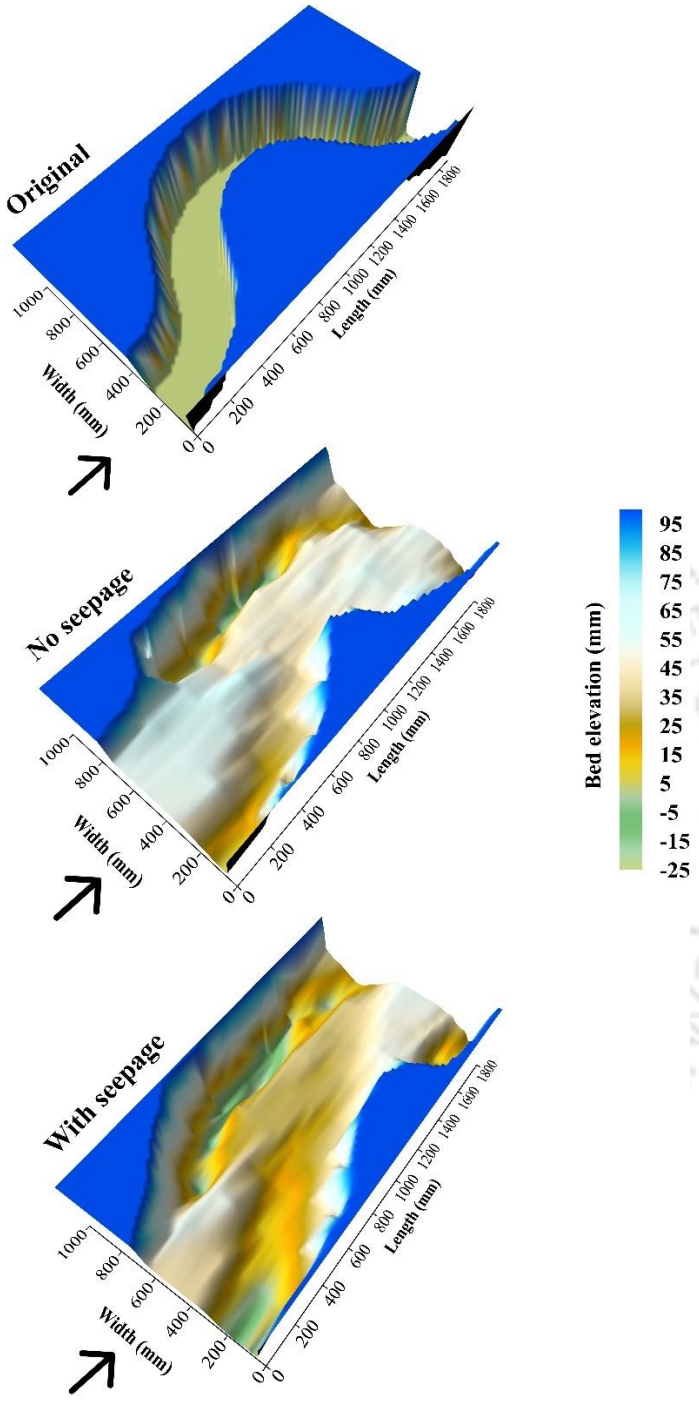

Figure 4.16 3-dimensional surface plots of the morphology along the mobile rectangular sinuous bend at $Q = 0.00793\ \mathrm{m}^3/\mathrm{s}$.

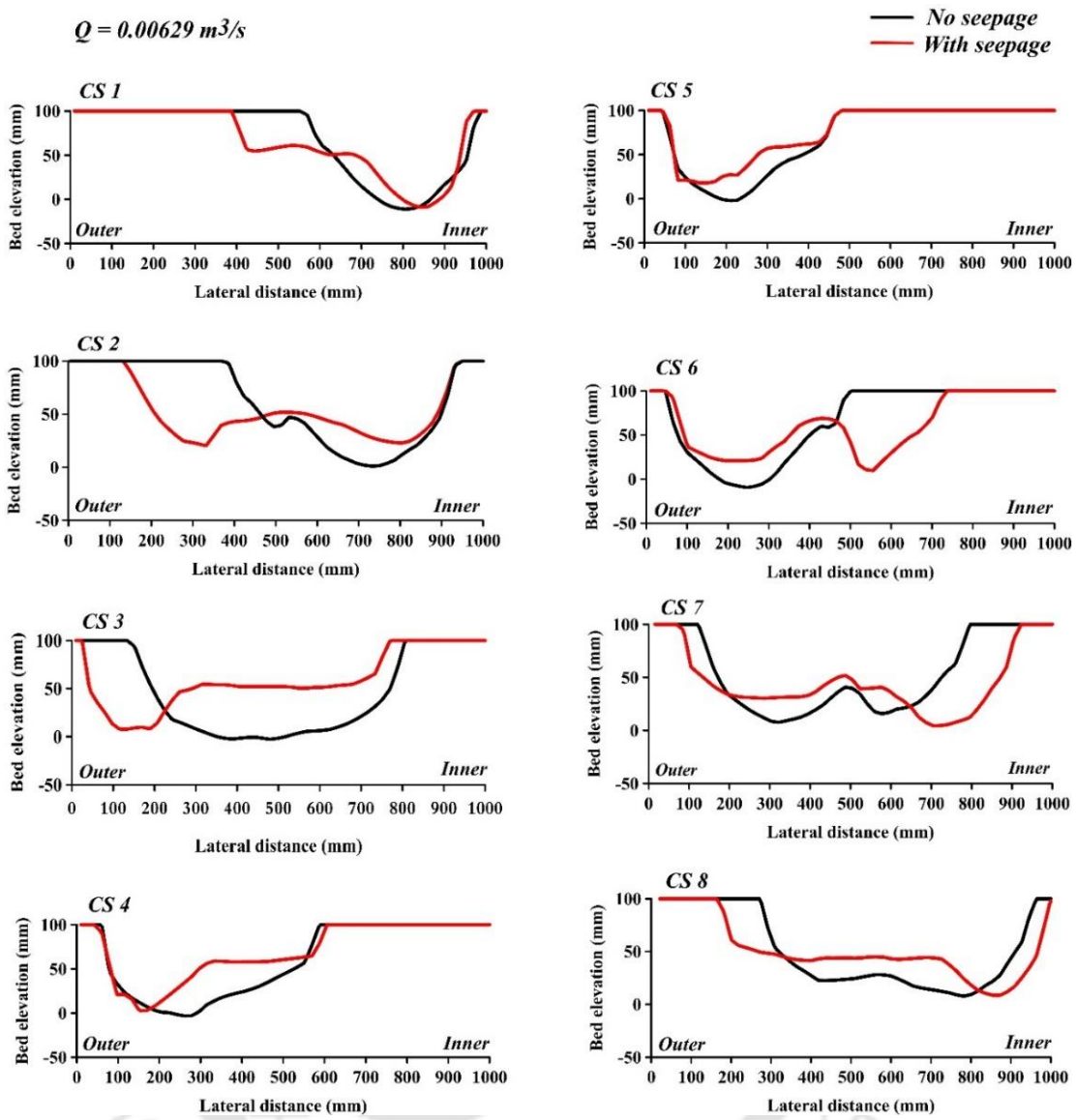

Figure 4.17 Cross-section profiles of the morphological changes in mobile rectangular sinuous channel of discharge $Q = 0.00629\ \mathrm{m}^3/\mathrm{s}$.

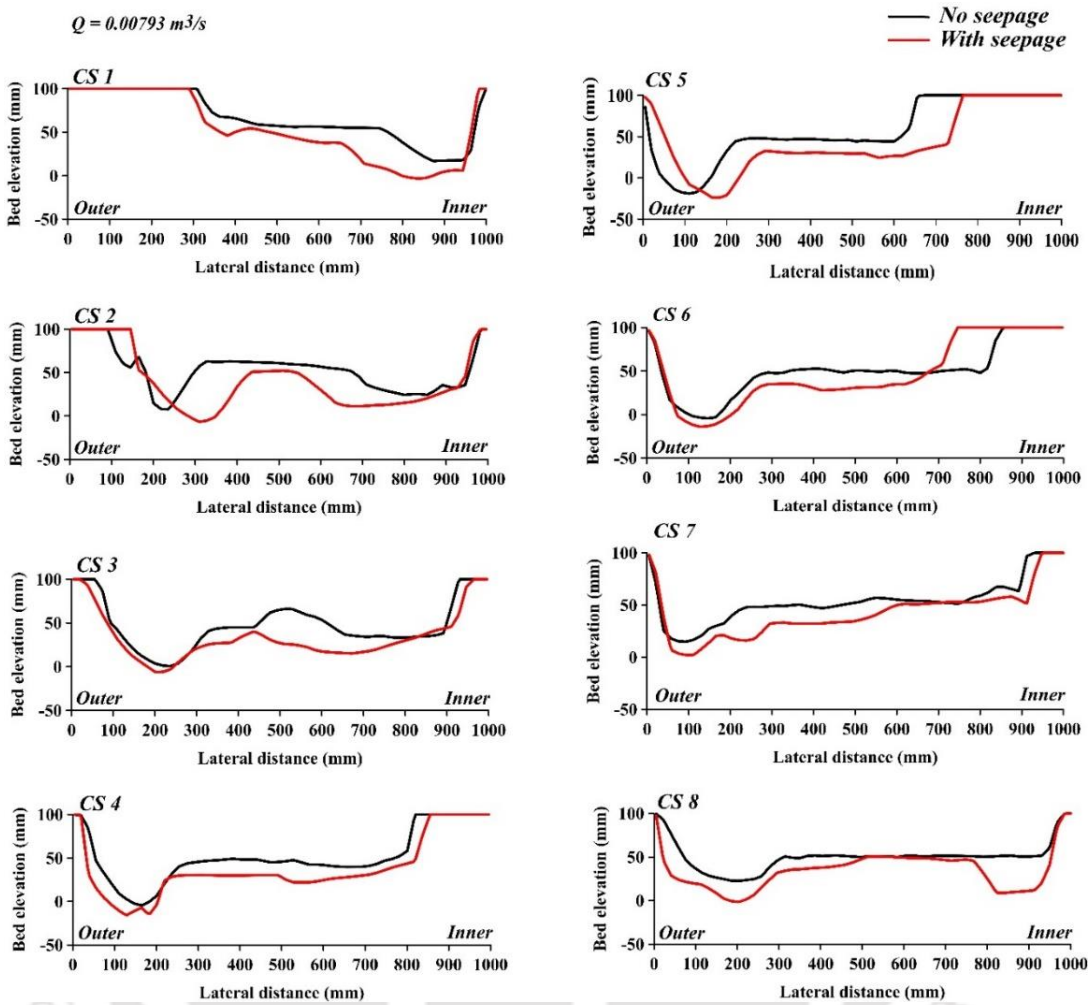

Figure 4.18 Cross-section profiles of the morphological changes in mobile rectangular sinuous channel of discharge $Q = 0.00793\ \mathrm{m}^3/\mathrm{s}$.

4.3.3 Effect of Downward Seepage on the Morphological Changes in Mobile Trapezoidal Sinuous Channel

The contour plots of the trapezoidal channel are shown in Figure 4.19. The plots do not provide much information at a glance. Observation from the rectangular sinuous channel (Figure 4.14) and of the trapezoidal sinuous channel (Figure 4.19) reveals that the trapezoidal channel was more stable than the rectangular channel. In the trapezoidal channel, the side slope of the channel was stable unlike the rectangular channel. The bankline of the channel had a side slope close to the dry angle of repose of the sand material. Hence, the trapezoidal channel inhibited extensive modification even with seepage and with the increase in discharge. Therefore, morphological changes in the

rectangular channel were more pronounced than the trapezoidal channel. However, there is further scope to study and observe the change with different side slope, different flow rates, and seepage rates.

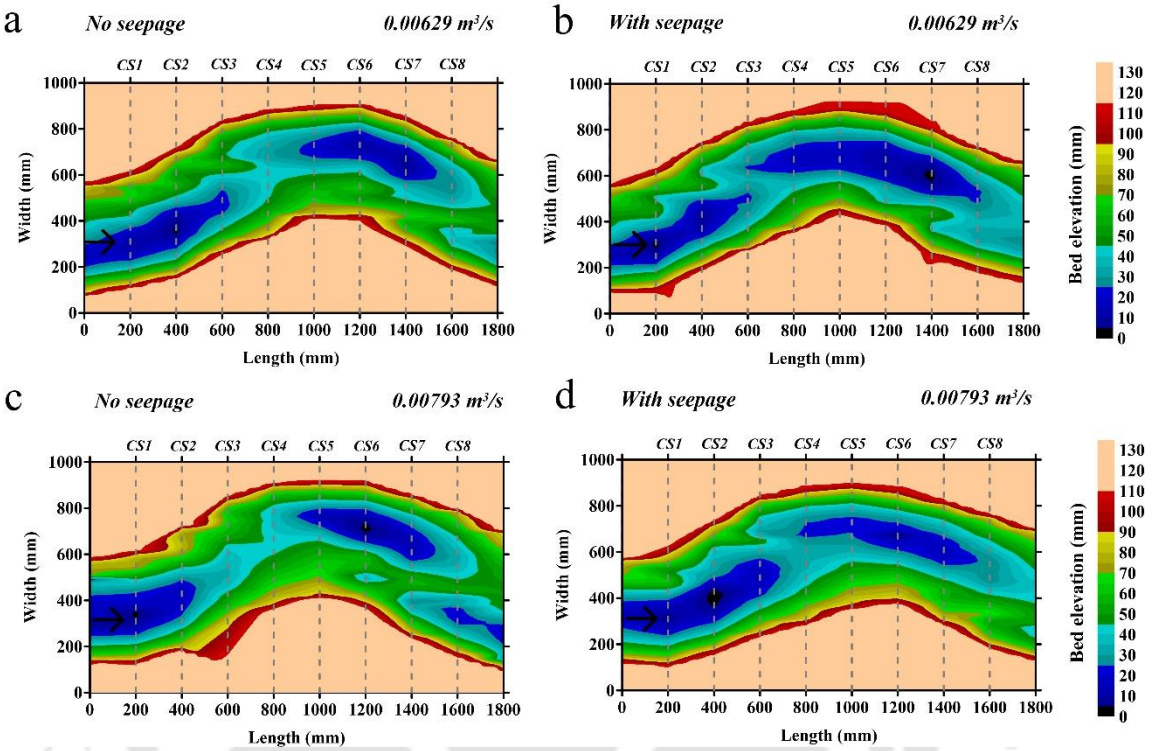

Figure 4.19 Contour plots of the morphological changes in mobile trapezoidal sinuous bend (a, c) no seepage and (b, d) with seepage flow.

The 3-dimensional surface plots present a clear representation of the morphology along the sinuous bend (Figures 4.20 and 4.21). High bed shear stress was found at the center of the channel bed, where maximum sediment transport was observed. The banks of the trapezoidal channel were almost stable with minimum changes at the bank. The stability of the trapezoidal channel was attained because of its channel shape. In the trapezoidal channel, the sinuosity was less, for which the channel may be subjected to less modification. However, the width of the sinuous channel has increased subjected to high flow rate and downward seepage (Figure 4.21).

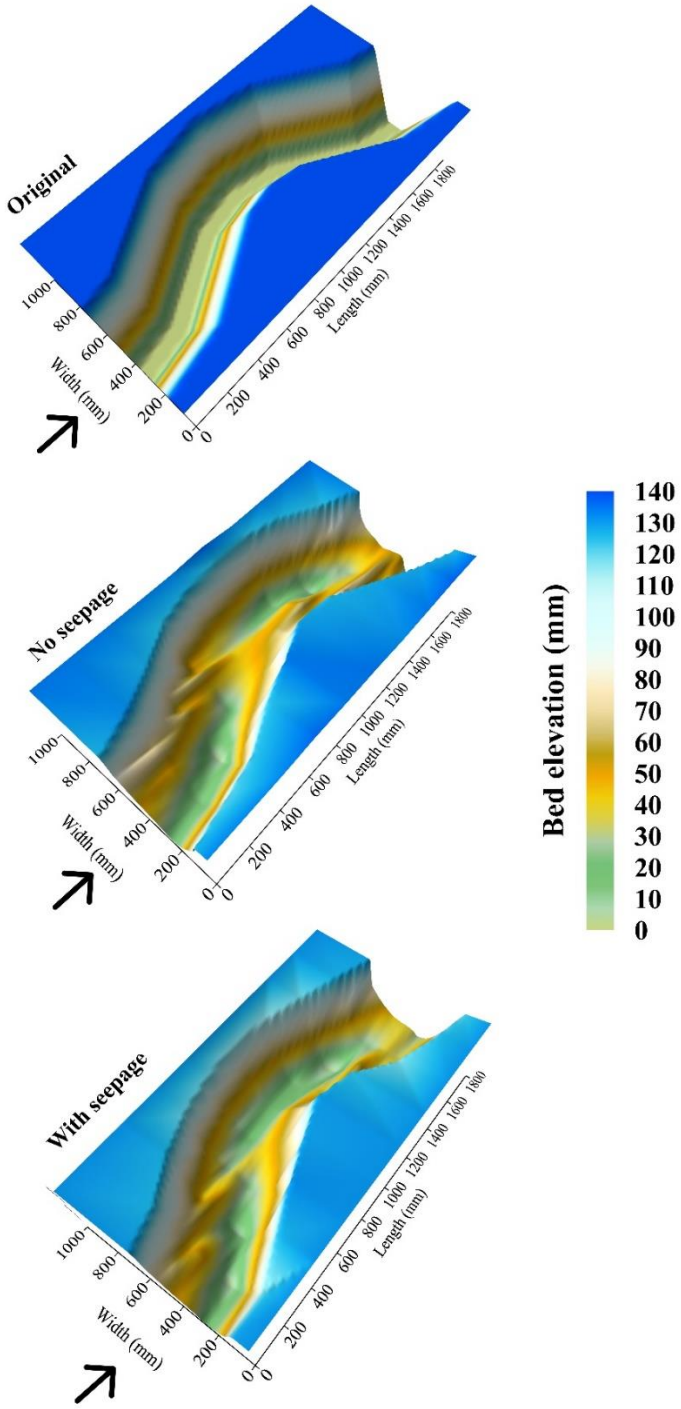

Figure 4.20 3-dimensional surface plots of the morphology along the mobile trapezoidal sinuous bend at $Q = 0.00629\ \mathrm{m}^3/\mathrm{s}$.

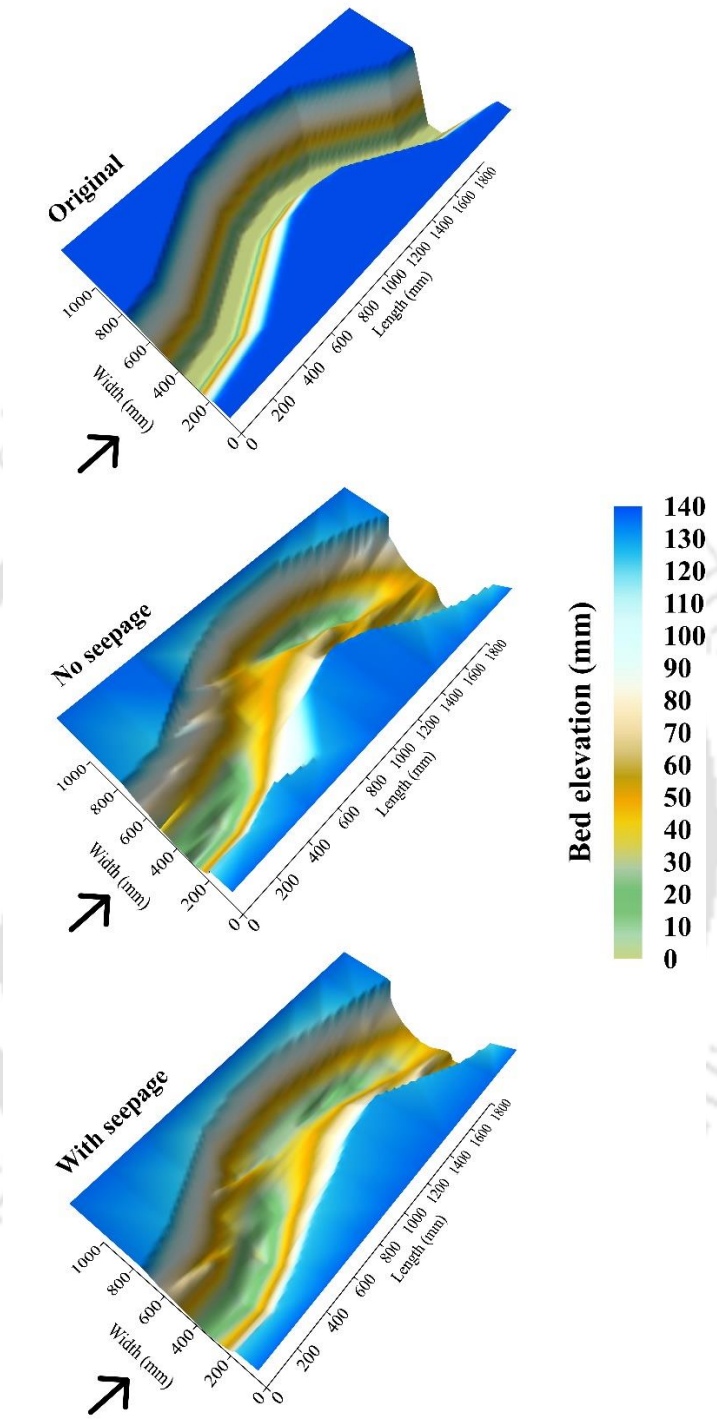

Figure 4.21 3-dimensional surface plots of the morphology along the mobile trapezoidal sinuous bend at $Q = 0.00793\ \mathrm{m}^3/\mathrm{s}$.

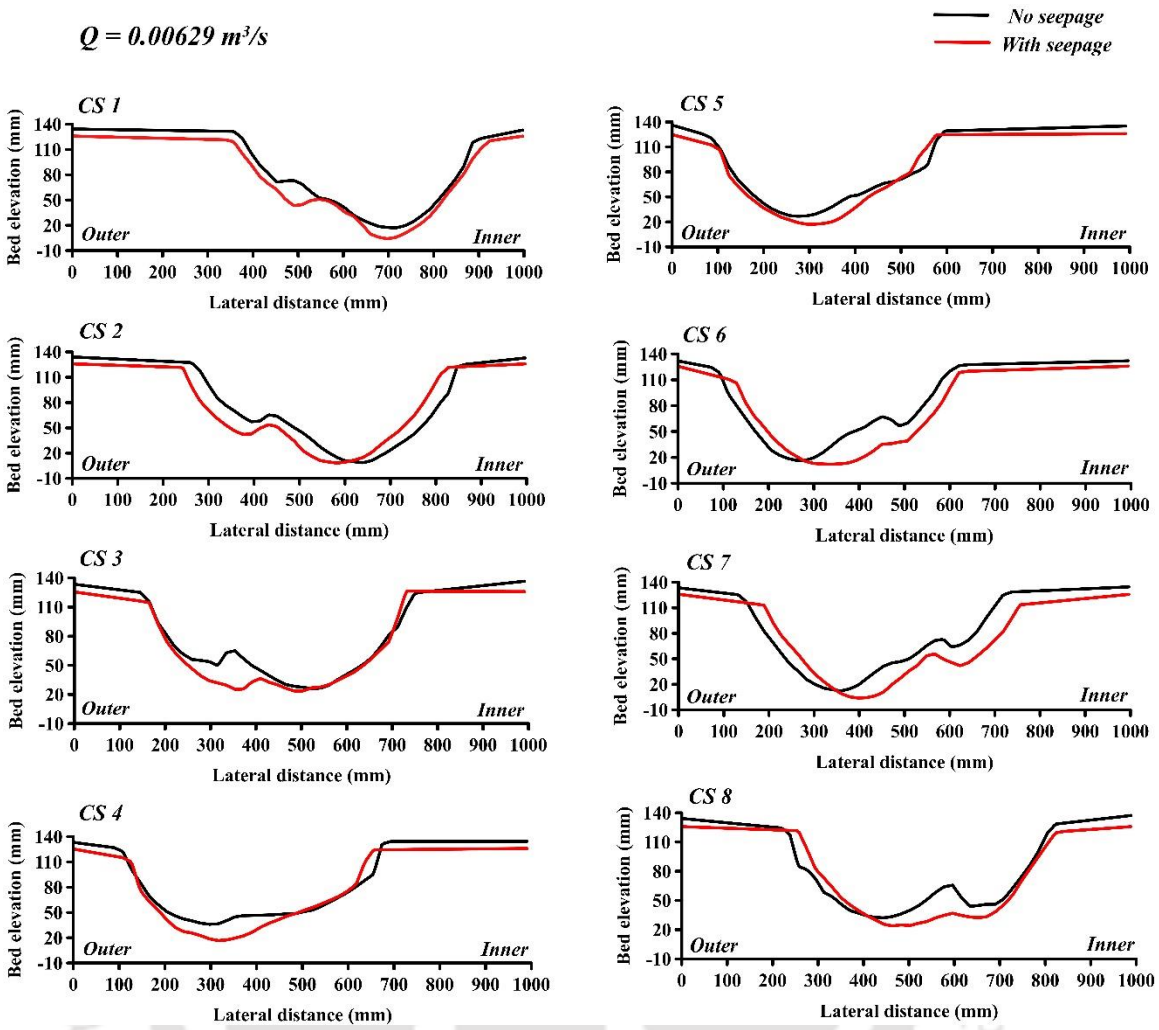

Figure 4.22 Cross-section profiles of the morphological changes in mobile trapezoidal sinuous channel of discharge $Q = 0.00629\ \mathrm{m}^3/\mathrm{s}$.

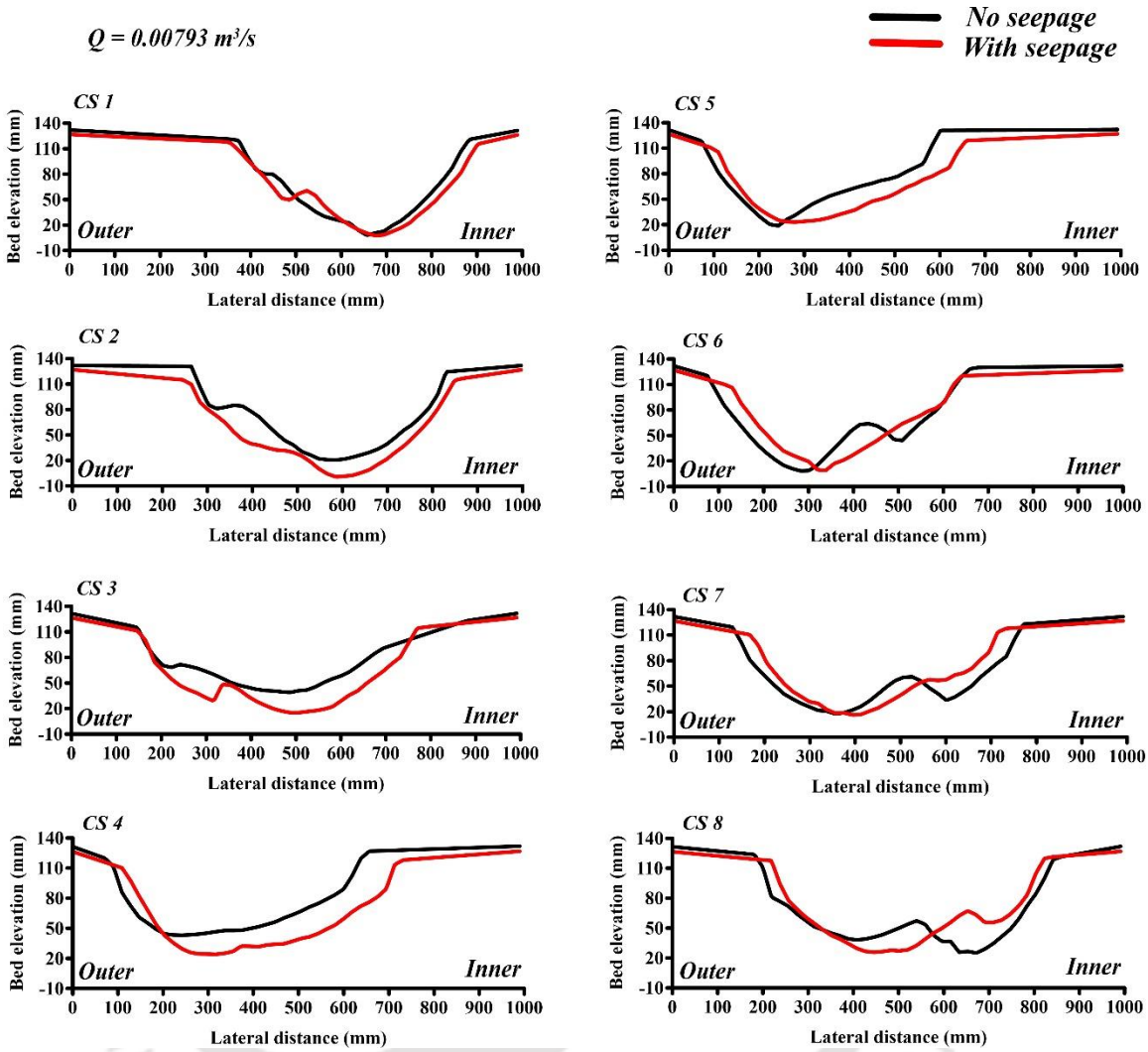

Figure 4.23 Cross-section profiles of the morphological changes in mobile trapezoidal sinuous channel of discharge at $Q = 0.00793\ \mathrm{m}^3/\mathrm{s}$.

The morphological changes across the trapezoidal sinuous channel were observed for no seepage and with downward seepage. The difference in bed elevation was distinctly noticed from the cross-sectional profiles as presented in Figure 4.22 ($Q = 0.00629\ \mathrm{m}^3/\mathrm{s}$) and Figure 4.23 ($Q = 0.00793\ \mathrm{m}^3/\mathrm{s}$). For both discharge rates, the profiles have shown some changes with downward seepage. The bed elevation has lowered with seepage, indicating sediment transport.

4.3.4 Summary

The deformation along the streambed and bank of the sinuous channels showed remarkable alteration with seepage. With the withdrawal of water from the main channel in seepage, the porous channel boundary encounters additional hydrodynamic force. This caused the channel to be fragile, which led to a morphological modification in the channel. Morphology of the channel was also influenced by the flow rate and geometry of the channel. Seepage with high flow rate has shown much difference in the channel planform. Scour around the outer bend and deposition around inner bend with seepage was visible. With high flow rate and seepage application, the rectangular channel has shown large modifications along the bend. In the trapezoidal channel, the modifications were less, particularly at the banks of the channel bend. This suggest the trapezoidal channel to be stable than the rectangular channel. However, the channel has widened with seepage in the trapezoidal channel. The trapezoidal channel experienced most of the modification at the center of the channel, where maximum bed shear was involved.

4.4 Discussions

The variation in the alluvial bed was visible in the channel. Researchers (Gautier et al., 2010; Hooke and Yorke, 2011) have examined the processes in sinuous channels ranging from small scale to large scale study to examine the interaction between flow and bed material. The migration of sediment over time and space is also of social-economic concern as this process may lead to erosion of the bank, a change in the channel centerline, and flooding (Güneralp and Rhoads, 2009; Larsen and Greco, 2002). This may lead to the construction of channel mitigation structures. Moreover, the flow variation in bends significantly affects the development of bed features along the sinuous channel. The dynamic process of the complex morphology in a sinuous bend can be characterized by linear and non-linear development of morphologies (Song et al., 2016). A developed sinuous channel is characterized by scour pool at the outer bend and deposition at the inner bend. This development can be attributed to the flow difference along the flow depth of the channel, where the surface water entering the channel bend move towards the outer bend and the bottom water move towards the inner bend. This flow variation is because of the channel curvature for which secondary flow circulation cells are observed at the channel

bends, and thereby it depicts the non-logarithmic streamwise velocity distribution. Rotating cells at the bends cause the sediment to move in the radial (transverse) direction. The transport of sediment from the outer bend is carried towards the inner bend where deposition is mostly observed. Several studies have reported the bank erosion due to maximum velocity at the outer bend (Blanckaert and De Vriend, 2005; Constantinescu et al., 2013; da Silva and Ebrahimi, 2017). However, this does not hold in all cases of meandering or sinuous channels. The maximum velocity was also found to exist near the inner region of the bend (Shams et al., 2002; de Vriend and Geldof, 1983; Xu and Bai, 2013). In this study, the velocity was found to be maximum at the deposition zone; hence the mean velocity cannot be the only defining factor to relate to the channel bed development.

The sand bed modifies itself temporally and spatially, and changes are primarily dependent on the channel geometry, flow conditions, and nature of the sediment. The interaction of the surface water and the groundwater plays a substantial role, which affects the flow behavior and the rate of sediment transport. Investigating the flow characteristics in the previous chapter, it was ascertained that the flow in the bend altered with downward seepage. With the altered nature of the flow with seepage, the channel bed experience modifications. The dominance of the fluctuating velocity rather than the mean velocity was found to hold good with the investigated flow characteristics. With the increase in seepage velocity, the fluctuating velocity exerted extra force on the channel bed particles, which lead to excess transport of sediment. The fluctuations from the mean velocity contribute largely to the bed deformation. In this context, high Reynolds shear was found towards the outer bend, which confirmed the transverse or radial sediment motion and assists in additional sediment transport. The turbulence parameters, such as, mean velocities, Reynolds stresses, normal stresses and bed stresses have increased with seepage in the vicinity of the channel bed. The stresses are found to be high near the outer bank compared to the inner bank and increased with downward seepage. Therefore, the contribution of the high velocity fluctuations conforms to the presented morphological features. Further, the octant analysis helped in recognizing the behavior of the bed changes. The positive radial velocity pushes the sediment towards the inner bend, causing deposition. The internal events of the bursting phenomenon influenced the particles to move from the outer bend to

the inner bend, causing erosion. These bursting events have significantly increased with downward seepage by a substantial percentage.

5

Conclusions and Recommendations

The experiments showed that downward seepage impacts the flow hydrodynamics, sediment transport, and corresponding morphological changes in an alluvial sinuous channel bed. The alteration of the channel bed with seepage condition provides us with an understanding of the mechanism of the seepage affected natural channel.

5.1 Effect of Downward Seepage on the Flow Turbulence in a Sinuous Channel

- High streamwise velocity was found near the region of deposition. With the increase in seepage velocity, the near-bed flow field was subjected to high streamwise velocities.
- The downward seepage exerted additional stress with high turbulent stresses along the channel bend.
- High fluctuating velocities resulted in greater momentum transport with seepage near the channel bed. The sediment motion across the channel bend was indicated with high (low) transverse Reynolds stress at the eroded (deposition) region. This indicates that the sediment particles with the flow move in the transverse direction.
- The turbulence intensities in the streamwise and transverse direction dominate the corresponding ones in the vertical direction. The average streamwise and transverse turbulence intensity across the bend apex increased with downward seepage.
- High turbulent kinetic energy at the outer zone corresponds to higher velocity fluctuations. A rise in turbulent kinetic energy was found near the channel bed.
- A remarkable increase in the bed shear caused modifications in the channel with downward seepage. The calculated bed shear stress is high at the outer bend of the channel.

- The bursting phenomena from the octant analysis addressed the momentum transfer between the water layer and the sediment channel bed. The events 2B (external ejection), 4B (external sweep), 4A (internal sweep), and 2A (internal ejection) are highest at the bend region, which causes the sediment to move from the outer bend to the inner bend of the channel.
- An increase in the entropy measures denotes the irregularity and high fluctuations with seepage flows, giving high entropy at the outer bend.

5.2 Effect of Downward Seepage on the Morphological Changes in a Sinuous Channel

- Bed development along the sinuous bend presented modifications with downward seepage.
- Erosion and deposition of sediment at the banks of the channel were prominent with downward seepage.
- The morphological changes were related to the flow rate, the geometry of the channel, the nature of sediment, and seepage rate.
- Scour area increased with downward seepage in the rigid boundary rectangular channel. The development along the channel, however, was distinct with an increase in time and seepage. The scour depth has significantly lowered with seepage.
- With high flow rate, scour and deposition developed in the mobile boundary rectangular channel. Extensive modifications along the channel bend were noticed, indicating sediment transport with seepage.
- The modifications in the mobile boundary trapezoidal channel were less compared to the rectangular mobile channel. The banks were stable, though the width of the channel increased with an increase in flow rate and seepage. However, with downward seepage, the streambed has lowered, particularly at the upstream of the bend apex.
- The migration of the sediment increased with downward seepage near the bend apex. The average bed celerity increased with downward seepage.

5.3 Recommendations from the Current Study

- Seepage flow causes modifications of the channel banks and channel bed. This modification, if neglected, can cause instability of the hydraulic structures. Therefore, the study of seepage should be considered before the construction of any hydraulic structure.
- With the increasing sediment motion due to seepage flow, there may be a need for sediment management downstream of hydraulic structure, and therefore proposal of river training works.
- In the vicinity of natural channels, construction of bore wells, open wells, or tube wells is not recommended, as it will advance the depletion of the groundwater.

5.4 Recommendations for Future Research

- Future work can be conducted to study the effect of point seepage or zone seepage on the hydrodynamics and morphology of sinuous channel.
- Upward and downward seepage can both be active in a channel reach as investigated in natural field conditions. Therefore, exploring the hydrodynamics and morphology under both the seepage activity would be more comparable to the real scenario.
- The sediment feeding at the upstream may have a substantial difference in the morphology of the sinuous channel. Therefore, the examination of morphology can be explored further with this consideration.
- Non-uniform bed material replicates the real field scenario in alluvial rivers. Thus, its use in laboratory setup can be explored further to study the seepage effects in sinuous channel.

5.5 Limitations of the present work

- Suspended sediment load was not considered in this study.
- Uniform sediment was used as the bed material. The use of non-uniform sediment which replicate the real field was not used in this study.

- Wooden baffles were used to diminish the unsteady fluctuations to achieve steady flow conditions at the test zone. It helped to weaken the flow fluctuations before its entry into the main channel.
- Seepage zones in real field measurement of an alluvial river channel are non-uniform, because of the difference in soil structure. This condition was not considered in this study. The application of non-uniform seepage zones or point seepage application could open up another scope of research.
- High flood level carrying huge sediment from the upstream may affect the hydromorphology in sinuous alluvial channel together with seepage. This condition was not considered in this study.

Appendix A

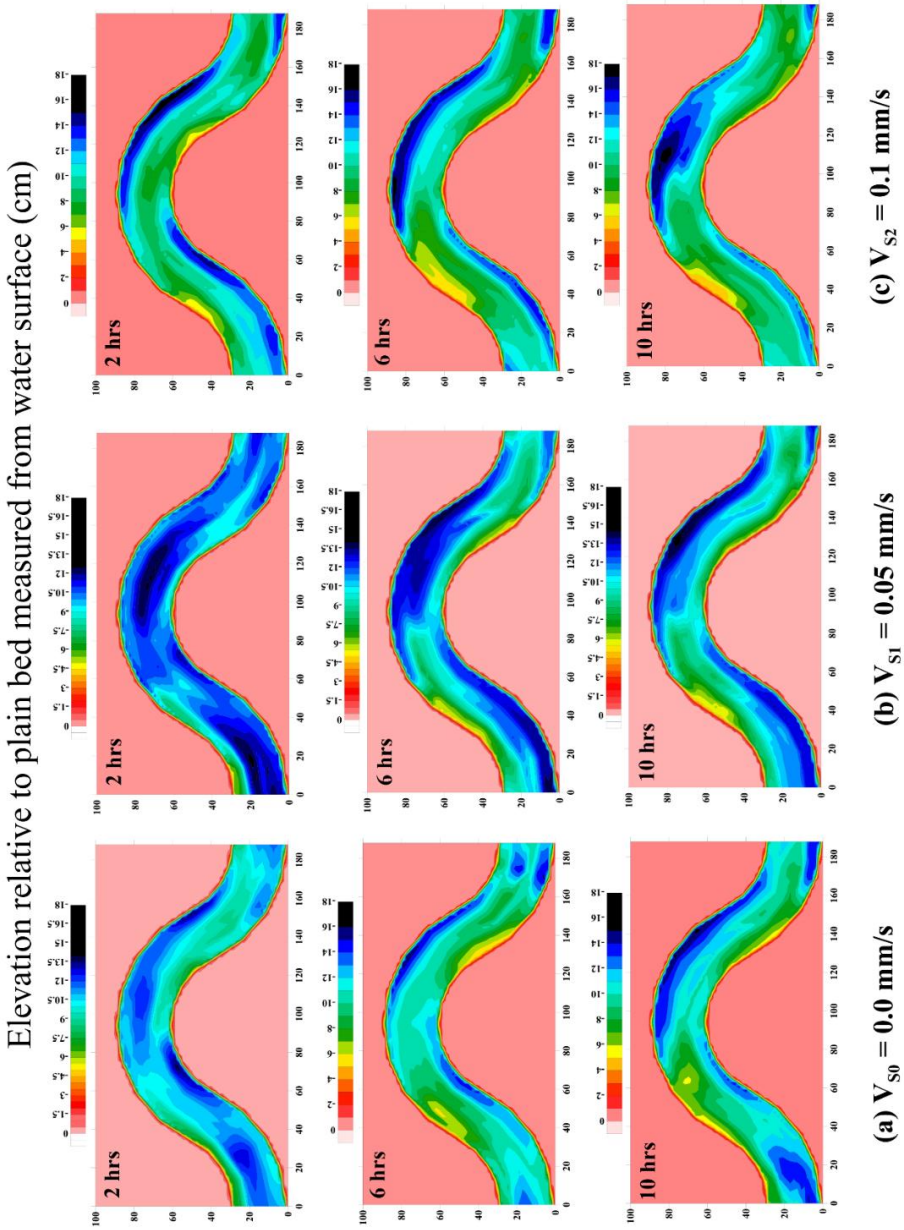

Figure A.1 Channel bed morphology (cm) along the sinuous bend with seepage velocity (a) V_{S0} = 0.0 mm/s, (b) V_{S1} = 0.05 mm/s and (c) V_{S2} = 0.1 mm/s.

References

Abad, J. D., and Garcia, M. H. (2009). Experiments in a high-amplitude Kinoshita meandering channel: 1. Implications of bend orientation on mean and turbulent flow structure. *Water Resources Research*, *45*(2).

Anwar, H. O. (1986). Turbulent structure in a river bend. *Journal of Hydraulic Engineering*, *112*(8), 657–669.

Azami, H., and Escudero, J. (2016). Improved multiscale permutation entropy for biomedical signal analysis: Interpretation and application to electroencephalogram recordings. *Biomedical Signal Processing and Control*, *23*, 28–41.

Bandt, C., and Pompe, B. (2002). Permutation entropy: a natural complexity measure for time series. *Physical Review Letters*, *88*(17), 174102.

Barman, B., Sharma, A., Kumar, B., and Sarma, A. K. (2017). Multiscale characterization of migrating sand wave in mining induced alluvial channel. *Ecological Engineering*, *102*, 199–206.

Bathurst, J. C., Hey, R. D., and Thorne, C. R. (1979). Secondary flow and shear stress at river bends. *Journal of the Hydraulics Division*, *105*(10), 1277–1295.

Berenbrock, C. (1999). Streamflow Gains and Losses in the Lower Boise River Basin, Idaho, 1996-97. *Water-Resources Investigations Report*, *99*, 4105.

Binns, A. D., and da Silva, A. M. F. (2015). Meandering bed development time: Formulation and related experimental testing. *Advances in Water Resources*, *81*, 152–160.

Biron, P. M., Robson, C., Lapointe, M. F., and Gaskin, S. J. (2004). Comparing different methods of bed shear stress estimates in simple and complex flow fields. *Earth Surface Processes and Landforms: The Journal of the British Geomorphological Research Group*, *29*(11), 1403–1415.

Biswas, P., and Barbhuiya, A. K. (2020). Scour at River Bend: A Parametric Study. *Iranian Journal of Science and Technology - Transactions of Civil Engineering*, *44*(3), 1001–1021.

Blanckaert, K., and de Vriend, H. J. (2005). Turbulence structure in sharp open-channel bends. *Journal of Fluid Mechanics*, *536*, 27–48.

Blanckaert, K. (2002a). Analysis of coherent flow structures in a bend based on instantaneous-velocity profiling. *3rd International Symposium on Ultrasonic Doppler Methods for Fluid Mechanics and Fluid Engineering, EPFL, Lausanne, Switzerland*.

Blanckaert, K. (2002b). Secondary currents measured in sharp open-channel bends. *River Flow 2002, 5th International Conference on Hydroinformatics River Flow*.

Blanckaert, K., and Graf, W. H. (2001). Mean flow and turbulence in open-channel bend. *Journal of Hydraulic Engineering*, *127*(10), 835–847.

Blanckaert, K., and Graf, W. H. (2004). Momentum transport in sharp open-channel bends. *Journal of Hydraulic Engineering*, *130*(3), 186–198.

Blanckaert, K., Kleinhans, M. G., Mclelland, S. J., Uijttewaal, W. S. J., Murphy, B. J., van de Kruijs, A., Parsons, D. R., and Chen, Q. (2013). Flow separation at the inner (convex) and outer (concave) banks of constant-width and widening open-channel bends. *Earth Surface Processes and Landforms*, *38*(7), 696–716.

Booij, R. (2003). Modeling the flow in curved tidal channels and rivers. *Proceedings of the International Conference on Estuaries and Coasts*, 786–794.

Boussinesq, J. (1868). Mémoire sur l'influence des frottements dans les mouvements réguliers des fluids. *Journal de Mathématiques Pures et Appliquées*, *13*(2), 377–424.

Camporeale, C., Perona, P., Porporato, A., and Ridolfi, L. (2007). Hierarchy of models for meandering rivers and related morphodynamic processes. *Reviews of Geophysics*, *45*(1).

Cao, D., and Chiew, Y. M. (2014). Suction effects on sediment transport in closed-conduit flows. *Journal of Hydraulic Engineering*, *140*(5), 1–9.

Carlson, R. A., and Petrich, C. R. (1999). New York Canal geologic cross-section, seepage gain/loss data, and ground water hydrographs: compilation and interim findings. *Treasure Valley Hydrologic Project Open File Report*.

Chavan, R., Gualtieri, P., and Kumar, B. (2019). Turbulent Flow Structures and Scour Hole Characteristics around Circular Bridge Piers over Non-Uniform Sand Bed Channels with Downward Seepage. *Water*, *11*(8), 1580.

Chen, X., and Chiew, Y. M. (2004). Velocity distribution of turbulent open-channel flow with bed suction. *Journal of Hydraulic Engineering*, *130*(2), 140–148.

Cheng, N. S., and Chiew, Y. M. (1999). Incipient sediment motion with upward seepage. *Journal of Hydraulic Research*, *37*(5), 665–681.

Coleman, S. E., and Melville, B. W. (1994). Bed-form development. *Journal of Hydraulic Engineering*, *120*(5), 544–560.

Constantinescu, G., Kashyap, S., Tokyay, T., Rennie, C. D., and Townsend, R. D. (2013). Hydrodynamic processes and sediment erosion mechanisms in an open channel bend of strong curvature with deformed bathymetry. *Journal of Geophysical Research*: *Earth Surface*, 118(2), 480–496. https://doi.org/10.1002/jgrf.20042

Crosato, A. (2008). *Analysis and modelling of river meandering*, Doctoral Thesis, University of Padua, Padua, Italy.

da Silva, A. M. F., and Ebrahimi, M. (2017). Meandering morphodynamics: Insights from laboratory and numerical experiments and beyond. Doctoral Dissertation, *American Society of Civil Engineers*.

da Silva, A. M. F., El-Tahawy, T., and Tape, W. D. (2006). Variation of flow pattern with sinuosity in sine-generated meandering streams. *Journal of Hydraulic Engineering*, *132*(10), 1003–1014.

da Silva, A. M. F., (1996). Turbulent flow in sine-generated meandering channels, *Doctoral Thesis*, Queen's University at Kingston, Canada.

Das, V. K., Barman, K., Roy, S., Chaudhuri, S., and Debnath, K. (2020). Near bank turbulence of a river bend with self similar morphological structures. *Catena*, *191*, 104582.

de Vriend, H. J., and Geldof, H. J. (1983). Main flow velocity in short river bends. *Journal of Hydraulic Engineering*, *109*(7), 991–1011.

Deshpande, V., and Kumar, B. (2016). Turbulent flow structures in alluvial channels with curved cross-sections under conditions of downward seepage. *Earth Surface Processes and Landforms*, *41*(8), 1073–1087.

Dey, S., Das, R., Gaudio, R., and Bose, S. K. (2012). Turbulence in mobile-bed streams. *Acta Geophysica*, *60*(6), 1547–1588.

Dey, S., and Nath, T. K. (2010). Turbulence Characteristics in Flows Subjected to Boundary Injection and Suction. *Journal of Engineering Mechanics*, *136*(7), 877–888.

Dey, S., Sarkar, S., and Ballio, F. (2011). Double-averaging turbulence characteristics in seeping rough-bed streams. *Journal of Geophysical Research: Earth Surface*, *116*(3), 1–16.

Dietrich, W. E. (1987). Mechanics of flow and sediment transport in river bends. *River Channels: Environment and Process*, *134*, 179–227.

Dietrich, W. E., and Smith, J. D. (1983). Influence of the point bar on flow through curved channels. *Water Resources Research*, *19*(5), 1173–1192.

Dietrich, W. E., Smith, J. D., and Dunne, T. (1979). Flow and sediment transport in a sand bedded meander. *The Journal of Geology*, *87*(3), 305–315.

Dukker, P., Bhutta, M. N., Roos, P., and Javed, I. (1994). Seepage Losses from Lower Gugera Branch Canal, Punjab, Pakistan. *IWASRI, Publication*, *134*, 24–25.

Einstein, H. A., and Harder, J. A. (1954). Velocity distribution and the boundary layer at channel bends. *Eos, Transactions American Geophysical Union*, *35*(1), 114–120.

Engel, F. L., and Rhoads, B. L. (2012). Interaction among mean flow, turbulence, bed morphology, bank failures and channel planform in an evolving compound meander loop. *Geomorphology*, *163*, 70–83.

Engel, F. L., and Rhoads, B. L. (2017). Velocity profiles and the structure of turbulence at the outer bank of a compound meander bend. *Geomorphology*, *295*, 191–201.

Engelund, F. (1974). Flow and bed topography in channel bends. *Journal of the Hydraulics Division*, *100*(11), 1631–1648.

Esfahani, F. S., and Keshavarzi, A. (2011). Effect of different meander curvatures on spatial variation of coherent turbulent flow structure inside ingoing multi-bend river meanders. *Stochastic Environmental Research and Risk Assessment*, *25*(7), 913–928.

Esfahani, F. S., and Keshavarzi, A. R. (2010). The Effect of Different Curvatures on Flow Structure inside the River Meander. *5th National Congress on Civil Engineering*, 2–9.

Faruque, M. A. Al, and Balachandar, R. (2011). Seepage effects on turbulence characteristics in an open channel flow. *Canadian Journal of Civil Engineering*, *38*(7), 785–799.

Fipps, G. (2005). Potential water savings in irrigated agriculture for the Rio Grande Planning Region. *Texas Water Resource Institute*, Texas A&M University System, College Station , TX.

Frothingham, K. M., and Rhoads, B. L. (2003). Three-dimensional flow structure and channel change in an asymmetrical compound meander loop, Embarras River, Illinois. *Earth Surface Processes and Landforms: The Journal of the British Geomorphological Research Group*, *28*(6), 625–644.

Furbish, D. J. (1988). River-bend curvature and migration: How are they related? *Geology*, *16*(8), 752–755.

Gautier, E., Brunstein, D., Vauchel, P., Jouanneau, J.-M., Roulet, M., Garcia, C., Guyot, J.-L., and Castro, M. (2010). Channel and floodplain sediment dynamics in a reach of the tropical meandering Rio Beni (Bolivian Amazonia). *Earth Surface Processes and*

Landforms, *35*(15), 1838–1853.

Goring, D. G., and Nikora, V. I. (2002). Despiking acoustic Doppler velocimeter data. *Journal of Hydraulic Engineering*, *128*(1), 117–126.

Graf, W. H., and Blanckaert, K. (2002). Flow around bends in rivers. *2nd International Conference New Trends in Water and Environmental Engineering for Safety and Life: Eco-Compatible Solutions for Aquatic Environments*, 1–9.

Güneralp, I., and Rhoads, B. L. (2009). Empirical analysis of the planform curvature-migration relation of meandering rivers. *Water Resources Research*, *45*(9).

Hatch, C. E., Fisher, A. T., Ruehl, C. R., and Stemler, G. (2010). Spatial and temporal variations in streambed hydraulic conductivity quantified with time-series thermal methods. *Journal of Hydrology*, *389*(3–4), 276–288.

Heller, V. (2011). Scale effects in physical hydraulic engineering models. *Journal of Hydraulic Research*, *49*(3), 293–306.

Henderson, F. M. (1966). Open Channel Flow. Macmillan Series in Civil Engineering. *A Book Published by The Macmillan Company, Library of Congress Catalog Card*, *66–10695*.

Henry, M., and Judge, G. (2019). Permutation Entropy and Information Recovery in Nonlinear Dynamic Economic Time Series. *Econometrics*, *7*(1), 10.

Hille, P., Vehrenkamp, R., and Schulz-Dubois, E. O. (1985). The development and structure of primary and secondary flow in a curved square duct. *Journal of Fluid Mechanics*, *151*, 219–241.

Hooke, J. M., and Yorke, L. (2011). Channel bar dynamics on multi-decadal timescales in an active meandering river. *Earth Surface Processes and Landforms*, *36*(14), 1910–1928.

Hooke, R. L. B. (1975). Distribution of Sediment Transport and Shear Stress in a Meander Bend. *The Journal of Geology*, *83*(5), 543–565.

Huggett, R. (2016). *Fundamentals of geomorphology*. Routledge, Abingdon, UK.

Ikeda, S., Parker, G., and Sawai, K. (1981). Bend theory of river meanders. Part 1. Linear development. *Journal of Fluid Mechanics*, *112*, 363–377.

Jamieson, E. C., Post, G., and Rennie, C. D. (2010). Spatial variability of three-dimensional Reynolds stresses in a developing channel bend. *Earth Surface Processes and Landforms*, *35*(9), 1029–1043.

Jerolmack, D. J., and Mohrig, D. (2005). A unified model for subaqueous bed form dynamics. *Water Resources Research*, *41*(12).

Jewel, A., Fujisawa, K., and Murakami, A. (2019). Effect of seepage flow on incipient motion of sand particles in a bed subjected to surface flow. *Journal of Hydrology*, *579*(July), 124178.

Johannesson, H., and Parker, G. (1989). Linear theory of river meanders. *River Meandering*, *12*, 181–213.

Jones, J. B., and Mulholland, P. J. (1999). Streams and ground waters. *Elsevier. Academic, San Diego, California.*

Karambas, T. V. (2003). Modelling of infiltration-exfiltration effects of cross-shore sediment transport in the swash zone. *Coastal Engineering Journal*, *45*(01), 63–82.

Kashyap, S., Constantinescu, G., Rennie, C. D., Post, G., and Townsend, R. (2012). Influence of channel aspect ratio and curvature on flow, secondary circulation, and bed shear stress in a rectangular channel bend. *Journal of Hydraulic Engineering*, *138*(12), 1045–1059.

Kavcar, P. C., and Wright, S. J. (2009). Experimental results on the stability of non-cohesive sediment beds subject to vertical pore water flux. *World Environmental and Water Resources Congress 2009: Great River* (Starrett S (ed.), American Society of Civil Engineers, Reston, VA, USA, pp. 1–10.

Keshavarzi, A., Hamidifar, H., and Ball, J. (2016). Bed morphology in vegetated estuarine river with mild-curved meander bend. *Hydrological Sciences Journal*, *61*(11), 2033–2049.

Keshavarzi, A. R., and Gheisi, A. R. (2006). Stochastic nature of three dimensional bursting events and sediment entrainment in vortex chamber. *Stochastic Environmental Research and Risk Assessment*, *21*(1), 75–87.

Keshavarzi, A., and Shirvani, A. (2002). Probability analysis of instantaneous shear stress and entraind particles from the bed. In *CSCE/EWRI of ASCE Environmental Engineering Conference,* Niagara Falls, Canada (Stiver WH and Zytner RG (eds))

Keshavarzy, A., and Ball, J. E. (1997). An analysis of the characteristics of rough bed turbulent shear stresses in an open channel. *Stochastic Hydrology and Hydraulics*, *11*(3), 193–210.

Khatua, K. K., Patra, K. C., Nayak, P., and Sahoo, N. (2012). Stage-discharge prediction for meandering channels. *International Journal of Computational Methods and Experimental Measurements*, *1*(1), 80–92.

Kinzli, K. D., Martinez, M., Oad, R., Prior, A., and Gensler, D. (2010). Using an ADCP to determine canal seepage loss in an irrigation district. *Agricultural Water Management*, *97*(6), 801–810.

Kline, S. J., Reynolds, W. C., Schraub, F. A., and Runstadler, P. W. (1967). The structure of turbulent boundary layers. *Journal of Fluid Mechanics*, *30*(4), 741–773.

Krishnamurthy, K., and Rao, S. M. (1969). Theory and experiment in canal seepage estimation using radioisotopes. *Journal of Hydrology*, *9*(3), 277–293.

Krogstad, P.-Å., and Kourakine, A. (2000). Some effects of localized injection on the turbulence structure in a boundary layer. *Physics of Fluids*, *12*(11), 2990–2999.

Kumar, P., and Foufoula-Georgiou, E. (1997). Wavelet analysis for geophysical applications. *Reviews of Geophysics*, *35*(4), 385–412.

Langbein, W. B., and Leopold, L. B. (1966). River meanders - theory of minimum variance. *U.S. Geological Survey, Professional Paper*, 422-H, pp. 15.

Langhoff, J. H., Rasmussen, K. R., and Christensen, S. (2006). Quantification and regionalization of groundwater--surface water interaction along an alluvial stream.

Journal of Hydrology, *320*(3–4), 342–358.

Larsen, E. W., and Greco, S. E. (2002). Modeling channel management impacts on river migration: a case study of Woodson Bridge State Recreation Area, Sacramento River, California, USA. *Environmental Management*, *30*(2), 209–224.

Leopold, L.B., and Langbein, W. B. (1966). *(098) River Meander - Scientific American*. *214*(6), 60–70.

Leopold, L.B., and Wolman, M. G. (1957). River channel patterns: braided, meandering, and straight. *US Government Printing Office.*

Li, K., Guo, Z., Wang, L., and Jiang, H. (2019). Effect of seepage flow on shields number around a fixed and sagging pipeline. *Ocean Engineering*, *172*, 487–500.

Li, X., Cui, S., and Voss, L. J. (2008). Using permutation entropy to measure the electroencephalographic effects of sevoflurane. *Anesthesiology: The Journal of the American Society of Anesthesiologists*, *109*(3), 448–456.

Li, X., Ouyang, G., and Richards, D. A. (2007). Predictability analysis of absence seizures with permutation entropy. *Epilepsy Research*, *77*(1), 70–74.

Li, Y., Li, G., Yang, Y., Liang, X., and Xu, M. (2018). A fault diagnosis scheme for planetary gearboxes using adaptive multi-scale morphology filter and modified hierarchical permutation entropy. *Mechanical Systems and Signal Processing*, *105*, 319–337.

Liang, D., Cheng, L., and Li, F. (2005). Numerical modeling of flow and scour below a pipeline in currents: Part II. Scour simulation. *Coastal Engineering*, *52*(1), 43–62.

Liu, X.-X., and Chiew, Y.-M. (2014). Effect of upward seepage on bedload transport rate. *Water Science and Engineering*, *7*(2), 208–217.

Liu, X., and Bai, Y. (2013). Three-dimensional bursting phenomena in meander channel. *Transactions of Tianjin University*, *19*(1), 17–24.

Liu, X. X., and Chiew, Y.-M. (2012). Effect of seepage on initiation of cohesionless sediment transport. *Acta Geophysica*, *60*(6), 1778–1796.

Lu, Y., and Chiew, Y.-M. (2007). Suction effects on turbulence flows over a dune bed. *Journal of Hydraulic Research*, *45*(5), 691–700.

Lu, Y., Chiew, Y. M., and Cheng, N. S. (2008). Review of seepage effects on turbulent open-channel flow and sediment entrainment. *Journal of Hydraulic Research*, *46*(4), 476–488.

Luchi, R., Zolezzi, G., and Tubino, M. (2010). Modelling mid-channel bars in meandering channels. *Earth Surface Processes and Landforms*, *35*(8), 902–917.

Maclean, A G. (1991a). Open channel velocity profiles over a zone of rapid infiltration. *Journal of Hydraulic Research*, *29*(1), 15–27.

Maclean, A. G., and Willetts, B. B. (1986). Measurement of boundary shear stress in non-uniform open channel flow. *Journal of Hydraulic Research*, *24*(1), 39–51.

Maclean, A. G. (1991b). Bed shear stress and scour over bed-type river intake. *Journal of Hydraulic Engineering*, *117*(4), 436–451.

Mallat, S. (1999). *A wavelet tour of signal processing*. Elsevier.

Marsh, N. A., Western, A. W., and Grayson, R. B. (2004). Comparison of methods for predicting incipient motion for sand beds. *Journal of Hydraulic Engineering*, *130*(7), 616–621.

Martin, C. A., and Gates, T. K. (2014). Uncertainty of canal seepage losses estimated using flowing water balance with acoustic Doppler devices. *Journal of Hydrology*, *517*, 746–761.

Matsuura, T., and Townsend, R. (2004). Stream-barb installations for narrow channel bends-A laboratory study. *Canadian Journal of Civil Engineering*, *31*(3), 478–486.

McKeogh, E. J., and Kiely, G. K. (1989). Experimental study of the mechanisms of flood flow in meandering channels. *Proceeding of 23 rd IAHR Congress, Ottawa, Canada*, 491–498.

Mianaei, S. J., and Keshavarzi, A. R. (2008). Spatio-temporal variation of transition probability of bursting events over the ripples at the bed of open channel. *Stochastic*

Environmental Research and Risk Assessment, *22*(2), 257–264.

Nakagawa, H., and Nezu, I. (1978). Bursting phenomenon near the wall in open-channel flows and its simple mathematical model. *Kyoto University, Faculty of Engineering, Memoirs*, *40*, 213–240.

Nezu, I. and Nakagawa, H. (1993). Turbulence in open-channel flows. *IAHR-Monograph*, AA Balkema, Rotterdam, The Netherlands, 1-281.

Nikora, V., Goring, D., McEwan, I., and Griffiths, G. (2001). Spatially averaged open-channel flow over rough bed. *Journal of Hydraulic Engineering*, *127*(2), 123–133.

Oldenziel, D. M., and Brink, W. E. (1974). Influence of suction and blowing on entrainment of sand particles. *Journal of the Hydraulics Division*, *100*(7), 935–949.

Olesen, K. W. (1985). Experiments with graded sediment in the DHL curved flume. *Report R 657-XXII M1771*, Delft Hydrulics Laboratory, Delft, Netherlands.

Omidvarnia, A., Mesbah, M., Pedersen, M., and Jackson, G. (2018). Range entropy: A bridge between signal complexity and self-similarity. *Entropy*, *20*(12), 962.

Patel, M., and Kumar, B. (2017). Flow and bedform dynamics in an alluvial channel with downward seepage. *Catena*, *158*, 219–234.

Patnaik, M., Patra, K. C., Khatua, K. K., and Mohanty, L. (2014). Modelling boundary shear stress in highly sinuous meandering channels. *ISH Journal of Hydraulic Engineering*, *20*(2), 161–168.

Patra, K. C., Kar, S. K., and Bhattacharya, A. K. (2004). Flow and velocity distribution in meandering compound channels. *Journal of Hydraulic Engineering*, *130*(5), 398–411.

Pincus, S. (1995). Approximate entropy (ApEn) as a complexity measure. *Chaos: An Interdisciplinary Journal of Nonlinear Science*, *5*(1), 110–117.

Pincus, S. M. (1991). Approximate entropy as a measure of system complexity. *Proceedings of the National Academy of Sciences*, *88*(6), 2297–2301.

Prinos, P. (1995). Bed-Suction Effects on Structure of Turbulent Open-Channel Flow. *Journal of Hydraulic Engineering*, *121*(5), 404–412.

Qi, M., Chiew, Y. M., and Hong, J. H. (2013). Suction effects on bridge pier scour under clear-water conditions. *Journal of Hydraulic Engineering*, *139*(6), 621–629.

Rahman, M., Nagata, N., Hosoda, T., and Muramoto, Y. (1996). Experimental study on morphological process of meandering channels with bank erosion. *Proceedings of Hydraulic Engineering*, *40*, 947–952.

Raja, R. K., Kumar, A., and Chhabra, S. S. (1983). Estimation of Seepage losses from an unlined channel-A field study by nuclear techniques. P*roceedings, Vol. II, Hydraulics, CBIP, Fiftieth Annual Research and Development Session*, Simla, Himachala Pradesh, India.

Rao, A. R., and Sitaram, N. (1999). Stability and mobility of sand-bed channels affected by see page. *Journal of Irrigation and Drainage Engineering*, *125*(6), 370–379.

Rao, A. R., and Sreenivasulu, G. (2009). Design of plane sand-bed channels affected by seepage. *Periodica Polytechnica Civil Engineering*, *53*(2), 81–92.

Rao, A. R., Sreenivasulu, G., and Kumar, B. (2011). Geometry of sand-bed channels with seepage. *Geomorphology*, *128*(3–4), 171–177.

Rao, N. H. (2007). Seepage losses from canal irrigation schemes Influence of surface and subsurface conditions and implications for conjunctive use. *International Journal of Water Resources Development*, *6*(1), 55–62.

Richardson, J. R., Abt, S. R., and Richardson, E. V. (1985). Inflow seepage influence on straight alluvial channels. *Journal of Hydraulic Engineering*, *111*(8), 1133–1147.

Richman, J. S., and Moorman, J. R. (2000). Physiological time-series analysis using approximate entropy and sample entropy. *American Journal of Physiology-Heart and Circulatory Physiology*, *278*(6), H2039-H2049.

Rosenberry, D. O., and Pitlick, J. (2009). Local-scale variability of seepage and hydraulic conductivity in a shallow gravel-bed river. *Hydrological Processes: An International Journal*, *23*(23), 3306–3318.

Rozovskii I.L. (1957). Flow of water in bends of open channels. *Academy of Sciences of the Ukrainian SSR*, Kiev, Ukraine.

Russell, P., and Vennell, R. (2019). High Resolution Observations of an Outer-Bank Cell of Secondary Circulation in a Natural River Bend. *Journal of Hydraulic Engineering*, *145*(5), 1–10.

Schumm, S. A. (1963). Sinuosity of alluvial rivers on the Great Plains. *Geological Society of America Bulletin*, *74*(9), 1089–1100.

Shams, M., Ahmadi, G., and Smith, D. H. (2002). Computational modeling of flow and sediment transport and deposition in meandering rivers. *Advances in Water Resources*, *25*(6), 689–699.

Sharma, H.D., Chawla, A.S. (1975). Manual of Canal Lining. Technical Report No. l4. Central Board of Irrigation and Power, New Delhi.

Sharma, A., Chavan, R., and Kumar, B. (2017). Multi-scale statistical characterization of migrating pier scour depth in non-uniform sand bed channel. *International Journal of River Basin Management*, *15*(3), 265–276.

Sharma, A., Huang, L., Fang, H., and Li, X. (2020). Effects of hydrodynamic on the mobility of phosphorous induced by sediment resuspension in a seepage affected alluvial channel. *Chemosphere*, *260*, 127550.

Shukla, M. K., and Mishra, G. C. (1994). Canal discharge and seepage relationship. *Proceeding 6th National Symposium on Hydro*, Shillong, India, *263*, 274.

Singh, A., Lanzoni, S., Wilcock, P. R., and Foufoula-Georgiou, E. (2011). Multiscale statistical characterization of migrating bed forms in gravel and sand bed rivers. *Warer Resources Research*, *47*(12), W12526.

Song, X., Xu, G., Bai, Y., and Xu, D. (2016). Experiments on the short-term development of sine-generated meandering rivers. *Journal of Hydro-Environment Research*, *11*, 42–58.

Song, Y., Crowcroft, J., and Zhang, J. (2012). Automatic epileptic seizure detection in EEGs based on optimized sample entropy and extreme learning machine. *Journal of Neuroscience Methods*, *210*(2), 132–146.

Soulsby, R. L., and Dyer, K. R. (1981). The form of the near-bed velocity profile in a tidally accelerating flow. *Journal of Geophysical Research: Oceans*, 86(C9), 8067–8074.

Sreenivasulu, G., Kumar, B., and Rao, A. R. (2011). Variation of stream power with seepage in sand-bed channels. *Water SA*, *37*(1).

Srinivasan, V., Eswaran, C., and Sriraam, N. (2007). Approximate entropy-based epileptic EEG detection using artificial neural networks. *IEEE Transactions on Information Technology in Biomedicine*, *11*(3), 288–295.

Stapleton, K. R., and Huntley, D. A. (1995). Seabed stress determinations using the inertial dissipation method and the turbulent kinetic energy method. *Earth Surface Processes and Landforms*, *20*(9), 807–815.

Sukhodolov, A., and Kaschtschejewa, E. (2010). Turbulent flow in a meander bend of a lowland river: Field measurements and preliminary results. *River Flow* (Dittrich A, Koll K, Aberle J and Geisenhainer P (eds)). Bundesanstalt für Wasserbau, Karlruhe, Germany, 309–316.

Tanji, K. K., and Kielen, N. C. (2002). Agricultural drainage water management in arid and semi-arid areas. *FAO*, Rome, Italy.

Termini, D. (2009). Experimental observations of flow and bed processes in large-amplitude meandering flume. *Journal of Hydraulic Engineering*, *135*(7), 575–587.

Thompson, C. E. L., Amos, C. L., Jones, T. E. R., and Chaplin, J. (2003). The manifestation of fluid-transmitted bed shear stress in a smooth annular flume-a comparison of methods. *Journal of Coastal Research*, *19*(4), 1094–1103.

Thomson, J. (1876). On the origin of windings of rivers in alluvial plains, with remarks on the flow of water round bends in pipes. *Proceedings of Royal Society of London*, *25*(171-178), 5–8.

Thorne, C. R., Zevenbergen, L. W., Pitlick, J. C., Rais, S., Bradley, J. B., and Julien, P. Y. (1985). Direct measurements of secondary currents in a meandering sand-bed river. *Nature*, *315*(6022), 746.

Thorne, P. D., Williams, J. J., and Heathershaw, A. D. (1989). In situ acoustic measurements of marine gravel threshold and transport. *Sedimentology*, *36*(1), 61–74.

Tilston, M., Rennie, C., Arnott, R. W. C., and Post, G. (2009). On the nature of coherent turbulent structures in channel bends: burst-sweep orientations in three-dimensional flow fields. *33rd IAHR Congress: Water Engineering for a Sustainable Environment*, 9–14.

Turner, I. L. (1995). Simulating the influence of groundwater seepage on sediment transported by the sweep of the swash zone across macro-tidal beaches. *Marine Geology*, *125*(1–2), 153–174.

Vermeulen, B., Hoitink, A. J. F., and Labeur, R. J. (2015). Flow structure caused by a local cross-sectional area increase and curvature in a sharp river bend. *Journal of Geophysical Research: Earth Surface*, *120*(9), 1771–1783.

von Schelling, H. (1951). Most frequent particle paths in a plane. *Eos, Transactions American Geophysical Union*, *32*(2), 222–226.

Watters, G. Z., and Rao, M. V. P. (1971). Hydrodynamic effects of seepage on bed particles. *Journal of the Hydraulics Division*, *97*(3), 421–439.

Whiting, P. J., and Dietrich, W. E. (1993a). Experimental studies of bed topography and flow patterns in large-amplitude meanders: 1. Observations. *Water Resources Research*, *29*(11), 3605–3614.

Whiting, P. J., and Dietrich, W. E. (1993b). Experimental studies of bed topography and flow patterns in large-amplitude meanders: 2. Mechanisms. *Water Resources Research*, *29*(11), 3615–3622.

Willetts, B. B., and Drossos, M. E. (1975). Local erosion caused by rapid forced infiltration. *Journal of the Hydraulics Division*, *101*(12), 1477-1488.

Xu, D., and Bai, Y. (2013). Experimental study on the bed topography evolution in alluvial meandering rivers with various sinuousnesses. *Journal of Hydro-Environment Research*, *7*(2), 92–102.

Xu, K., and Wang, J. (2017). Weighted fractional permutation entropy and fractional sample entropy for nonlinear Potts financial dynamics. *Physics Letters A*, *381*(8), 767–779.

Yalin, M. S. (1992). *River Mechanics. Pergamon Press*. Oxford, UK.

Yalin, M. S. (1977). *Mechanics of sediment transport*. 2nd edition, Pergamon Press, Oxford UK.

Yalin, M. S., and da Silva, A. M. F. (2001). Fluvial processes. IAHR monograph. *International Association for Hydraulic Research, Delft*.

Yan, X., Rennie, C. D., and Mohammadian, A. (2020). A three-dimensional numerical study of flow characteristics in strongly curved channel bends with different side slopes. *Environmental Fluid Mechanics, 0123456789*.

Yen, B. C. (2002). Stochastic inference to sediment and fluvial hydraulics. *Journal of Hydraulic Engineering*, *128*(4), 365–367.

Yu, M., Xie, Y., Wu, S., and Tian, H. (2019). Sidewall shear stress distribution effects on cohesive bank erosion in curved channels. *Proceedings of the Institution of Civil Engineers: Water Management*, *172*(5), 257–269.

Zhang, L., Zhang, F., Cai, A., Song, Z., and Tong, S. (2020). Comparison of methods for bed shear stress estimation in complex flow field of bend. *Water (Switzerland)*, *12*(10), 1–16.

Zhou, S., Qian, S., Chang, W., Xiao, Y., and Cheng, Y. (2018). A novel bearing multi-fault diagnosis approach based on weighted permutation entropy and an improved SVM ensemble classifier. *Sensors*, *18*(6), 1934.

Zhu, X., Xu, H., Zhao, J., and Tian, J. (2017). Automated epileptic seizure detection in scalp EEG based on spatial-temporal complexity. *Complexity*, *2017*.

Zunino, L., Zanin, M., Tabak, B. M., Pérez, D. G., and Rosso, O. A. (2009). Forbidden patterns, permutation entropy and stock market inefficiency. *Physica A: Statistical Mechanics and Its Applications*, *388*(14), 2854–2864.